Lawrence Berkeley National Laboratory
Lawrence Berkeley National Laboratory

Title
PHYSICS OF ULTRA-PURE GERMANIUM

Permalink
https://escholarship.org/uc/item/7mp4x58b

Author
Haller, Eugene E.

Publication Date
1980-09-01

eScholarship.org Powered by the California Digital Library
University of California

LBL-10326 c.2
Preprint

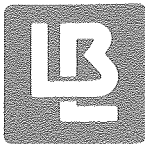

Lawrence Berkeley Laboratory

UNIVERSITY OF CALIFORNIA

Engineering & Technical Services Division

Submitted to Advances in Physics

PHYSICS OF ULTRA-PURE GERMANIUM

Eugene E. Haller, William L. Hansen, and Frederick S. Goulding

RECEIVED
LAWRENCE
BERKELEY LABORATORY

September 1980

DEC 11 1980

LIBRARY AND
DOCUMENTS SECTION

TWO-WEEK LOAN COPY

This is a Library Circulating Copy which may be borrowed for two weeks. For a personal retention copy, call Tech. Info. Division, Ext. 6782.

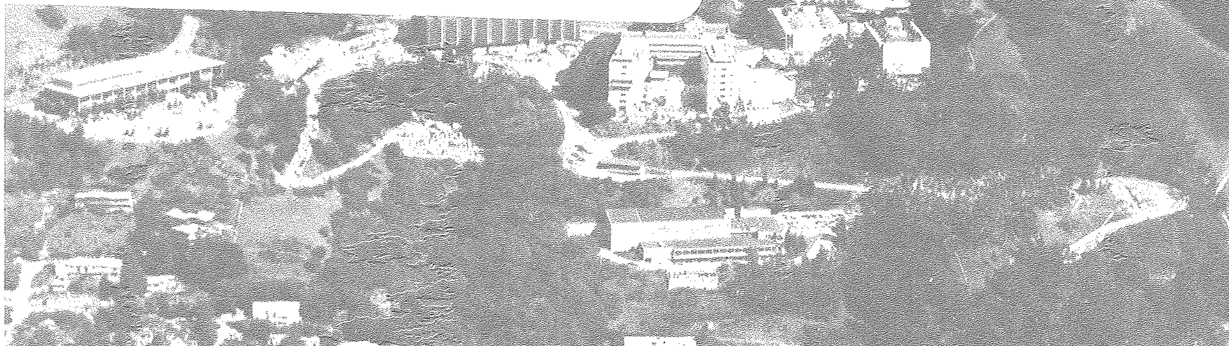

Prepared for the U.S. Department of Energy under Contract W-7405-ENG-48

LBL-10326 c.2

DISCLAIMER

This document was prepared as an account of work sponsored by the United States Government. While this document is believed to contain correct information, neither the United States Government nor any agency thereof, nor the Regents of the University of California, nor any of their employees, makes any warranty, express or implied, or assumes any legal responsibility for the accuracy, completeness, or usefulness of any information, apparatus, product, or process disclosed, or represents that its use would not infringe privately owned rights. Reference herein to any specific commercial product, process, or service by its trade name, trademark, manufacturer, or otherwise, does not necessarily constitute or imply its endorsement, recommendation, or favoring by the United States Government or any agency thereof, or the Regents of the University of California. The views and opinions of authors expressed herein do not necessarily state or reflect those of the United States Government or any agency thereof or the Regents of the University of California.

Submitted to Advances in Physics LBL-10326

PHYSICS OF ULTRA-PURE GERMANIUM

Eugene E. Haller, William L. Hansen and Frederick S. Goulding

Lawrence Berkeley Laboratory
University of California
Berkeley, California 94720 U.S.A.

September 1980

Prepared for the U. S. Department of Energy
under Contract No. W-7405-ENG-48

TABLE OF CONTENTS

	Page No.
1. Introduction	1
2. Purification and Crystal Growth	3
2.1. Purification	3
2.2. Crystal Growth	6
3. Analytical Methods	9
3.1. Traditional Techniques	9
3.2. Photothermal Ionization Spectroscopy	16
3.3. Deep Level Transient Spectroscopy	20
3.4. High Q Electron Paramagnetic Resonance	23
4. Point and Line Defects	24
4.1. Elemental Impurities of the Third and Fifth Group	24
4.2. Deep Impurities	25
4.3. Neutral Impurities	29
4.4. Complexes	33
4.4.1. General Remarks	33
4.4.2. Hydrogen-related acceptors and donors: A(H,Si), A(H,C) and D(H,O)	34
4.4.3. Lithium-related donors D(Li) and D(Li,O)	39
4.4.4. Divacancy-hydrogen acceptor $A(V_2H)$	42
4.4.5. Copper-related acceptors A(C,H,Li)	43
4.5. Dislocations	45
5. Summary and Conclusions	47
6. Acknowledgment	48

Abstract

A broad review of the physics of point defects, i.e., electrically active and neutral impurities and impurity complexes is given. Basic material science which is crucial for understanding the physics is summarized in an introductory section. It is followed by the detailed description of the novel measurement techniques--Photothermal Ionization Spectroscopy, High-Q Electron Paramagnetic Resonance and Deep Level Spectroscopy. These spectroscopic techniques have had a profound impact on the investigations of ultra-pure germanium. The major part of this work deals with the physics of point defects in ultra-pure germanium. The high purity of this semiconductor allows the undisturbed observation of highly excited bound states of shallow donors and acceptors. Many new previously unknown acceptor and donor centers have been discovered in ultra-pure germanium. The nature of several of these centers can be understood in terms of a complex consisting of two impurities--a light interstitial atom (e.g. hydrogen or lithium) tunneling between four identical real space positions in the vicinity of a substitutional impurity (e.g. carbon, silicon, oxygen or copper), or a defect (e.g. divacancy). The motion of the tunneling impurity is shown to influence the electronic structure of the complex leading to a symmetry of higher order than tetrahedral. Experimental results are presented which are fully consistent with the tunneling model. Besides the review of recently published results, new findings on the solubility of substitutional copper in ultra-pure crystals grown under a variety of conditions and on the two donors lithium D(Li) and lithium-oxygen D(Li,O) are presented.

Physics of Ultra-Pure Germanium*

Eugene E. Haller, William L. Hansen and Frederick S. Goulding

Lawrence Berkeley Laboratory
University of California
Berkeley, California 94720 U.S.A.

1. Introduction

The development of large, ultra-pure germanium single crystals has greatly stimulated interest in the physics of germanium in recent years. This pure semiconductor, probably the purest substance produced by man, has resulted in the development of various novel analytical techniques. It has led to the discovery and understanding of many new impurity complexes [1], has given an opportunity to test the limits of validity of solid state theories [2] and has helped in the exploration of a new state of matter, the electron-hole liquid [3]. It is interesting to recognize that the incentive for the development of ultra-pure germanium was not generated by physics or material science but originated directly from the need to understand the basic mechanisms involved in nuclear radiation detectors so as to improve their performance and the reliability of the fabrication process [4]. Such detectors are, compared with typical semiconductor devices, gigantic diode structures with depletion layers up to several centimeters thick and areas of many square centimeters. To obtain such thick depletion layers and collect all the ionization generated in the layers at a reverse bias of a few thousand volts, a semiconductor is

*This work is supported by the Office of Health and Environmental Research of the Department of Energy under Contract W-7405-ENG-48.

required with a net concentration of shallow centers (i.e., the difference between the donor and acceptor concentration) of around $10^{10}cm^{-3}$ and with a very low concentration of deep levels. Therefore, an electrically active net-impurity concentration of no more than 1 atom in 4×10^{12} germanium atoms is essential. Fortunately, in the early days of semiconductor nuclear radiation detectors, a compensation technique was developed which made use of the drifting of interstitial lithium donors in an electric field. The donors compensate the acceptors in gallium-doped germanium [5]. The process, called "lithium drifting", is self-regulating insofar that local over- or under-compensation leads to electric field gradients that rapidly correct the compensation imbalance. Applying reverse bias to the junction formed by a lithium (n^+)-doped region and the gallium (p)-doped base region causes a steady widening of the compensated region as the lithium ions drift in the electric field. The drift process is sensitive to oxygen interference and, in germanium, the compensation is not stable at room temperature when the reverse bias is removed.

The deficiencies in these detectors led to a search for ways to produce ultra-pure germanium. A feasibility study was presented in 1966 by R. N. Hall [6]. By 1970 the first crystals with net-impurity concentrations between 10^{10} and $10^{11}cm^{-3}$ were grown [7]. While a number of laboratories have now successfully produced such crystals [8], the high costs and difficult technology have resulted in very few sources of the material. It is interesting to observe that, from a wealth of potential ways to purify germanium and to grow ultra-pure crystals, only one set of techniques has proven successful in the various laboratories.

The processes of purification and crystal growth strongly influence the kinds and concentrations of impurities and of residual point and line defects. Therefore, a rather detailed review of the basic elements of these material processes will be given as background for the explanation of the newly discovered impurity complexes discussed later in this chapter. These processes will therefore be the subject of the next section.

The development of ultra-pure germanium has largely been predicated on the introduction of new analytical techniques mainly of a spectroscopic character. These techniques are particularly important for measurements on ultra-pure semiconductors (sections 3.2.-3.4.) and since they are not in wide use, we will describe them in greater detail than we do the classical techniques.

2. Purification and Crystal Growth

2.1. Purification

We will discuss here only the steps required to decrease the impurity concentration in the purest, commercially available, polycrystalline germanium down to the $10^{10}cm^{-3}$ concentration range. Analysis shows that commercially produced "intrinsic germanium", which is used as starting material, normally contains phosphorus, boron and aluminum at levels of 10^{12} to $10^{13}cm^{-3}$. Beyond these impurities which produce shallow levels [9], no other electrically-active impurities are found in significant concentrations. We have not investigated the neutral impurities (e.g. silicon, oxygen and hydrogen) in starting materials since their concentration

in the final crystals is determined by the crystal growing technique used to grow ultra-pure germanium crystals (see Section 2.2).

The principle of solid-liquid impurity segregation [10] can be used to accomplish a reduction of impurity concentrations by two to three orders of magnitude. Every impurity species establishes a well defined ratio of concentrations in liquid (C_l) and solid (C_s) germanium if the two phases are in contact in equilibrium. This ratio is called segregation coefficient K where:

$$K = C_s/C_l \tag{2.1}$$

The interface equilibrium is reached via diffusion and the segregation is therefore disturbed by any finite crystal growth velocity and consequent freezing of liquid germanium. In this case an effective segregation coefficient, closer to unity, is observed.

Zone purification and multiple crystal growth [11] have both been commonly used to purify germanium. The first of these methods is based on passing a narrow liquid zone of germanium slowly through a long bar of polycrystalline or single-crystal germanium held in a container called a "boat". A zone is melted at one end of the bar by heating by means of a localized radio frequency field; the molten zone is then moved through the bar to the other end and the process is repeated several times "collecting" impurities by segregation. In principle, the smaller the segregation coefficient is, the easier it is to remove an impurity. The second method, multiple Czochralski crystal growth, uses the fact that impurities with segration coefficients less than unity accumulate in the melt during crystal growth, concentrating the impurities in the "tail" end of the crystal. Subsequent

crystals are then grown from the pure "seed" ends of the previous generations thereby achieving purification. Theoretically both methods can produce crystals of any desired purity. However, interactions between the germanium, the container and the ambient atmosphere in the refiner/crystal puller interfere drastically with the purification process at concentration levels between 10^{10} and $10^{11}cm^{-3}$. In the case of graphite containers the interaction consists of transfer of residual impurities from the graphite into the liquid germanium. The purest graphite available is found to contaminate germanium with phosphorous (a shallow donor) and boron (a shallow acceptor) at concentrations $>10^{11}cm^{-3}$. The most suitable container material, synthetic quartz [12], contaminates germanium with phosphorus ($<2x10^{10}cm^{-3}$) and leads to the formation of ternary or higher order compounds involving silicon, oxygen and aluminum. Such compounds do not exhibit effective segregation [13] and they appear to partially dissociate in the solid germanium releasing electrically active aluminum [13] (a shallow acceptor). Effective purification in quartz demands that aluminum be removed before the germanium melt contacts the quartz or alternatively that methods be devised to precipitate the aluminum-containing compounds. For example, a possible method is to first purify in a graphite container to remove aluminum and then in quartz to remove boron and phosphorus. Other solutions are still being investigated.

The atmosphere surrounding the melt also has a strong influence on purification, not as a source of impurities, but as a medium controlling the thermochemistry of impurities in the liquid germanium. Gas mixtures can be used which can range from pure, palladium-diffused hydrogen which is strongly reducing, through inert gases (e.g. noble gases) to strongly oxidizing mixtures containing water or oxygen. The composition of the atmosphere controls

the equilibrium between impurity complexes and their dissociation products. The situation has been discussed thermochemically for compounds in liquid germanium [14]. The general results of this investigation indicate that reducing atmospheres are more suitable for purification by the liquid-solid segregation process. The situation is actually more complicated than is indicated by these general comments. High vacuum, at first sight very "pure", is not a suitable ambient. This is probably because the mean free paths of atoms or molecules (which can contaminate the germanium) become very long and the liquid germanium behaves as a powerful getter. A reducing gas "blanket" is in general preferred for this reason.

2.2. Crystal Growth

Much of the discussion of the previous section concerning container materials and ambient atmosphere is also relevant for the crystal growth process. In addition, the isotherms in the crystal puller must be shaped so that a monocrystal of the desired size and crystalline perfection can be pulled. This may dictate compromises which produce detrimental conditions for the purity control. For example, materials used to shape the temperature distribution may be sources of impurities.

The ultra-pure germanium single crystals discussed here are grown by the Czochralski method [15]. The crucible-free techniques, (e.g. float zoning) are not suitable for large diameter germanium crystals because of the high density and small surface tension of germanium.

Experience has shown that a pure hydrogen atmosphere in the crystal puller leads to crystals which produce the best nuclear radiation detectors. This strongly reducing atmosphere seems to prevent the formation of quartz

precipitates in the crystals [16] which interfere with perfect charge collection. However, hydrogen is, because of its high thermal conductivity, an inconvenient crystal-growth atmosphere from the point of view of temperature distribution. Hydrogen is soluble in germanium [17] and is now known to form complexes with various point defects (see sections 4.4). These complexes are important for the electrical properties of germanium; for example, the divacancy-hydrogen center (V_2H) [18], has a single acceptor level at E_V + 0.072 eV, causing trapping of holes which degrades the performance of nuclear radiation detectors. The concentration of vacancies, which controls that of divacancies, can be kept small if dislocations are present at a concentration >100cm^{-2}. On the other hand, the dislocation density should not exceed $10^5 cm^{-2}$ because dislocations also produce charge trapping. The acceptable concentration range of dislocations is rather narrow in practice since dislocations multiply rapidly when the temperature distribution in the crystal puller is not perfect.

The optimum container for the ultra-pure germanium melt is a synthetic quartz crucible [12]. This crucible is chemically etched before each crystal growth to avoid cross contamination from one crystal to the next. The whole amount of molten germanium must be pulled as a single boule since the quartz crucible will break if liquid germanium freezes in it.

The previous paragraphs indicate the fine process tuning required when purifying and growing germanium single crystals suited for nuclear radiation detectors. Of course, the process becomes considerably less critical when certain parameters are not important and when the net impurity concentration can reach >5 x $10^{10} cm^{-3}$. Some of the crystals discussed in later sections on impurity complexes were grown as experimental crystals under special conditions.

Before closing this section, let us analyze briefly an impurity profile of a typical ultra-pure germanium crystal. Figure 1 shows the net-impurity concentration $|N_A - N_D|$ of a crystal grown under the standard conditions discussed earlier (i.e. 1 atm. of pure hydrogen, synthetic quartz crucible). The net impurity concentration, as determined by conductivity measurements and Hall effect at 77K lies close to $3.5 \times 10^{10} cm^{-3}$ near the seed end of the crystal. Photothermal Ionization Spectroscopy indicates that the majority impurity is aluminum in the p-type section. The minority impurity is phosphorus. A large fraction of the aluminum does not segregate because of complex formation with silicon and oxygen from the crucible. Phosphorus, on the other hand, segregates normally leading to a continuous increase in donor concentration towards the tail end. At the point where 63% of the melt was frozen, a change from p- to n-type is observed. In the lower section of the crystal phosphorus is the majority impurity. The dashed and dotted curves are the calculated concentration profiles of aluminum and phosphorus. They add up to the measured profile (continuous line). Effective segregation coefficients for phosphorus and aluminum of 0.25 and 1.0 respectively lead to the best fit.

Deep level impurities have not been detected in this crystal. This general result is not suprising since such impurities exhibit very small segregation coefficients and they also exhibit low solubilities compared with elemental impurities of valency 3 and 5. Of the three major neutral impurities--hydrogen, silicon and oxygen--only oxygen can be measured with good sensitivity and accuracy using the lithium precipitation technique [19]. Such measurements indicate oxygen concentrations $[O] = 5$ to $10 \times 10^{13} cm^{-3}$ near the seed end of crystals grown in the manner described earlier. [O]

increases towards the tail end, indicating either segregation or accumulation for some reason. At the point where ~ 90% of the melt was frozen the value of $[O] = 2 \times 10^{14} cm^{-3}$. An in-depth discussion of neutral impurities will follow in section 4.3.

3. Analytical Methods

3.1 Traditional Techniques

The primary goal in the development of ultra-pure germanium is obviously the reduction of electrically active centers, donors and acceptors. The net concentration of such species can be measured with very high sensitivity because the intrinsic conduction of the host crystal can always be reduced by cooling to temperatures where the impurity conduction becomes dominant. The analysis of neutral centers is much more difficult. This task is generally less crucial but it is assuming increasing importance because several electrically active centers have been discovered which consist of complexes of "neutral" impurities and defects.

The aim of this section is to survey the traditional measurement techniques and to present typical examples. Recently developed methods will be discussed in more detail.

The easiest electrical property to measure is probably the gross conductivity of an ultra-pure germanium crystal. To obtain useful information the crystal must be cooled to the extrinsic conduction range.

For net-impurity concentrations of $10^{11}cm^{-3}$ and low compensation, this implies using temperatures T < 200K. Contacts play an important part in precise conductivity measurements. They should be ohmic; therefore a linear V-I dependence should be observed for both polarities. A special complication occurs in producing ohmic contacts on ultra-pure germanium crystals since they cannot be heated to temperatures above 300°C without the high probability of contamination by fast diffusing impurities. Satisfactory contacts can be formed at room temperature by using a liquid indium-gallium eutectic for p-type and liquid indium-mercury eutectic for n-type crystals. The extrinsic conductivity range and shallow level freeze-out region can be explored with such contacts although the voltage-current linearity range is limited to small current densities ($<100\mu Acm^{-2}$). Samples are chemically etched [24] on all surfaces before application of the eutectic. Our experience shows that such etched surfaces do not contribute any excess conduction when kept clean and dry.

Better contacts can be produced using processes that involve some heating. For example, implanting boron ions at an energy of 25--100 keV and to a dose of 10^{14}-$10^{15}cm^{-2}$ followed by annealing for one hour at 250°C leads to contacts which are ohmic on p-type crystals down to at least 1.2K [1]. Similarly, diffusion of lithium at 300°C for 10 to 30 minutes into the surface of n-type crystals produces ohmic contacts. The disadvantage of lithium diffused contacts is the presence of lithium and lithium-oxygen donors to a few hundred microns depth in the crystal. These extra donors interfere in all impurity spectroscopy methods. Phosphorus implantation at energies of 25 keV and a dose of 10^{14} - $10^{15}cm^{-2}$ followed by a two-stage annealing cycle produces degenerately doped n^{+}-contacts [20].

However extreme care must be taken in surface preparation and the relatively high temperature needed for perfect annealing (~ 300°C) makes this type of contact difficult to prepare.

Conductivity measurements are well suited for quick, non-destructive survey measurements. A whole crystal can be analyzed by applying current contacts to the seed and tail ends and measuring voltages along the side surface of the crystal. The crystal is immersed in liquid nitrogen and a constant current is passed through it. Measurement of the voltage differences across adjacent suitably-spaced contacts leads to an axial conductivity "profile" which can be converted into a net-impurity profile if radial concentration variations can be neglected and if it is assumed that the mobility of the electrons or holes is known. Both conditions are usually met in ultra-pure germanium crystals. The following equation relates conductivity and net-impurity concentration $|N_A - N_D|$:

$$\sigma = |N_A - N_D| e\mu \qquad (3.1)$$

μ = mobility (44,000$cm^2 V^{-1} s^{-1}$ at 77K for both electrons and holes).
e = charge on the electron (= 1.6×10^{-19}As). The net-impurity profile in Figure 1 was obtained from such conductivity measurements.

Hall effect measurements are slightly more complicated but also more informative. The net-impurity concentration and the type of conduction (p or n) can be obtained over a wide temperature range independent of the mobility:

$$R_H = \frac{C}{|N_A - N_D|\ e} = \frac{\Delta V t}{IB} \qquad (3.2)$$

R_H is the Hall constant, ΔV is the Hall-voltage and B is the magnetic field strength perpendicular to the current I. The crystal sample has width t. The factor C depends on temperature, crystal type and crystal orientation. It is always close to unity and has been experimentally determined for n- and p-type crystals [21,22]. Since the geometric constraints can be relaxed if the van der Pauw measurement geometry is chosen [23], we have used this geometry in our experiments. A typical example of a Hall effect measurement over a wide temperature range is shown in Figure 2. Here, the logarithm of the net-hole concentrations of two samples is plotted in function of the inverse absolute temperature. The dislocated sample (+) is truly pure in the sense that no deep levels are present and the net shallow level concentration is $2 \times 10^{10} cm^{-3}$. The three ranges of conduction are very distinct. As the sample is cooled, at T = 180K, the intrinsic range changes to extrinsic and at about 14K the freeze-out region begins. The dislocation-free sample (0) contains an additional deep acceptor. From the temperature where 50% of the deep levels are frozen out and from the slope of the freeze-out, the position of this deep acceptor level is found to be E_V + 72 meV. This acceptor has been extensively studied and is believed to be a divacancy-hydrogen complex [18] (see also section 4.4.4).

Since conductivity and Hall-effect measurements are based on electrical and magnetic measurements, they are sensitive to the state of the surfaces, contacts, sample geometry and homogeneity. In order to test the uniformity of a single crystal, samples of a few cubic millimeters must be examined. In general, one does not need smaller samples in any of the applications or physics experiments involving ultra-pure germanium. The surfaces have little effect if they have been polish-etched [24] and are kept extremely clean. Contacts have been discussed before.

The experimental errors in such measurements are composed of a series of small errors which are difficult to analyze accurately. From cross checking the results obtained with different methods, we guess that these purely electrical measurements are accurate to between 5 and 10%. Consequently, all physical entities derived from such measurements exhibit errors of such magnitude, e.g., it is obvious that one cannot determine the nature of shallow acceptors and donors from the carrier freeze-out at low temperature. The ground state energies of the group III/V impurities leading to shallow acceptors/donors lie too close together.

As mentioned at the beginning of this section, it is much more difficult to investigate neutral impurities in ultra-pure germanium. The best known neutral impurities are hydrogen, carbon, oxygen and silicon. Undoubtedly there are other neutral impurities present in ultra-pure crystals. Their effect must, however, be extremely subtle or their concentrations very small. Of the four impurities mentioned, only oxygen can be analyzed down to concentrations around $10^{12}cm^{-3}$ because it can be incorporated into a complex with lithium to form a shallow donor D(Li,O) which can be measured electrically. The lithium precipitation technique [19] is based on the supersaturation of lithium in a sample and the subsequent precipitation of the dissolved lithium into lithium clusters and complexes. The supersaturation is obtained by diffusing lithium into a crystal sample from an infinite source (i.e., lithium evaporated onto the crystal) at a temperature T_1 (typically approximately 400°C). Rapid cooling to a lower temperature T_2 (typically room temperature) creates supersaturation of lithium. Because lithium is a shallow donor, its concentration can be measured as a function of time using a simple four-point probe conductivity measurement. The oxygen concentration affects both the precipitation rate and the final donor

concentration. A group of precipitation curves is presented in Figure 3. All samples were saturated with lithium at 425°C for 24 hrs. Curves (1) and (2) were obtained with samples from a crystal grown in a quartz crucible and a hydrogen atmosphere. The final donor concentration is ~ $1 \times 10^{14} cm^{-3}$ which corresponds to the original oxygen concentration in the crystal (finally bound in LiO donors). A sample of a crystal grown from a graphite crucible in a hydrogen atmosphere leads to curve (4). The precipitation rate is much smaller and the end value of the donor concentration is $4.5 \times 10^{13} cm^{-3}$. This value is very close to the intrinsic carrier concentration of germanium at room temperature ($3.5 \times 10^{13} cm^{-3}$) and is, therefore, only an upper limit for the original oxygen concentration. We have allowed such samples to precipitate at 0°C and have obtained a smaller donor concentration. Since the sensitivity limit of this method is set by the intrinsic carrier concentration at the precipitation temperature, even lower temperatures can be used to reduce the oxygen detection limit but the precipitation rate then becomes very small. Curve (3) is a special case where the crystal was grown from a melt contained in a quartz crucible and in a hydrogen atmosphere just as were the crystals of curves (1) and (2), but pure silicon was added to the germanium melt producing [Si] = $9.3 \times 10^{17} cm^{-3}$ at the position in the crystal where the sample was taken. Obviously, the silicon greatly affects the oxygen concentration. The crystal behaves similarly to the one grown in a carbon crucible and it exhibits much lower oxygen concentration than those grown in quartz where no silicon doping was added. This is an important result which will be discussed in section 4.4.2.

Of the three remaining known neutral impurities--hydrogen, carbon and silicon--the first one has been studied extensively [17] at temperatures close to the melting point by time-resolved diffusion through thin-walled

single-crystal germanium cylinders using a mass spectrometer for hydrogen detection. Such diffusion studies cannot be used in an analytical way to measure the hydrogen concentration present in germanium. However, the results indicate that hydrogen is interstitially dissolved at high temperatures and that it has a maximum solubility of a few times $10^{14}cm^{-3}$ near the melting point (935°C). We assume that a large fraction of the hydrogen is trapped in the crystal during the crystal growth process. We are not aware of any method for measuring such small concentrations of hydrogen in germanium single crystals. A large problem for any method is the water absorbed on the surface of the germanium [25]. Nuclear reactions [26] have been proposed as a technique to analyze hydrogen in semiconductor crystals but the sensitivity is limited to a few parts per million which is much too insensitive for our purpose.

Non-gaseous impurities can be detected using Spark Source Mass Spectrometry (SSMS). Detection limits of several parts per billion (ppb i.e., 1 in 10^9 weight) are typical for elements with no matrix interference or high instrument background. Silicon has been analyzed in this way down to concentrations of $3.5 \times 10^{14}cm^{-3}$ (3ppb). SSMS measurements always show high levels of sodium (10 to 40ppb) and potassium (5 to 10ppb) in our crystals [27]. Since we have been unable to correlate any effects or complexes with these impurities, we suspect that surface contamination of the sample when used as the spark source falsifies the results. No other elements have been detected in our normal germanium crystals using this method.

None of the described methods is sensitive enough to detect carbon in germanium. Metallurgical studies indicate that carbon and germanium do not form any compounds and are not miscible [28]. This information is not very relevant for the concentration levels of interest here. Because there is

strong evidence that carbon is involved in some acceptor complexes, we are in the process of designing an experiment using the radiocarbon (^{14}C) as a tracer. A slice of a crystal grown out of a pyrolytic graphite-coated crucible containing ^{14}C will be used to fabricate a standard p-i-n nuclear radiation detector [4]. This detector will register the beta decays of the ^{14}C atoms with almost 100% efficiency. In a low background counting area, we expect to be able to detect a carbon concentration as low as ~ $10^{10} cm^{-3}$ [76]. Our current experiment could be developed into a method for detection of any suspected impurity which has isotopes which are reasonably long lived. Any semiconductor which can be made into a p-n diode with a low reverse leakage current could in principle be investigated.

3.2. Photothermal Ionization Spectroscopy

Photothermal Ionization Spectroscopy (PTIS), often now called Photoelectric Spectroscopy in the Russian literature, is based on a two-step ionization process discovered by Lifshitz and Nad [29]. They found sharp features in photoconductivity measurements at photon energies below the threshold energy of shallow levels in germanium. They attributed these sharp features to optical transitions of a bound electron from the ground state to one of the excited states and subsequent excitation into the conduction band by the absorption of lattice phonons. This interpretation was supported by the temperature dependence of the intensity of the photoconductivity peaks [30] and also by theoretical work [31]. The method has excellent sensitivity because it is based ultimately on an electrical measurement. In addition, it is a spectroscopic method, and the spectral information exhibits excellent resolution allowing unique identification of donors and acceptors in germanium.

In Figure 4, the two-step process is schematically presented for the case of a donor. In order to fully appreciate how powerful this kind of spectroscopy is, we have to go back to some basic features of shallow levels in germanium. Such centers are often called "hydrogenic" [32] because an electron (or hole) is bound in the Coulomb field of a singley-charged donor (or acceptor) as in the case of a hydrogen atom. The theory of a locally-fixed charge in a semiconductor, the impurity atom, binding an electron or a hole is called effective mass theory (EMT) and was developed twenty-five years ago [33]. Replacing the mass of the free electron with an appropriately averaged effective mass m^* and taking into account the dielectric constant ε of the host lattice, the classical equation for the hydrogen atom gives a good estimate for the ground state energy:

$$E_n = - \frac{e^4 m^*}{2\varepsilon^2 \hbar^2} \quad (3.3)$$

e is the charge of the electron and $\hbar$ is Planck's constant $\div 2\pi$. Using the correct anisotropic mass tensor one obtains for the ground state energy of a single valley donor $E_{gs} = 9.9$ meV [32], a value more than one thousand times smaller than the hydrogen ground state energy (13.6 eV). This theoretical value for the ground state is very close to experimentally determined ground states of typical shallow donors in germanium.

Using the same constants, the Bohr radius r is given by the equation:

$$r_n = \frac{\varepsilon \hbar^2}{e^2 m^*} \quad (3.4)$$

The ground state has a Bohr radius of ~ 80Å. This means that the bound

electron or hole moves through a volume much larger than that occupied by its parent impurity. The wave function of an excited state is shaped by the host crystal and a Coulomb potential and is almost independent of the local lattice distortions at the impurity core especially in the case of p-like excited states. This is the main reason why the excited states are virtually identical for all the donors and for all acceptors, a fact well supported by early infrared absorption measurements [34].

The large size of bound excited state wave functions leads to interference between atoms at relatively small impurity concentrations ($>10^{12}cm^{-3}$). Ultra-pure germanium has the unique advantage that such interference is almost non-existent. Using Photothermal Ionization Spectroscopy, one can take full advantage of this situation. The sensitivity for detection of species reaches concentrations as low as $10^{7}cm^{-3}$ (i.e. ~ 1 impurity in 10^{16} Ge atoms) [35]. The bound excited states can develop completely undisturbed and exhibit extremely narrow levels (<10 μeV wide) in almost perfect crystals.

Fourier Transform Infrared Spectroscopy [36] is used with great advantage at the long wavelength (λ ~ 100μm) and the resolution needed in PTIS ($\Delta E<10$ μeV). Figures 5A and 5B show the basic setup used to perform Photothermal Ionization Spectroscopy using a Michelson Interferometer. In Figure 5A, the interferometer is shown schematically. It consists of an IR-source (typically a high-pressure mercury lamp or a Nernst glower), the mirrors M_p, M_f and M_m and the beam splitter BS (mylar). The IR-radiation is modulated by moving the mirror M_m either in steps (sampling the interfer- ogram) or continuously. The light is collected by a funnel into a polished brass pipe which guides the IR-radiation through a mechanical chopper Ch to the sample (#6 in Figure 5B). In our case, this is a cube of ultra-pure germanium (~ 7mm on the side) which is

lightly pressed with a spring (#8) against a base plate containing a temperature sensor (#7) inside a brass cavity (#5). Cooling is provided via a copper coldfinger (#3) immersed in liquid helium (#2) inside an all-glass dewar (#1). Heating to temperature $T > 4.2K$ is achieved by passing current through a resistor (#4). More detailed descriptions of Fourier Transform Spectroscopy in general and its specific application in PTIS can be found in the literature [36].

A typical interferogram obtained with a pure germanium sample containing mainly the residual impurity aluminum is shown in Figure 6. The 'beat' character of the amplitude of the sinusodial interferogram indicates mixing of two strong lines in the spectrum. Figure 7 shows the Cosine Fourier Transform of the interferogram. Besides the dominant C and D lines [34] of the shallow acceptor aluminum there are many weaker lines present. They are due to higher bound excited states of aluminum and to the shallow acceptors boron and gallium.

The basic PTIS method reveals only centers which produce a free charge carrier when they change their charge state through the absorption of a photon and a phonon. It is therefore restricted to levels in the lower half of the band-gap for p-type crystals and to levels in the upper half of the bandgap for n-type crystals. This restriction can be removed by shining band-edge light ($h\nu \approx E_{gap}$) onto the crystal [37]. Depending on various factors, a substantial population of neutral minority centers is thereby created. These centers generate free minority carriers when they absorb a photon and a phonon of appropriate energies producing a change in the conductivity of the sample. In ultra-pure germanium, the conductivity decreases when minority carriers are produced leading to negative peaks in the

spectra. A possible explanation is that generation of minority carriers leads to recombination of majority and minority carriers, reducing the dominant conductivity by hole conduction. That this explanation is not complete is indicated by the fact that experiments with pure silicon have shown spectra with all positive lines [1]. Figure 8 shows the spectrum obtained with the same sample as used to obtain the spectrum in Figure 7 but with band-edge light illumination. In addition to the acceptor lines the hydrogenic set of lines belonging to phosphorus is now present.

PTIS is very sensitive and exhibits excellent energy resolution for shallow levels. The sensitivity decreases rapidly with increasing ground state energy due mainly to the rapid decrease of the absorption cross-section and the broadening of the ground state with the increasing depth of the level. The deepest center which has been investigated successfully in germanium (using PTIS) is the acceptor level created by substitutional copper at E_V + 43 meV [38]. Excellent sensitivity and high resolution have made PTIS the preferred technique for many investigations including impurity analysis [1,39,40, 41,42], uniaxial stress studies [43,44,45,46], impurities in a magnetic field [47] and the temperature dependence of the intensity of PTIS lines [48]. Because we will rely very strongly on PTIS results in later sections, we would like to conclude this section by pointing out that "hydrogenic" relates only to the excited state spectrum of a neutral acceptor or donor. It does not refer to the composition of any impurity complex, many of which do contain hydrogen!

3.3 Deep Level Transient Spectroscopy

Deep Level Transient Spectroscopy (DLTS) has been used recently in many semiconductor studies and excellent reviews of the method have appeared [49].

Its application to study deep levels in thick diodes made from ultra-pure germanium is obvious and in principle, rather simple [50]. The reverse bias applied to a partially depleted diode is repetitively reduced by a square pulse to a lower value. During the application of the pulse the depletion layer width decreases and the capacity increases accordingly. If deep majority levels are present they can be neutralized in the temporarily undepleted section of the diode. After the bias has returned to its pre-pulse value these deep levels release their charge with a characteristic time constant τ :

$$\tau = cT^{-2} \exp\ (-\ \Delta E/kT) \tag{3.5}$$

ΔE is the energy difference between the nearest bandedge and the deep level (meV), T is the absolute temperature (K) and k is the Boltzmann constant (= 0.0863 meV K^{-1}). The constant C is composed of the capture cross section of the deep level, the thermal velocity of the free majority carriers and the concentration of the latter. The depletion layer width will be larger directly after the reapplication of the full bias because the deep levels have been neutralized. The capacity of the diode will be correspondingly smaller than the pre-pulse value and will return with the characteristic time constant τ of the deep levels to the quiescent value. Where multiple deep levels are present the decay time constants will mix together. However, it is most convenient to select to measure the amplitude of a single time constant-component at one time and to scan the temperature of the sample. Each level will then release its charge at its own particular temperature. One way to select a certain time constant is shown in Figure 9. The capacity of the partially depleted diode is measured with a one megahertz bridge (Capacitance DLTS). The bias is applied through one leg, the pulse temporarily reducing the bias through the other leg of the bridge.

A Miller correlator [51] with appropriate base line restoring and switching transient suppressing circuits multiplies the capacitive transient signal with an internally created exponentially decaying voltage. The output of the correlator is a maximum when the two time constants are identical. Various other schemes using a boxcar integrator [52] or a lock-in amplifier [53] have been successfully applied to this problem. The temperature of the diode is slowly changed between 10 and 300K using a closed cycle helium refrigerator. The spectra in Figures 10 and 11 are typical result obtained with ultra-pure germanium diodes. The crystal used for the spectrum in Figure 10 was grown in a hydrogen atmosphere and contained copper which was introduced on purpose using thermal diffusion from the surface into a crystal slice. The various deep levels are due to the multiple acceptor level produced by substitutional copper and to several copper-hydrogen complexes (see sections 4.4.5). The diodes used for nuclear radiation detection exhibit large surfaces which are not covered by contacts. Surface states on these surfaces can cause capacitive transients and appear in the DLT spectrum. Figure 11 shows spectra of the same diode with three different surface conditions.

The time constant associated with the series resistance of the undepleted region and the depletion layer capacitance limits the capabilities of this technique to observe fast transients. The purer the germanium and the thicker the diode, the longer this built-in time constant becomes for a given depletion depth. It is often necesssary to either use a capacitance bridge with lower frequency or to fabricate sample diodes specifically suited for capacitance DLTS.

3.4 High-Q Electron Paramagnetic Resonance

Electron Paramagnetic Resonance (EPR) has been used extensively for the study of donors in germanium [54]. A small crystal sample is inserted in a microwave resonance cavity. Donor electrons absorb microwave power when they are precessing in an external magnetic field in resonance with the microwave frequency. The power absorption or more commonly its derivative is observed by measuring the amplitude of the microwaves reflected back from the cavity. The hyperfine interaction between the donor electron spin and the nuclear spin of the donor impurity produces multiple resonances. In general, the spin Hamiltonians of group V donor nuclei are isotropic leading to EPR spectra which are crystal-orientation independent. The lithium-oxygen donor D(Li,O) is an exception and will be described in section 4.4.3. The sensitivity of EPR can be increased substantially if ultra-pure germanium is used as a low loss (high Q) dielectric cavity. The high dielectric constant ($\epsilon_{Ge} = 16$) increases the energy density and the small concentration of impurities leads to very small losses. Q-factors close to 10^6 have been observed [43]. Figure 12 shows a typical resonance mode of an ultra-pure germanium cylinder inside a TE 011 cavity as shown in Figure 13. The particular mode is completely insensitive to the position of the tuning plunger and to mechanical vibrations. As little as 10^{11} shallow donors have been observed with a signal to noise ratio greater than unity at an integrating time constant of 1 second. This sensitivity extends the EPR technique toward the range of impurity concentrations typical for ultra-pure germanium.

4. Point and Line Defects

4.1 Elemental Impurities of the Third and Fifth Group

The elemental impurities of the third and fifth group of the periodic table are probably the most thoroughly studied point defects. Their technical importance in the development of the transistor and other electronic devices led to the accumulation of a vast amount of experimental and theoretical knowledge of most aspects of these impurities. Despite this, the advent of high purity germanium has provided a tool to study previously unobserved properties. As pointed out in section 3.2, the shallow-level impurities are described accurately with the hydrogenic model [33] and the wave functions of the highly excited states reach so far into the crystal that overlap of these states occurs at impurity concentrations as low as $\sim 10^{12} cm^{-3}$. Ultra-pure germanium is unique in permitting observation of the undisturbed, hydrogenic bound states up to high quantum numbers. An example of PTIS of a germanium sample containing mostly aluminum as an impurity is shown in Figure 7.

The experimental results observed in this work have stimulated extensive theoretical treatment of hydrogenic excited states of shallow levels in germanium and silicon [2]. The level assignments of the acceptor states in Table 1 are taken from recent theoretical work by Baldereschi and Lipari. The energy differences between equivalent excited states are identical for different acceptors and donors. This shows that the influence of the impurity core on the p-like bound excited states is negligible.

An uncertainty exists in the accurate determination of the ground state energy of shallow acceptors. The very early infrared absorption studies of Jones and Fisher [34] indicated that an energy of 2.53 meV has to be added to the energy of the D-transition (Γ_8) in order to obtain the ground state energy. This has recently been supported by studies of the dependence of the intensities of lines on temperature in PTIS studies [47,48]. Theoretical calculations stand in contrast to this result [2] and they indicate that a larger gap of 2.88 meV should exist between the top of the valence band and the Γ_8-state. Band tailing and overlap of very highly excited states may explain the difference between theory and experiment.

The high resolution PTI spectra of elemental impurity levels obtained in ultra-pure germanium are most important in the development of purification techniques and crystal growth. The identification of the residual chemical impurities is unambiguous and using the ratio of corresponding lines and the net-concentration obtained by Hall effect measurements, it is possible to determine both the concentration and identity of the impurity. Table 1 contains transition energies and the ground state energy of several elemental acceptors which have been studied with Photothermal Ionization Spectroscopy in ultra-pure germanium crystals.

4.2 Deep Impurities

Impurities producing deep levels, or simply deep impurities, are not as well known and understood as shallow impurities, either experimentally or

theoretically. Since nearly all electronic devices* demand low concentrations of deep traps, every effort has been made to remove, rather than understand such impurities. Also, an accurate theoretical description of deep impurities, depends on detailed knowledge of the impurity core--the region close to the impurity atom. Since this information is extremely difficult to obtain, the theory of deep levels has received little attention until recently [55].

Practical detector applications of ultra-pure germanium also demand the lowest possible concentration of deep levels so every effort is made to remove deep impurities. This task is relatively easy because of the low solubility and small segregation coefficient of most deep impurities. Despite this favorable situation for purification, several deep acceptors have been studied in ultra-pure germanium.

For example, Photothermal Ionization spectra of neutral beryllium, a double acceptor, have been reported [39]. The most striking feature is that the bound excited state spectrum is perfectly hydrogenic, and is identical to shallow acceptor spectra as shown in Figure 14. This observation indicates the short range character of the lattice disturbance caused by the substitutional beryllium atom. The ground state energy derived from the spectrum is $E_{gs} = E_V + 24.42$ meV (see Table 1). Figure 14 also shows the PTI spectrum of neutral zinc, another double acceptor with a perfectly

*Exceptions are devices which rely on short free-carrier lifetimes (e.g., switching diodes).

hydrogenic spectrum which yields $E_{gs} = E_V + 32.66$ meV (see Table 1). Considerable theoretical interest exists in the spectra of singly-ionized double acceptors. No such PTI spectra have been reported so far. Such results could clarify the situation of the spectral C-line assignment. At the present time it seems that this line is probably due to the transition from the ground state to two bound excited states ($1\ \Gamma_7^-$ and $3\ \Gamma_8^-$) which are accidentally almost degenerate.

The third elemental deep impurity which we will discuss is copper. Hall and Racette have studied this impurity in doped and moderately pure germanium [56]. They determined the ratio of interstitial to substitutional copper as a function of the type and concentration of the shallow impurity background. On the basis of early ion-drift experiments in an electric field at temperatures close to the melting point of germanium, it was concluded that interstitial copper is a positive ion and should be a donor [57]. No donor level in the bandgap has been experimentally observed and we have found no indication of such a level in ultra-pure germanium. We conclude that interstitial copper is a deep donor with its energy level inside the valence band. Substitutional copper has three acceptor levels in the bandgap. If copper is present in sufficiently high concentrations ($\sim 10^{12} cm^{-3}$), it can be observed with PTIS. The ground state energy of neutral copper has been deduced from its hydrogenic spectrum. It is $E_{gs} = E_V + 42.88$ meV (see Table 1). Also, from the analysis of DLT spectra, one finds for the lowest level of copper, $E_{gs} = E_V + 44$ meV (see Figure 10).

Using the commonly accepted degeneracy factor for single acceptors $g = 4$, our Hall effect measurements of ultra-pure germanium samples containing copper, yield a value $E_{gs} = E_V + 44$ meV. The excellent agreement

between these results indicates that the ground state of copper is of a rather uncomplicated nature leading to the same value for optical, dynamic and static thermal ionization measurements.

The second level of copper at ~ E_V + 330 meV cannot be investigated by PTIS. Large concentrations are necessary to obtain precise values for this level with Hall effect measurements because it lies very close to the middle of the bandgap. Only DLTS measurements have the sensitivity and energy resolution needed to determine accurate values. A thermal emission rate $e = 6.1 \times 10^8 (K^{-2} s^{-1}) T^2 \exp(-0.310\ eV/kT)$ has been reported [50].

Because copper is easily introduced in its interstitial form into a germanium crystal at low temperature by accident we are interested in determining its solubility in ultra-pure germanium. The crystals used were grown under various conditions and showed different concentrations of the dislocation etch pit density. The Cu solubility results obtained indicate that the solubility (substitutional) is extremely sensitive to crystal parameters such as dislocation density. This finding has never been reported in the literature. Table 2 summarizes the crystal parameters and the concentration of the E_V + 44 meV level in six different samples which were saturated at 400°C under an inert gas atmosphere with copper. Of course, all the crystals studied were intrinsic at the Cu diffusion temperature. The samples were rapidly quenched and Hall effect measurements were made over the range from room temperature to ~ 10K. Despite the preliminary nature of the results reported in Table 2, we can conclude that the presence of hydrogen increases the concentration of the substitutional copper species and that oxygen seems to counteract the effect of hydrogen. The highest concentration

of substitutional copper is found in hydrogen-grown, dislocation-free crystals. Such crystals are known to contain vacancy and hydrogen-related complexes (see 4.4.4) which seem to be a source of the vacancies that enhance copper solubility. We have no explanation for the undetectably low copper concentration in nitrogen-grown, dislocation-free crystals; despite several attempts, we have never observed the $E_V + 44$ meV level in these crystals.

4.3 Neutral Impurities

Little attention has been given to neutral impurities in semiconductors. This is natural since neutral impurities do not directly affect the properties that are important in electronic devices. Interest is now growing because hydrogen has been found to play a very important role in the physics of amorphous silicon. This work postdates by several years that on ultra-pure germanium where hydrogen had been found to influence the acceptor and donor concentrations. More recent work has shown that a large family of electrically active complexes containing hydrogen together with other impurities and point defects exist. They will be discussed in a separate section (4.4.1--4.4.5). Here we will discuss a few neutral elemental impurities which are known to exist in ultra-pure germanium.

Hydrogen is found in almost all metals and semiconductors because of its small atomic size. The most complete study of hydrogen in germanium is that of Frank and Thomas [17]. They carried out time resolved permeation studies which yielded the diffusion coefficient D and the solubility S of hydrogen between 800°C and 910°C:

$$D = 2.7 \times 10^{-3} \exp(-\frac{0.38eV}{kT}) \; (cm^2 s^{-1}) \tag{4.1}$$

The solubility in hydrogen at 1 atmosphere is:

$$S = 1.6 \times 10^{24} \exp(-\frac{2.3eV}{kT}) \; (cm^{-3}) \tag{4.2}$$

The solubility is proportional to the square root of the partial hydrogen pressure p. At the melting point of germanium (935°C) the solid solubility lies between 10^{14} and $10^{15} cm^{-3}$ at 1 atmosphere of pressure. An accurate value is difficult to obtain and it is not clear if the hydrogen solubility is retro-grade as are the solubilities of many elemental impurities [58]. We assume that a large fraction of the hydrogen dissolved near the melting point is trapped in our crystals during growth leading to a hydrogen supersaturation. Direct evidence for hydrogen precipitation is seen in Figure 15. The chemically etched (100) surface of a partially dislocated crystal is shown. The dislocated section exhibits etch pits only related to dislocations. The dislocation-free section is covered with smooth shallow pits which are present only in crystals grown in a hydrogen atmosphere and always in these crystals. We conclude that these smooth pits are due to hydrogen precipitates. In dislocated crystals or parts of crystals hydrogen presumably precipitates at the dislocations and does not result in the smooth etch pits. In our crystals the size and concentration of the hydrogen-related smooth pits vary along the crystal growth axis. The pits are larger and less abundant ($<100\ cm^{-2}$) near the seed end than near the tail end ($>1000\ cm^{-2}$). We assume that this is due to our particular crystal puller in which the seed end cools more slowly than the tail end, thereby permitting the out-diffusion of some hydrogen and also giving more time for the formation of large precipitates.

Extrapolation of equation (4.2) down to room temperature indicates virtually zero hydrogen solubility. As we will show in the sections on impurity complexes (4.4.1--4.4.5), hydrogen concentrations larger than $\sim 10^{12} cm^{-3}$ must be present in our crystals grown in a hydrogen atmosphere. It is interesting to consider the form and location of hydrogen in the lattice. Several sites which hydrogen occupies have recently been discovered. All these sites are interstitial and are near a substitutional or interstitial impurity so they must be considered as complexes. Since only those complexes that are electrically active can be investigated with high sensitivity, neutral complexes must be present at high concentrations in order to be directly observable. They are therefore not generally observed. Molecular hydrogen has been suggested as a low temperature form of hydrogen in semiconductors and recent measurements of the diffusion coefficient of hydrogen at 400°C indicate mechanisms such as complexing, molecule formation or trapping [59]. They yield a value more than two orders of magnitude smaller than the value that is obtained by extrapolation from high temperatures (Eq. 4.1).

From the careful analysis of hundreds of germanium crystals grown in a hydrogen atmosphere, we conclude that any acceptor site or strain center has the potential to attract and trap hydrogen. Details of the forces which bind the hydrogen atoms to certain sites are not well understood. A simplistic view which is consistent with most of the experimental observations is that hydrogen donates its electron to electron-deficient sites thereby leading to a higher degree of lattice perfection. The recent developments regarding hydrogen in high-purity germanium are of great interest in impurity physics and will bear on the work on hydrogenated amorphous silicon [60].

Oxygen is another impurity which is electrically inactive in silicon and germanium at low concentrations. An oxygen site which can be observed (at moderately high concentrations) by IR-absorption is the bond-centered interstitial position in which the oxygen atom is located somewhat off the direct line between the two neighboring germanium atoms [61]. Other oxygen sites that have been studied include, as in the case of hydrogen, association with impurities and point defects. For example, the lithium-oxygen complex produces a shallow donor level that will be discussed in section 4.4.3. The formation of this complex is the key to the very sensitive lithium precipitation technique which is discussed in section 3.1 [19].

Due to its tendency to bond to two neighboring germanium atoms, oxygen diffuses much more slowly than typical interstitial impurities. It therefore behaves primarily as the stationary impurity in complex formation. Knowledge of oxygen is still very incomplete and studies using ultra-pure germanium should do much to elucidate details of oxygen behavior in semiconductors.

Silicon is another impurity of considerable interest in high-purity germanium. In its substitutional position, a silicon atom replaces a germanium atom almost perfectly. Both the local strain produced by its smaller size and its greater affinity for oxygen have been found to be important in ultra-pure germanium crystals. The strain results in complex formation with hydrogen which leads to the shallow acceptor described in section 4.4.2. An observable effect of the silicon strain field is the increased line width in the photothermal ionization spectra of shallow impurities. The formation of complexes influences zone purification as described in section 2.1. It has been shown that additions of silicon to a germanium melt contained in a quartz boat suppresses "free" oxygen (see Figure 3) thereby facilitating normal segregation of aluminum [13].

Carbon is assumed to have very similar effects as silicon. Carbon is believed to form a shallow acceptor complex with hydrogen. So far no carbon has been detected in germanium. We hope that we will soon learn more about the solubility of carbon in germanium after our ^{14}C experiment has been completed (see section 3.1. and Ref [76]).

4.4 Complexes

4.4.1 General Remarks. While the effects of complex formation are almost impossible to observe directly in doped semiconductors, they become amenable to study in high purity germanium crystals. For this reason, this work has contributed much to the solid-state physical understanding of these basic mechanisms.

A general pattern of complex formation has emerged; all the observed complexes consist of a combination of an immobile component (often substitutional in the lattice) and a mobile interstitial component. The mobile light component is trapped in a potential well surrounding the fixed heavy component and it tunnels between potential minima around the well. In this model the motion of the atoms in real space has a pronounced effect on the electronic structure of the ground state [45]. One of the important changes is the symmetry of the electronic wave function of such complexes as compared with substitutional elemental impurities. The mixing of the real space positions of the tunneling atom with the conduction band valleys (in the case of donors) or the top of the valence band (in the case of acceptors), leads to increased multiplicity of the ground-state manifold of the complex centers. Depending on the splitting of the various components

of the ground-state manifold, rather complicated absorption spectra consisting of several hydrogenic sets of lines are obtained. The strengths of corresponding lines in the various spectral sets indicate the relative populations of the particular ground-state manifold components. These populations would be expected to depend strongly on temperature and the experimentally observed temperature dependence is a strong argument supporting the validity of our model. More subtle effects caused by the tunneling vary from one kind of a complex to another and they will be discussed in the corresponding sections.

4.4.2 Hydrogen-Related Acceptors and Donors: A(H,Si), A(H,C), D(H,O). R. N. Hall [62] discovered that a shallow accepter level was created by heating high-purity germanium crystals to 700K and rapidly quenching to room temperature. Annealing to slightly above room temperature removes the acceptors and a shallow donor level appears. Isochronal annealing experiments show that the donor totally disappears when the crystal is heated to 420K and the sample appeared to be in its original state; in fact, the whole process could be repeated. Typical isochronal annealing curves for this case are shown in Figure 16A. These were measured on a sample cut from the tail end of a high-purity germanium crystal grown using the normal process discussed earlier (quartz crucible, hydrogen atmosphere). Based on this work, Hall proposed that the donor and acceptor levels were related and were due to a defect site containing oxygen.

Since then it has become evident that only germanium crystals grown in a hydrogen atmosphere from a melt contained in quartz show the so called "fast" acceptors and donors, and therefore, it was proposed that hydrogen was

involved in the formation of these centers. This was subsequently pı the PTIS measurement (see Figure 17) of an isotope shift in the groun of the "fast" acceptor as well as the "fast" donor in crystals grown in a deuterium atmosphere compared with those grown in a hydrogen atmosphere [63]. By growing crystals in a mixture of deuterium and hydrogen and performing the PTIS measurements shown in Figure 18, we were able to establish that only a single hydrogen atom is involved in the complex [64]. If two hydrogen atoms were incorporated in a complex, three combinations would be possible: two hydrogen atoms, one hydrogen and one deuterium atom or two deuterium atoms. This would lead to three sets of hydrogenic lines. In fact, only two sets of lines are observed corresponding to either hydrogen or deuterium atom in the complex.

Experiments using silicon doping have revealed the importance of this element in the formation of the "fast" centers [13]. In silicon-rich crystals the conversion from the acceptor to the donor is suppressed as shown in Figure 16B. The acceptor anneals out at about 350K. Such crystals also exhibit very low concentration of free oxygen as determined by the lithium precipitation technique (see section 4.3 and Figure 3). These experimental findings suggest the following interpretation. Since silicon-free crystals such as those grown in graphite crucibles did not exhibit the "fast" acceptor, it is clear that silicon plays a crucial role in formation of this acceptor. Crystals grown in quartz crucibles and silicon-doped crystals show the acceptor. Therefore it is reasonable to conclude that the "fast" acceptor consists of hydrogen and silicon, now identified by the nomenclature A(H,Si), also called A_1 and A_3 in early papers [1]. The donor, on the other hand, needs the presence of hydrogen as well as <u>free</u> oxygen. It is therefore believed to be a hydrogen-oxygen complex D(H,O). Crystals

grown in graphite also exhibit a quench-in acceptor similar to A(H,Si) which we designate A(H,C), formerly called A_6 [1].

A further experimental result that is observed is the extremely small line widths of the hydrogen-related spectra. For example, it is very obvious that the lines of the donor D(H,O) in Figure 17 are much narrower than those of phosphorus, a substitutional donor. Uniaxial stress experiments lead to the explanation for the narrow line widths observed. The lines of D(H,O) as well as A(H,Si) and A(H,C) do not change their position under small uniaxial stress in the [111] direction which means that the ground states of these centers are stress independent. At very high stresses the lines of the acceptors split up like the corresponding excited states. This stress dependence is totally different from the one exhibited by simple substitutional acceptors [65] or donors [66] and the result shows that a different symmetry must exist in the two types.

In the case of normal shallow donors, the lower component of the ground-state manifold is a singlet which departs from the conduction band minimum quadratically under uniaxial compressional stress. In these cases, the upper ground-state manifold component splits up into a doublet and a singlet [66] and the stress dependence of the various components is shown in Figure 19. The stress behavior of the donor D(H,O) is totally different. The line positions are stress independent up to a certain stress amplitude where they suddenly reduce sharply in intensity and a new set of lines appears at lower energies indicating a new, shallower ground state (see Figure 20 and Table 3). This sudden change in ground-state energy occurs for stress in any direction and has been explained in terms of a symmetry change of the ground-state wave function from s-like (unstressed) to p-like (stressed) [46].

In the case of an elemental substitutional acceptor, a symmetric split of the fourfold degenerate ground state occurs into two doublets (Γ_{5+6}, Γ_4) under uniaxial stress parallel to <111>. This can be seen for the aluminum acceptor spectrum in Figure 21. In contrast, the lines of the complex acceptor A(H,C) do not shift under small uniaxial stress. As stress is increased all lines broaden due to the splitting of the excited state. It is clear that the ground-state component of A(H,C) observed indirectly in the hydrogenic spectrum in Figure 21 does not split under stress and is therefore of different symmetry than that of elemental substitutional impurities (Γ_8^+). The dynamic tunneling model for acceptors [45] predicts a multiplicity of sixteen for the ground-state manifold. Group-theoretical considerations lead to three quadruplets and two doublets. The doublets belong to Γ_6 or Γ_7 and do not split under stress. Being Kramers doublets, they should split in a magnetic field--a further possible test for the model which has not yet been explored. Depending on the temperature of a sample and the energy difference between the two doublets, a second set of hydrogenic lines can be observed due to transitions from the upper doublet to the excited states. For A(H,Si) this energy difference amounts to 1.07 meV (= 8.63 cm^{-1}). Between 5 and 10K, the upper doublet state is occupied during an appreciable fraction of the time according to a Boltzmann factor $\exp(\Delta E/kT)$. The intensity ratio of lines due to the upper doublet state to those due to the lower state follows precisely the Boltzmann factor as shown in Figure 22, fully supporting this model. Two typical spectra of A(H,Si) are shown in Figure 23. The splitting between the doublets is an indirect measure of the tunneling frequency of the hydrogen, yielding a rough estimate of a tunneling element of 0.8 meV (= 1.9 x 10^{11}Hz).

For the acceptor A(H,C), the energy difference between the two doublets is 1.98 meV, which is so large that the line series belonging to the upper doublet had not been observed before the dynamic tunneling model predicted its existence. When measurements were carried out at a higher temperature the upper doublet set was promptly found, as can be seen in Figure 24. As in the case of A(H,Si), the ratios of the corresponding lines in the two sets follow precisely a Boltzmann factor with $\Delta E = 1.98$ meV.

These observations have resulted in perfect agreement between theory and experiment. It is of interest to explore the possibility of observing features due to the three quadruplets. It is impossible to populate states higher than about 2 meV above the lowest lying ground-state component by continuously increasing the sample temperature since, with the very large density of states near the band minimum, direct ionization from the ground state into the valence band quickly becomes dominant resulting in a rapid decrease in the number of neutral acceptors and with this, a decrease in the photothermal signals. Theory indicates that the energy differences between the various quadruplets should be of the same order of magnitude as the splitting between the doublets. Because transitions between ground-state components produced by the absorption of photons are forbidden, they cannot produce absorption lines. Another pumping mechanism would have to be found to populate the higher-lying quadruplets in order to make them observable.

The dynamic tunneling model is also applicable to other centers found in germanium and silicon. It has been proposed that normal muonium, a positive muon (μ^+) capturing an electron is trapped at substitutionally dissolved carbon in germanium as well as in silicon, resulting in the acceptor A(Mu,C) [67]. The subsequent increase in symmetry could explain the isotropic spin Hamiltonian of normal muonium [68]. The acceptor nature, in analogy to the

A(H,C) complex, would explain why normal muonium is observed in p-type but not in n-type crystals. In n-type crystals all the acceptors stay ionized at all temperatures. The ionized $A(Mu,C)^-$ has two electrons which cancel their spins leading to a center with the pure muon spin. In other words, the $A(Mu,C)^-$ signal cannot be differentiated from the μ^+ signal. Experiments carried out with crystals with and without carbon have results in agreement with these models.

In conclusion, we would like to point out that there is no unanimous proof that the dynamic tunneling model is the only one fitting the experimental observations. However, so far it has been the only simple model which has been successfully applied to several complexes and that fits all the experimental findings: stress dependence, temperature dependence and impurity correlation.

Table 4 contains the energies for the major transitions from the ground state ($1\Gamma_8^+$) to the bound excited states of the hydrogen-related centers A(H,Si) and A(H,C) and for several still unknown centers. These unknown acceptors are most probably complexes involving electrically neutral impurities. The acceptors A_3, A_4 and A_5 always and only appear in crystals grown in a nitrogen atmosphere from a quartz crucible coated with pyrolytic graphite. This correlation suggests complexes which contain nitrogen and/or carbon. The acceptor A_7 has so far not been correlated with any parameter.

4.4.3 Lithium-Related Donors: D(Li) and D(Li,O). Lithium, disolved interstitially, produces a shallow donor D(Li) which has been known for a long time [69]. It has found wide practical use because lithium can be diffused and drifted into germanium as well as silicon at conveniently low temperatures (<500K). It can compensate acceptors in large volumes using

the lithium-ion drift process [5]. Both lithium diffusion and drifting are strongly influenced by the presence of oxygen because of the formation of LiO complexes which are almost immobile. Early IR-transmission experiments showed that germanium samples containing lithium showed extra lines in the hydrogenic line spectrums [70]. Photothermal Ionization Spectroscopy showed that the extra lines exhibited extraordinarily small widths and that they formed their own complete set of hydrogenic lines [43]. The set was assigned to a donor S (for sharp!) and it was speculated that it was due to the LiO complex [41,42]. Later work suggested that both spectra observed in lithium-doped germanium belong to LiO_x complexes [71].

We have now undertaken a careful study with a large number of ultra-pure germanium crystals exhibiting low ($<10^{13}cm^{-3}$) and high ($>10^{14}cm^{-3}$) oxygen concentrations. The first important finding is that the sharp line set S is insensitive to externally applied uniaxial stresses exactly as described in the previous section for D(H,O). Careful examination of the spectra revealed that two sets of very broad lines at lower energies were associated with the same donor. They converged into two sharp sets of lines at higher stress. None of these lines belong to the simple lithium donor as can be seen from Figure 25. The upper spectrum was obtained with an oxygen-rich crystal in which practically all the lithium atoms are attached to oxygen atoms. In the lower half of the figure obtained from a sample with much less oxygen, we observe an extra set of lines due to free lithium. Looking at the unstressed spectra (Figure 26), the confusion in the interpretation of early experiments is easy to understand. The D(Li) lines almost coincide with the broad line sets of D(Li,O) and could not be resolved from them in these experiments. These piezospectroscopy studies show that the ground state of D(Li,O) must be a complicated manifold and that the ground state of D(Li) does not exhibit a measurable chemical split.

Further experimental evidence was obtained from High Q Electron Paramagnetic Resonance (see section 3.4). Cylinders of ultra-pure germanium doped with D(Li,O) and with their axis parallel to [$\bar{1}$10] were mounted in a TE011 cavity of a 25 GHz heterodyne EPR spectrometer. The derivative of a typical absorption signal with the $\vec{B}$-field direction close to the [001] direction is shown in Figure 27. All the lines are observed to move as the angle θ between $\vec{B}$ and the [001] direction is changed. In Figure 28 the g values are plotted in function of Θ. The plot can be explained with single valley donors aligned in the <111> direction.

How can these data be interpreted? It was the LiO donor study which first suggested the dynamic tunneling model for a donor complex. Mixing of the four real space positions along <111> together with the four conduction band minima produces a 16-fold ground-state manifold [43]. The splitting at zero stress and at high stress together with the observed line intensity ratios seriously restrict the choice of the free parameters. The diagonalization of the 16 x 16 ground-state matrix can be performed analytically and the tunneling element t is found to be of the order of ~28μeV corresponding to a tunneling frequency of 6.8 GHz. The single-valley electron nature of the EPR spectra is explained by the fact that this is much smaller than the EPR frequency so the electron appears to be located in one valley during a typical resonance event. The changes in the ground-state manifold under stress in the [111] direction is shown in Figure 29. The minute bend in the lowest lying ground-state component leading to a shift of about 1 μeV cannot be detected. The lines due to this state remain unchanged under stress thereby explaining the exceptionally narrow hydrogenic line set. The two broad line sets are caused by two clusters of ground-state components which are split and shifted by random minute stresses in the crystal superimposed

on any external applied stress. As stated in the last section, there is no absolute proof that the dynamic tunneling model is correct but it is certainly very successful in explaining all the observed phenomena. The line positions for the Li and LiO donors are presented in Table 5. The very small ground-state shift of D(Li) with the opposite sign of substitutional donors indicates that there is virtually no valley-orbit splitting.

4.4.4 Divacany-Hydrogen Acceptor $A(V_2H)$. During the discussion in section 4.3 of hydrogen being one of the important neutral impurities, we used Figure 15 to show that hydrogen precipitation takes place in dislocation-free crystals. As illustrated in Figure 2, an acceptor at a level $E_V + .072$ eV is associated with dislocation-free material. The concentration of this acceptor is found to directly depend on the annealing temperature. Increasing the annealing temperature of a crystal sample leads rapidly to a new higher concentration while reducing the temperature to a new lower value leads only slowly to a new correspondingly lower concentration. This behavior is typical of a dissociation-recombination process. The proposed reaction can be described in the following way:

$$V_2H + H \underset{\text{dissoc.}}{\overset{\text{recomb.}}{\rightleftarrows}} V_2H_2 \quad . \qquad (4.3)$$

The V_2H complex is assumed to be the observed acceptor while H and V_2H_2 are neutral defect species. A quantitative model for the annealing kinetics has been developed [18]. The symmetry and the microscopic structure of the V_2H center, however, are not yet understood. The center is just beyond the reach of the high-resolution Photothermal Ionization Spectroscopy so that neither isotope shifts nor stress experiments can be used to explore its composition and symmetry.

The steady state concentration of the divacancy-hydrogen acceptor is plotted as a function of the inverse (annealing) temperature in Figure 30. Heating small Ge samples beyond 400°C leads to an irreversible reduction in the divacancy-hydrogen acceptor concentration presumably due to the dissociation of V_2H and outdiffusion of hydrogen. The slope of the equilibrium concentration curve in Figure 30 corresponds to an activation energy of ~0.7 eV. This value is composed of several physical quantities and cannot therefore be readily used for further interpretation of the proposed model.

Results of radiation damage studies in germanium doped with group V elements and lithium have been interpreted with divacancy-donor (V_2D) models [72]. There exists a clear tendency for the acceptor level associated with such complexes to become shallower for lighter donor atoms. The V_2H complex is about 30 meV shallower than the V_2Li complex—in agreement with the experimentally established trend. Recent radiation damage experiments with dislocated, high-purity germanium crystals grown in a hydrogen atmosphere further support the V_2H model insofar as they have shown that the acceptor level assigned to V_2H can be created in such crystals by irradiation with 1 MeV gamma rays [73].

4.4.5 Copper-Related Acceptors A(H,Li,Cu). The acceptor levels associated with substitutional copper have been discussed in section 4.2. We pointed out that copper is a very complicated case of an impurity because it exists in two forms—interstitially and substitutionally. The large differences in solubility suggest that copper will be involved in many interactions. Indeed, complex formations between copper and hydrogen and lithium have been identified and there will certainly be further complexes consisting of copper and other impurities and/or defects. For example, a clear candidate would be a CuO complex.

No fully quantitative studies of copper complex formation have been carried out. All early experiments concentrated on analysis of the composition and on energy levels. The complexity of the system means that a full study of all parameters is not likely to be justified. The first pair of hydrogenic sets of lines correlated with copper and hydrogen are shown in the photothermal ionization spectrum in Figure 31. [74]. It is not clear whether the two sets of lines belong to one acceptor with a split ground state [in analogy to the A(H,Si) and A(H,C) acceptors] or indeed if two different acceptors are present. A simple uniaxial stress experiment could answer this question. Hall effect measurements and deep level transient spectroscopy on identical samples showed that there are at least two deep acceptor levels associated with copper-hydrogen complexes. Figure 32 shows Hall results on such a sample. The levels due to complexes at E_V + 80 meV and E_V + 175 meV are all found in the DLT spectrum in Figure 10.

By diffusing lithium into copper-containing samples, further acceptors can be created which are associated with copper-lithium complexes [74]. Figure 33 shows the PTI spectrum of all known semi-shallow, copper- and lithium-related levels. The spectra are perfectly hydrogenic as can be seen from the comparison with the Al spectrum. Hall effect measurements of a copper and lithium-containing sample are shown in Figure 34. Deep levels different from the copper- and hydrogen-containing samples appear at E_V + 100 meV and E_V + 270 meV.

Some clear trends become evident in other copper-related complexes which have been seen. The hydrogen-containing complexes produce shallower energy levels than the lithium-containing complexes which in turn are shallower than the energy levels of the bare substitutional copper. These trends can be understood from a slightly simplistic but nevertheless attractive point of view which sees hydrogen and lithium as interstitial impurities which can

donate their electron to electron-deficient sites (acceptors) thereby reducing the mismatch between the host lattice and the point defect. Hydrogen acts in this sense almost like a donor in forming pairs with acceptors. As a very deep donor, hydrogen can be present in the crystal at large concentrations without influencing electrical measurements; on the other hand lithium, as a shallow donor, changes the electrical properties of the crystal very much.

4.5 Dislocations

Dislocations have played an important role both in the development and in many of the applications of ultra-pure germanium single crystals. Dislocations can act as nucleation centers for excess hydrogen or sinks for vacancies; conversely, the total absence of dislocations leads to precipitates in hydrogen-atmosphere-grown crystals (see Figure 15) and to the formation of the divacancy-hydrogen complex (see section 4.4.4). Both these centers are detrimental to perfect charge collection over large distances (cm), a prerequisite for high quality nuclear radiation detectors. For such applications, a dislocation density in the range of ~100 to $1000 cm^{-2}$ is ideal. On the other hand, dislocation-free, ultra-pure germanium crystals have been very useful in the study by Jeffries *et al* [3] of large, strain-field confined electron hole drops (EHD) where such crystals exhibit EHD lifetimes ten times longer than in dislocated crystals.

Whereas a considerable amount of detailed knowledge on the mechanical properties of dislocations exists, there is still very little detailed understanding of the electronic phenomena introduced in crystals by dislocations. Furthermore, the interaction between impurities and dislocations is

a subject that must receive more attention. We are confident that the interaction between substitutional impurities leading to shallow levels (group III and group V elements) and dislocations in ultra-pure germanium must be negligible. Proof of this is evident in Figure 2 where besides the appearance of an acceptor level at $E_V + 0.072$ eV in the dislocation-free part of the crystal (which we attribute to a divancancy complex), no differences can be detected in the shallow level concentrations in the dislocation-free and in the dislocated areas of the crystal. Measurements on a very large number of crystals (p- and n-type) support this assumption. Interstitial impurities which diffuse over large distances at temperatures slightly above room temperature might possibly have a much larger influence on the mechanical and electrical properties of dislocations. It is reasonable to assume that hydrogen plays the most important role as the most abundant neutral interstitial impurity. Evidence for this is obtained from DLTS and Hall effect studies of dislocated crystals grown in a hydrogen and a nitrogen atmosphere where a broad acceptor band appears in both types of crystals but it is shallower in the hydrogen-containing crystal. This observation is analogous to the shift of deep acceptors towards the valence band when they form complexes with hydrogen.

Experiments with dislocations in ultra-pure germanium have so far been rather qualitative. However, this will probably change because the pure germanium crystals give us, for the first time, a chance to observe very subtle effects due to a small number of dislocations. This is in contrast with the rather violent artificial introduction of large numbers of dislocations using bending and twisting of single crystals--a technique that has been employed in earlier studies of dislocations.

5. Summary and Conclusions

The reduction in the concentration of electrically active impurities in large, ultra-pure germanium single crystals to the $10^{10}cm^{-3}$ range (about two orders of magnitude purer than earlier materials) has produced a wealth of new results in the physics and chemistry of semiconductors and has led to the development of new measurement techniques. The discovery and subsequent investigation of unknown shallow levels has led to the recognition of the importance of neutral impurities. Such impurities (hydrogen, oxygen, silicon and carbon) can form complexes themselves and together with electrically active impurities to produce shallow acceptors and donors which exhibit novel ground-state manifold structures. Studies of these complexes have resulted in the model whereby tunneling of a light, interstitial impurity occurs in the vicinity of a heavy impurity. With this model, the old lithium and lithium-oxygen donor problem has finally been resolved.

For all of these investigations, a high resolution technique was necessary and Photothermal Ionization Spectroscopy with and without uniaxial stress has proved to be the most powerful tool. It combines the sensitivity of an electrical measurement with the high resolution of an optical spectroscopy. Fourier Transform Spectroscopy increases the ease and reduces the time it takes to record high resolution spectra by several orders of magnitude compared with conventional grating instruments. High Q Electron Paramagnetic Resonance using an ultra-pure semiconductor as the cavity has proven a very useful additional tool. By shaping the sample into a large cylindrical resonant cavity the sample volume can be made large and the technique can be sensitive to small impurity concentrations.

It is important to recognize that it appears at the present time that

impurity complexes involving mainly neutral impurities are limiting the shallow and deep level concentrations. Any further attempts to improve the purity must concentrate on the reduction of these neutral impurities in parallel with the standard group III and V elemental acceptors and donors. The most important of the neutral impurities seems to be hydrogen. Hydrogen is, in its atomic form, very mobile and it forms bonds with a large variety of electron-deficient sites (shallow and deep acceptors, line defects etc.). The importance of hydrogen in amorphous semiconductors has been recognized for a long time and we foresee that the understanding of the role of hydrogen in crystalline and amorphous materials will profit from each other.

Due to our specific involvement with ultra-pure germanium, we have concentrated on impurity-related questions. There are, of course, many other fields in which ultra-pure germanium has been found to be useful. We have briefly mentioned electron-hole drop studies. Photoluminescence and exciton studies, radiation damage, ion implantation and annealing (thermal, laser and electron beam), far infrared photoconductors, low-temperature-operated field effect transistors, X-ray transmission and muon spin resonance have all made use of these well-characterized crystals.

The need for a nuclear radiation detector material which is stable at room temperature has led to an exciting new material. Only the combined application of physics, chemistry and material science has brought about the degree of understanding indicated in this chapter.

6. Acknowledgment

We are indebted to P.L. Richards for the extensive use of his infra-red facilities and his continuing interest and advice. Many of our colleagues and collaborators have aided in furthering the understanding of ultra-pure germanium. Without the help of L.M. Falicov, G.S. Hubbard, B. Joos and A. Seeger we could not have adanced to the point at which we are today.

FIGURES

Number

1 Net-shallow level concentration $|N_A - N_D|$ along the growth axis of an ultra-pure germanium single crystal. At the seed end (0% of melt frozen) the aluminum acceptor dominates, yielding the crystal p-type. Near the tail end the phosphorus concentration exceeds the aluminum concentration, $|N_A - N_D|$: continuous curve; aluminum concentration: dashed curve; phosphorus concentration: dotted curve.

2 Arrhenius plot of the free hole concentration p (log p versus 1000/T). The dislocation-free sample contains an acceptor level at E_V + 72 meV.

3 Decay of the donor concentration in function of time in a lithium saturated sample. The end values correspond to the LiO donor concentration. The four decay curves are discussed in the text.

4 The two-step absorption process which leads to Photothermal Ionization.

5 A) Schematic of a Michelson Interferometer as it is used in Far Infrared Spectroscopy.
B) Helium dewar with insert. The numbers are referred to in the text.

6 Cosine part of the Photoconductivity Interferogram of an ultra-pure germanium sample containing mainly aluminum as the residual acceptor impurity. The beat character is caused by two strong lines (C and D).

7 Fourier Transform Spectrum of the Interferogram shown in Figure 6. The assignment of the lines is according to Reference [34]. Aluminum (Al) is the dominant acceptor. The hydrogenic sets of lines due to boron (B) and gallium (Ga) are also present.

8 Spectrum of the same crystal as used for Figures 6 and 7 but under band-edge light illumination. The minority levels are populated and lead to negative lines (P = phosphorus).

9 Schematic of a Deep Level Transient Spectrometer (capacity mode) using a Miller Correlator as the filter network.

10 DLT spectrum of a ultra-pure germanium diode which contains copper and copper-hydrogen acceptor levels. The correlator time constant was 3 ms.

11 DLT spectra of one diode with different surface conditions.

12 Resonance mode excited in a dielectric Ge cavity with $Q \sim 5 \times 10^5$. The klystron frequency is 23 GHz.

13 Schematic drawing of the cavity containing the large germanium single crystal sample acting as a dielectric cavity.

14 Photothermal Ionization Spectra of three neutral deep acceptors and the shallow acceptor aluminum. The X-axis scale is identical for all four spectra but the origin is shifted so that the corresponding lines do line up.

15 Preferentially etched (100) surface of a partially dislocated hydrogen-atmosphere-grown germanium crystal. A high density of precipitates causes the small pits in the dislocation-free area. The large etch pits are due to dislocations.

16 Isochronal annealing curves for rapidly quenched germanium samples. A = standard crystal; B = crystal doped with [Si] = $3 \times 10^{17} cm^{-3}$. The donor formation is fully suppressed in the silicon-doped crystal.

17 PTI spectra of two rapidly quenched Ge samples, one cut from a crystal grown in a hydrogen atmosphere, the other from a crystal grown in a deuterium atmosphere. The donors D(H,O) and D(D,O) exhibit an isotope shift of ΔE_{gs} = 51 μeV in their ground state. The acceptors A(H,Si) and A(D,Si) show an isotope shift of ΔE_{gs} = 21 μeV.

18 PTI spectra of samples from three crystals grown in pure hydrogen, pure deuterium and a 1:1 mixture of the two gases. The mixed gas grown crystal only shows two line series indicating that only one hydrogen or deuterium atom is part of the donor complex.

19 Evolution of the ground and excited states of the phosphorus donor in germanium under [111] uniaxial compression. The asymptote (dash-dot) to the singlet ground state cuts the Y-axis at precisely 3Δ above the ground state at zero stress.

20 Three PTI spectra of a sample containing phosphorus (P) and the hydrogen-oxygen donor complex (D) at different [111] uniaxial compressional stress values.

21 Spectra of a p-type Ge sample containing the elemental acceptors Al, B, Ga and the acceptor complex A(H,C). The line splitting of the elemental acceptors is due mainly to the ground state splitting under [111] uniaxial compression. The lines of A(H,C) do not split indicating a ground state symmetry different from elemental acceptors.

22 The ratio of the intensities of the C lines in the two series of A(H,Si) (circles) and the D lines in the same series (plus signs) are proportional to a Boltzmann factor exp (1.07 meV/kT). The ratio of the sum of the intensities of the C lines of A(H,Si) to the intensity of the aluminum acceptor C line is temperature independent (squares). The same holds for the D lines (x's).

23 PTI spectra recorded at two temperatures of a sample containing the acceptor complex A(H,Si).

24 PTI spectra recorded at two temperatures of a sample containing the acceptor complex A(H,C).

25 PTI of two samples containing lithium-oxygen and lithium donors. The uniaxial compression separates the Li and the LiO-lines.

26 Spectra of the same two samples used in Figure 25 but at zero stress. The Li and LiO lines mixed together.

27 Derivative of an EPR absorption spectrum of a sample containing LiO donor complexes.

28 The g factors of the LiO donor complex indicate single-valley electrons.

29 Evolution of the LiO donor complex ground state manifold in function of [111] uniaxial compression.

30 Steady state concentration of the V_2H acceptor at $E_V + 0.072$ eV in function of the inverse temperature.

31 PTI spectrum of a p-type sample containing two sets of hydrogenic lines due to one or two copper- and hydrogen-related centers [A(H,Cu)].

32 Hall effect measurement of the free-hole concentration versus 1000/T of a sample containing A(H,Cu). The insert shows the deep level region magnified. Curve b indicates a deep level at $E_V + 175$ meV, curve a is obtained with a sample free of deep levels.

33 PTI spectra of two acceptor complexes A(Li,Cu) and A(H,Li,Cu) aligned with the aluminum spectrum. All three spectra are perfectly hydrogenic.

34 Hall effect measurement of the free-hole concentration versus 1000/T of a sample containing A(H,Li,Cu) complexes. The region where the crystal becomes intrinsic is magnified in the insert. For comparison, curve a obtained with a deep-level-free sample is shown.

REFERENCES

[1] E. E. Haller, Izv. Akad. Nauk SSSR, Phys. Ser. 42 No. 6, 1131 (1978). [Bull. Acad. Sci. USSR Phys. Ser. 42 No. 6, 8 (1979)]. Because of translation difficulties, please request the original English version.

[2] A. Baldereschi and N. O. Lipari, Phys. Rev. B 8, 2697 (1973); Phys. Rev. B 9 1525 (1974), Proc. XIII Int. Conf. Phys. Semicond., Rome, September 1976, ed. F. G. Fumi, (North-Holland; Amsterdam, 1976) p. 595.

[3] T. M. Rice, Solid State Physic 32, 1 (1977) eds., H. Ehrenreich, F. Seitz and D. Turnbull, Academic Press, N.Y.; J. C. Hensel, T. G. Phillips and G. A. Thomas, ibid 88; C. D. Jeffries, Science 189, 955, (1975).

[4] E. E. Haller and F. S. Goulding, Handbook on Semiconductors, Vol. 4, Ch. 6C, ed. C. Hilsum, North-Holland Publ. Co. (1980) in print.

[5] E. M. Pell, J. Appl. Phys. 31, 291 (1960).

[6] R. N. Hall, "Semiconductor Materials for Gamma Ray Detectors," p. 27, Proc. of the meeting June 24, 1966 N.Y. N.Y., eds. W. L. Brown (BTL) and S. Wagner (BNL).

[7] General Electric Company R and D Center, Schenectady, New York, USA [see also: R. N. Hall and T. J. Soltys, IEEE Trans. Nucl. Sci. NS-18, No. 1, 160, (1971)] and Lawrence Berkeley Laboratory, University of California, Berkeley, California, USA. [See also W.L. Hansen, Nucl. Instr. and Meth. 94, 377 (1971)].

[8] Metallurgie Hoboken-Overpelt, Division of Chemical Products, Olen, Belgium and ORTEC Inc. EG&G, Oak Ridge Tennessee, USA.

[9] S. M. Sze and J. C. Irvin, Solid State Electr. 11, 599 (1968).

[10] W. G. Pfann, Trans. AIME 194, 747 (1957), also Metallurg. Rev. 2, 5, 29 (1957).

[11] W. G. Pfann, Zone Melting, John Wiley and Sons N.Y.-London (1966), second ed.

[12] Synthetic quartz "Suprasil", by Amersil Inc. Sayreville, N.J., USA and "Spectrosil" by Thermal American Fused Quartz Co., Montville, N.J., USA have successfully been used to purify and grow ultra-pure germanium.

[13] E. E. Haller, W. L. Hansen, G. S. Hubbard and F. S. Goulding, IEEE Trans Nucl. Sci. NS-23, No. 1, 81 (1976).

[14] L. S. Darken, Jr., IEEE Trans. Nucl. Sci. NS-26, No. 1, 324 (1979).

[15] J. Czochralski, Z. Phys. Chemie 92, 219 (1918).

[16] R. N. Hall, IEEE Trans. Nucl. Sci. NS-19, No. 3, 266 (1972).

[17] R. C. Frank and J. E. Thomas, J. Phys. Chem. Solids 16, 144 (1960).

[18] E. E. Haller, G. S. Hubbard, W. L. Hansen and A. Seeger, Inst. Phys. Conf. Ser. No. 31, 309 (1977).

[19] R. J. Fox, IEEE Trans. Nucl. Sci. NS-13, 367 (1966).

[20] G. S. Hubbard, E. E. Haller and W. L. Hansen, IEEE Trans. Nucl. Sci. NS-24, No. 1, 161 (1977).

[21] H. Miyazawa and H. Maeda, J. Phys. Soc. Jap. 15, 1924 (1960).

[22] A. C. Beer and R. K. Willardson, Phys. Rev. 110, 1286 (1958). Also, J. H. Yee, S. P. Swierkowski, G. A. Armantrout and R. Wichner, J. Appl. Phys. 45, 3949 (1974).

[23] L. J. van der Pauw, Philips Res. Repts. 13, 1 (1958).

[24] A mixture of 4:1 nitric and hydrofluoric acids was used for etching. Rinsing with electronic grade methanol was followed by blowing dry with a pure N_2-jet.

[25] K. P. Artemov, V. Z. Goldberg, I. P. Petrov, V. P. Rudakov, I. N. Serikov and V. A. Timofeev, Atomnaya Energiya, 34, 265 (1973).

[26] B. L. Cohen, C. L. Fink and J. H. Degnan, J. Appl. Phys. 43, 19 (1972). Also, S. T. Picraux, Physics Today, 42, Oct. (1977).

[27] A. J. Tavendale, private communication.

[28] M. Hansen and K. Anderko, Constitution of Binary Alloys, McGraw Hill Book Co. Inc. N.Y. Toranto, London (1958).

[29] T. M. Lifshits and F. Ya. Nad, Dokl. Akad. Nauk SSSR 162, 801 (1965); Soviet Phys. - Doklady 10, 532 (1965). For an extensive review see: Sh.M. Kogan and T. M. Lifshits, Phys. Stat. Sol. (a) 39, 11 (1977).

[30] T. M. Lifshits, N. P. Likhtman, and V. I. Sidorov, Fiz. Tekh. Poluprov. 2, 782 (1968), Soviet Physics Semiconductors 2, 652 (1968).

[31] Sh. M. Kogan and B. I. Sedunov, Fiz. tverd. Tela 8, 2382 (1966); Soviet Phys. - Solid State 8, 1898 (1967).

[32] R. A. Faulkner, Phys. Rev. 184, 713 (1969).

[33] C. Kittel and A. H. Mitchell, Phys. Rev. 96, 1488 (1954).

[34] For donors see: J. H. Reuszer and P. Fisher, Phys. Rev. 135, A1125 (1964). For acceptors: R. L. Jones and P. Fisher, J. Phys. Chem. Solids 26, 1125 (1965).

[35] Sh. M. Kogan, Fiz. Tekh. Poluprov. 7, 1231 (1973), Soviet Phys. Semicond. I, 828 (1973).

[36] R. J. Bell, Introductory Fourier Transform Spectroscopy, Academic Press, New York (1972).

[37] T. M. Lifshits, N. P. Likhtman, and V. I. Sidorov, Zh. eksper. teor. Fiz., Pisma 7, 111 (1968); Soviet. Phys. - J. exper. theor. Phys. Letters 7, 2076 (1968).

[38] N. R. Butler and P. Fisher, Bull. Am. Phys. Soc. Series II, 19 No. 1, 92 (1974).

[39] E. E. Haller and W. L. Hansen, Sol. State Commun. 15, 687 (1974); E. E. Haller and W. L. Hansen, IEEE Trans. Nucl. Sci. NS-21, 279 (1974) and E. E. Haller, W. L. Hansen and F. S. Goulding, IEEE Trans. Nucl. Sci. NS-22, 127 (1975).

[40] M. S. Skolnick, L. Eaves, R. A. Stradling, J. C. Portal and S. Askenazy, Sol. State Commun. 15, 1403 (1974).

[41] S. D. Seccombe and D. M. Korn, Sol. State Commun. 11, 1539 (1972).

[42] W. K. H. Schoenmaekers, P. Clauws, K. van den Steen, J. Broeckx and R. Henck, IEEE Trans. Nucl. Sci. NS-26, No. 1, 256 (1979) and P. Clauws, K. van den Steen, J. Broeckx and W. Schoenmaekers, Inst. Phys. Conf. Ser. 46, 218 (1979).

[43] E. E. Haller and L. M. Falicov, Phys. Rev. Lett. 41, 1192 (1978); also: Inst. Phys. Conf. Ser. 43, 1039 (1979).

[44] A. G. Kazanskii, P. L. Richards and E. E. Haller, Sol. State Commun. 24, 603 (1977).

[45] E. E. Haller, B. Joós and L. M. Falicov, Phys. Rev. B21, 4729 (1980).

[46] B. Joós, E. E. Haller and L. M. Falicov, Phys. Rev. B, 22, 832 (1980).

[47] H. W. H. M. Jongbloets, J. H. M. Stoelinga, M. J. H. van de Steeg and P. Wyder, Physica 89B, 18 (1977).

[48] H. W. H. M. Jongbloets, J. H. M. Stoelinga, M. J. H. van de Steen and P. Wyder, Phys. Rev. B20, 3328 (1979).

[49] G. L. Miller, D. V. Lang and L. C. Kimerling, Annual Review of Material Science, 377, Annual Review Inc. (1977).

[50] E. E. Haller, P. P. Li, G. S. Hubbard and W. L. Hansen, IEEE Trans. Nucl. Sci. NS-26, No. 1, 265 (1979).

[51] G. L. Miller, J. V. Ramirez and D. A. H. Robinson, J. Appl. Phys. 46, 2638 (1975).

[52] D. V. Lang, J. Appl. Phys. 45, 3022 (1974).

[53] L. C. Kimerling, IEEE Trans. Nucl. Sci. NS-23 No. 6, 1497 (1976).

[54] G. W. Ludwig and H. H. Woodburg, Solid State Physics, Vol. 13, 223 ed. F. Seitz and D. Turnbull, Academic Press Inc., New York (1962). Also, D. K. Wilson, Phys. Rev. 134, A265 (1964).

[55] M. Jaros, Inst. Phys. Conf. Ser. 43, 281 (1979).

[56] R. N. Hall and J. H. Racette, J. Appl. Phys. 35, 379 (1964).

[57] C. S. Fuller and J. C. Severiens, Phys. Rev. 96, 21 (1954).

[58] F. A. Trumbore, Bell Syst. Techn. J. 39, 205 (1960).

[59] R. N. Hall and T. J. Soltys, IEEE Trans. Nucl Sci. NS-25, No. 1, 385 (1978).

[60] W. E. Spear and P. G. Le Comber, Solid State Commun. 17, 1193 (1975); W. Paul, A. J. Lewis, G. A. N. Connell, and T. D. Moustakas, Solid State Commun. 20, 969 (1976); and G. Muller and S. Kalbitzer, in: Amorphous and Liquid Semiconductors, Ed. W. E. Spear, CICL, Univ. of Edinburgh, 1977 (p. 347).

[61] B. Pajot, Analusis 5, No. 7, 293 (1977).

[62] R. N. Hall, Inst. Phys. Conf. Ser. 23, 190 (1975); also, R. N. Hall IEEE Trans. Nucl. Sci. NS-21, No. 1, 260 (1974).

[63] E. E. Haller, Phys. Rev. Lett. 40, 584 (1978).

[64] E. E. Haller, Inst. Phys. Conf. Ser. 46, 205 (1979).

[65] D. H. Dickey and J. O. Dimmock, J. Phys. Chem. Solids 28, 529 (1967); also R. L. Jones and P. Fisher, Phys. Rev. B2, 2016 (1970).

[66] H. Fritzsche, Phys. Rev. 125, 1560 (1962).

[67] E. E. Haller, W. L. Hansen, A. Seeger, D. Herlach, K.-P. Doering, H. Bossy, M. Gladisch, H. Matsu, H. Metz, H. Orth, G. zu Pulitz, J. Vetter and E. Yagi, "The Nature of Muonium in Germanium and Silicon", Proc. Intern. μSR2 Conference, Vancouver, Aug. 11-15, 1980.

[68] P. F. Meier, "Exotic Atoms' 79", 331-354, eds. K. Crowe, J. Duclos, G. Fiorentini and G. Torelli, Plenum Press (1980).

[69] H. Reiss, C. S. Fuller and F. J. Morin, Bell Syst. Tech. J. 35, 535, (1956).

[70] R. L. Aggarwal, P. Fisher, V. Mourzine and A. K. Ramdas, Phys. Rev. 138, A882 (1965).

[71] E. M. Bykova, L. A. Goncharov, T. M. Lifshits, V. I. Sidorov, and R. N. Hall, Fiz. Tekh. Poluprov. 9, 1853 (1975), [Sov. Phys. Semic. 9, 1288 (1976)].

[72] T. V. Mashovets, Inst. Phys. Conf. Ser. 31, 30 (1977).

[73] E. D. Vassilyeva, V. V. Emtsev, E. E. Haller and TV Mashovets, Sov. Phys. Semic. (1980), submitted.

[74] E. E. Haller, G. S. Hubbard and W. L. Hansen, IEEE Trans. Nucl. Sci. NS-24 No. 1, 48 (1977).

[75] M. S. Skolinck, "Shallow and Deep Impurities in Germanium", Landolt-Bornstein, Numerical Data and Functional Relationships in Science and Technology, ed. O. Mandelung, Springer New York, to be published.

[76] Preliminary results indicate a carbon concentration between 10^{14} and $10^{15}cm^{-3}$.

TABLE 1

The Strongest Transitions of Neutral Elemental Acceptors in Ultra-Pure Germanium
(all values are in units of meV ± .01 meV)

Transition (Ref 34)	D	C	B	A_4	A_3	A_2	A_1	Groundstate energy*
Endstate Assignment (Ref 2)	$2\Gamma_8^-$	$1\Gamma_7^-, 3\Gamma_8^-$	$4\Gamma_8^-$	$5\Gamma_8^-$				
B	7.94	8.69	9.32	9.57	9.66	9.78	9.86	10.47
Al	8.27	9.03	9.65	9.93	10.00	10.13	10.20	10.80
Ga	8.44	9.19	9.81	10.09	10.15	10.29	10.36	10.97
In	9.11	9.86	10.51	10.75	10.83	10.96	11.03	11.64
Be	21.89	22.68	23.31	23.71		23.85		24.42
Zn	30.13	30.88	31.53	31.87		32.04		32.66
Cu	40.35	41.10	41.72	--	42.13	42.35	--	42.88

*The ground state energy was determined by adding 2.53 meV to the transition energy of the D-line (Ref 34, 48). Recent theory (Ref 2) predicts an energy difference of 2.88 meV which would increase all the ground state energy values in the table by 0.35 meV.

TABLE 2

Crystal Number	Growth Conditions: Crucible	Growth Conditions: Atmosphere (1 atm)	Dislocation Etch Pit Density (cm^{-2})	Neutral Impurity Concentrations (cm^{-3}): [H]	[C]	[O]	[Si]	Net Shallow Impurity Concentration N_A-N_D(cm^{-3})	Copper Concentration (cm^{-3})
342	Synthetic quartz	Hydrogen	$\sim 10^3$	$\sim 10^{14}$	low	$<10^{14}$	$\sim 10^{14}$	-3.5×10^9	8.2×10^{11}
373	Synthetic quartz	Hydrogen	0	"	"	"	"	8.5×10^{10}**	4.8×10^{12}
235	Graphite	Hydrogen	$\sim 10^3$	"	high	$<10^{13}$	low	9.1×10^{10}	3.2×10^{12}
436*	Synthetic quartz	Hydrogen	$\sim 10^3$	"	low	$<10^{13}$	3×10^{17}	7.0×10^{10}	$\sim 2.0 \times 10^{11}$
136	Synthetic quartz	Nitrogen	$\sim 5 \times 10^3$	low	"	$>4 \times 10^{14}$	$\sim 10^{14}$	1.2×10^{11}	1.5×10^{11}
132	Synthetic quartz	Nitrogen	0	"	"	$>4 \times 10^{14}$	$\sim 10^{14}$	3.3×10^{11}	$<2.0 \times 10^{10}$

*Crystal #436 has been doped with elemental high-purity silicon.

**Crystal #373 contains in addition to the shallow centers, $1.4 \times 10^{11} cm^{-3}$ V_2H acceptors at E_V + 72 meV.

TABLE 3

The Strongest Transitions of the Shallow Donor Complex $D(H_2O)$
(all energy values are in units of meV ± .005 meV)
(other notation for this complex: "C" Ref 40, 41, 62)

Transition Endstate Assignment (Ref 32)	2P ± 1	3P ± 1	4P ± 1	4F ± 1	5P ± 1	5F ± 1	6P ± 1	Binding Energy* of Lowest Groundstate Manifold Component
at zero stress	10.736	11.420	11.704	11.849	11.985	12.055	12.131	12.498
at high stress	8.058	8.741	9.028	9.174	9.313	--	--	9.820

*This energy was obtained by adding the theoretically derived binding energy of the 2P ± 1 state 1.762 meV to the energy of the 1S - 2P ± 1 transition (Ref 32).

TABLE 4

The Strongest Transitions of Neutral Shallow Acceptor Complexes in Ultra-Pure Germanium
(all values are in units of meV ± .01 meV)

Transition (Ref 34)	D	C	B	A_4	A_3	A_2	A_1	Groundstate Energy*	Groundstate Splitting
Endstate Assignment (Ref 2)	$2\Gamma_8^-$	$1\Gamma_7^-$, $3\Gamma_8^-$	$4\Gamma_8^-$	$5\Gamma_8^-$					
A(H,Si) other notations: A_1,A_2 Ref (1), X Ref (40)	7.71 8.78	8.44 9.53	-- 10.17	-- 10.41	-- 10.50	-- 10.64	-- 10.71	10.24 11.31	1.07
A(H,C) other notations: A_6 Ref (1), Y Ref (39)	7.42 9.39	8.17 10.14	-- 10.77	-- 11.04	-- 11.13	-- 11.24	-- 11.32	9.95 11.93	1.98
A_3 — nitrogen atmosphere,	7.34	8.10	--	--	--	--	--	9.87	--
A_4 — graphite crucible related	7.89	8.64	9.27	9.54	9.61	9.73	9.82	10.42	--
A_5 — centers, Ref (1)	8.44	9.19	9.82	10.09	10.15	--	--	10.97	--
A_7 unknown other notation: X Ref (39)	8.13	8.89	9.53	--	--	--	--	10.66	--

*See Table 1.

TABLE 5

The Strongest Transitions of the Donors D(Li) and D(Li, O)
(all energy values are in units of meV ± .003 meV)

Transition Endstate Assignment (Ref 32)		2P ± 1	3P ± 1	4P ± 1	4F ± 1	5P ± 1	5F ± 1	6P ± 1	Binding Energy*** of Ground state
D(Li)	zero stress	8.286	8.974	9.259	9.406	9.546	9.609	--	10.048
D(Li)	high stress	8.317	9.004	9.288	9.436	9.573	9.637	9.728	10.079
D(Li,O) zero stress	broad lines*	7.70	--	--	--	--	--	--	9.46
		8.27	8.96	9.25	--	--	--	--	10.03
	sharp lines**	8.736	9.419	9.706	9.850	9.981	10.057	10.133	10.498
D(Li,O) high stress F || [111]		8.029	8.714	9.004	9.147	--	--	--	9.791
		8.120	8.803	9.092	9.233	9.376	9.436	--	9.982
		8.748	9.436	9.720	9.862	9.996	--	--	10.510

* The error in the transition energies leading to the broad lines is ± .05 meV.

** The sharp set of lines has been assigned in the past to a donor "S" (Ref 40, 62) and "A" (Ref 41).

*** See Table 4.

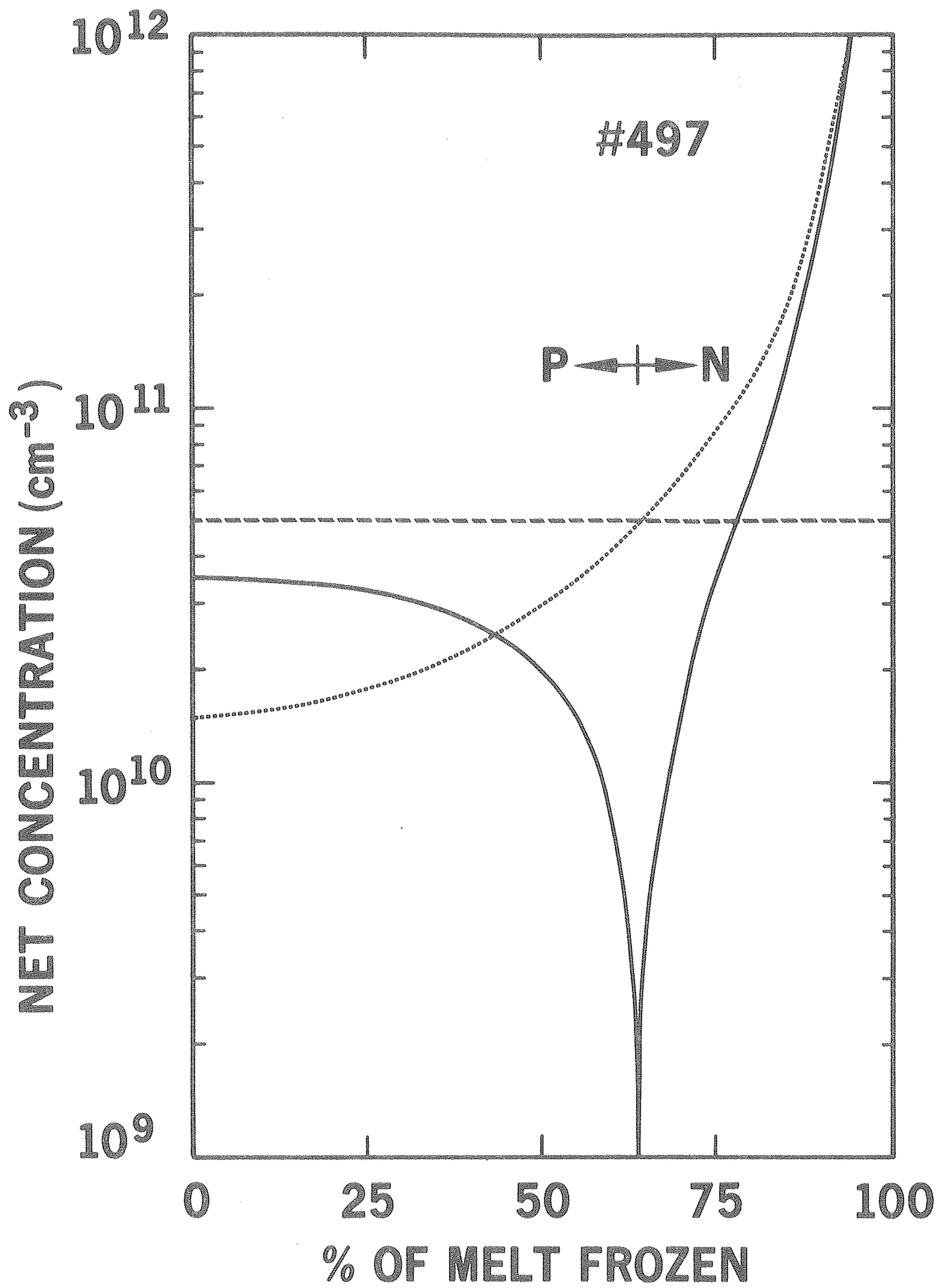

Figure 1.

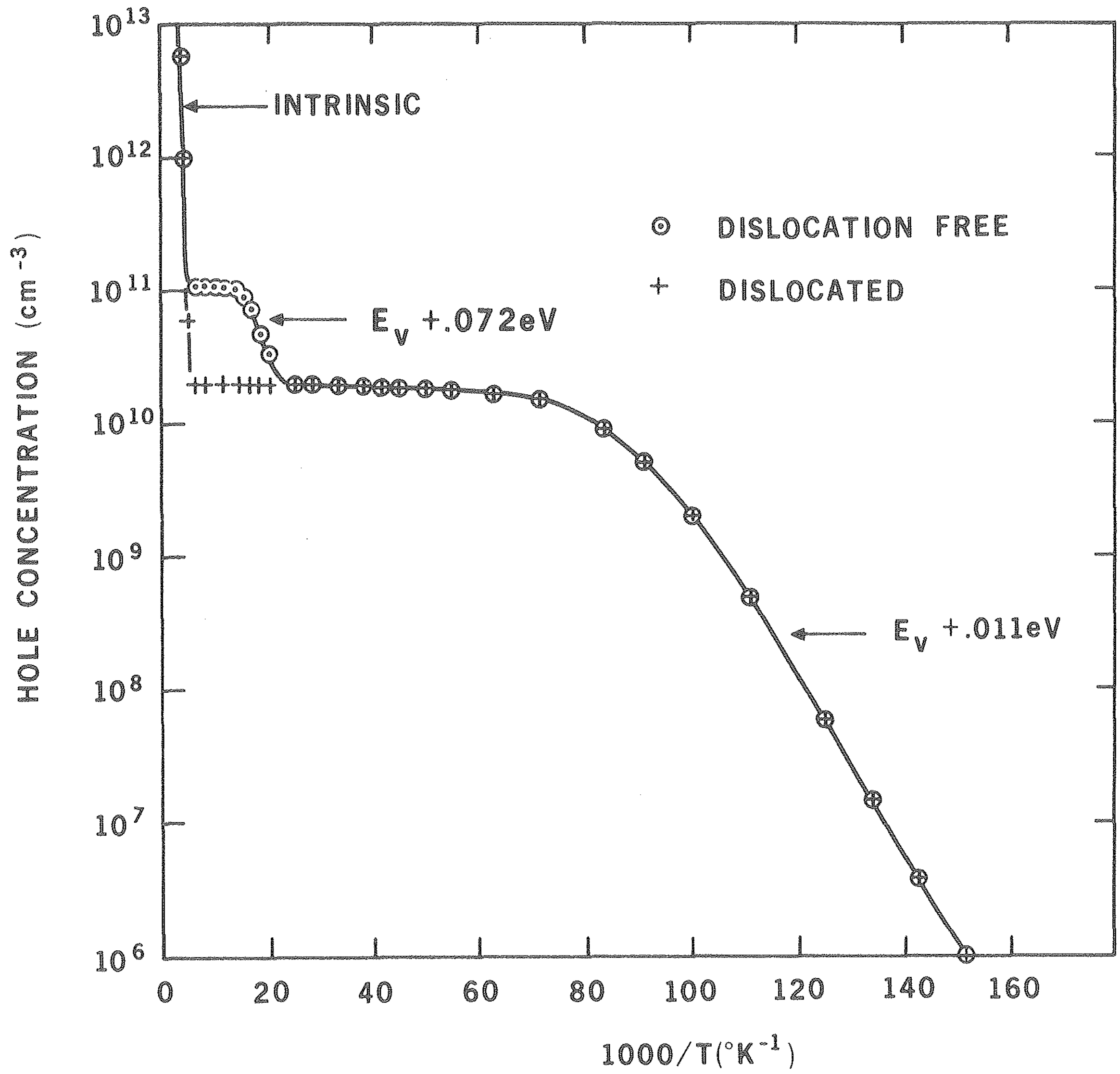

Figure 2.

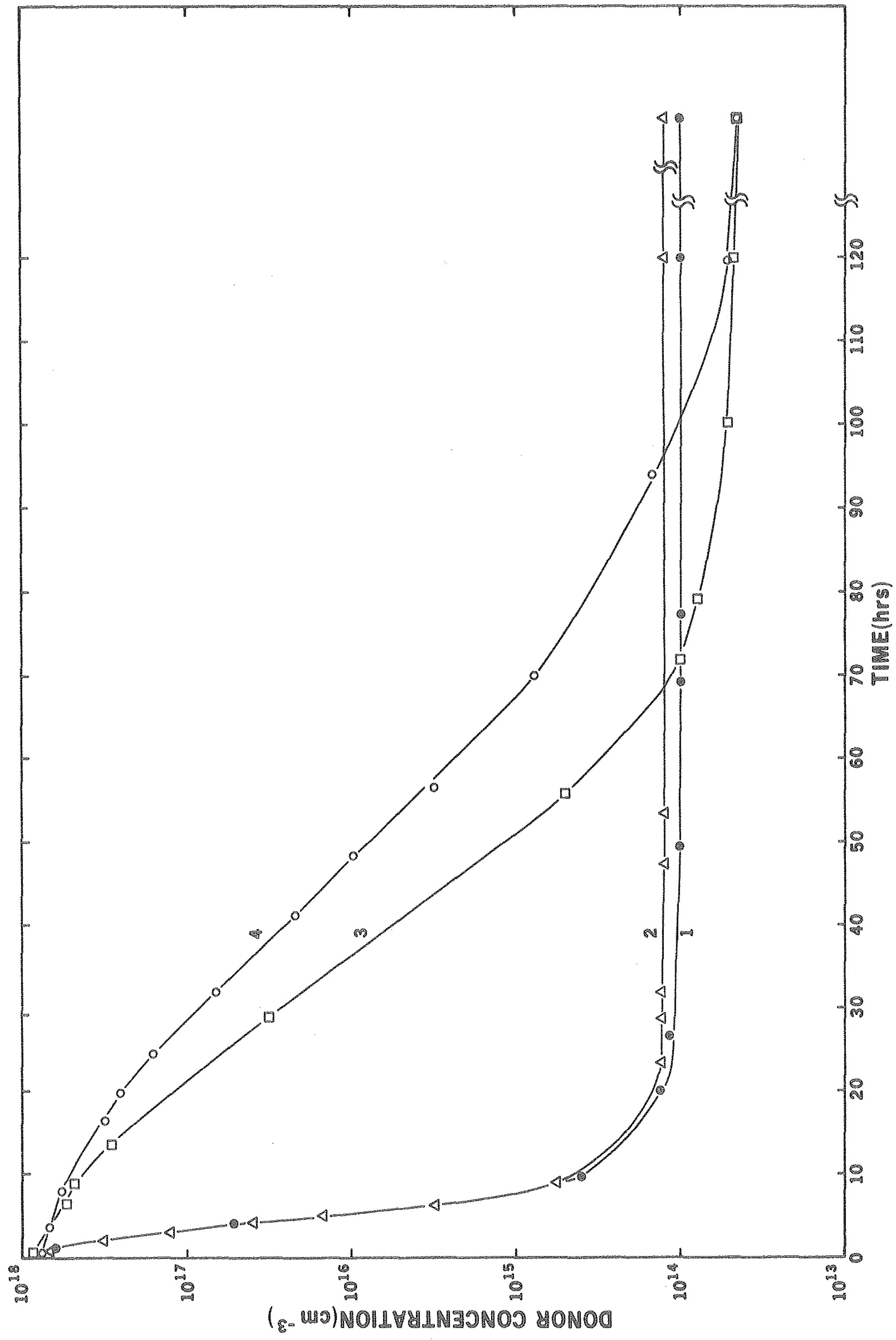

Figure 3.

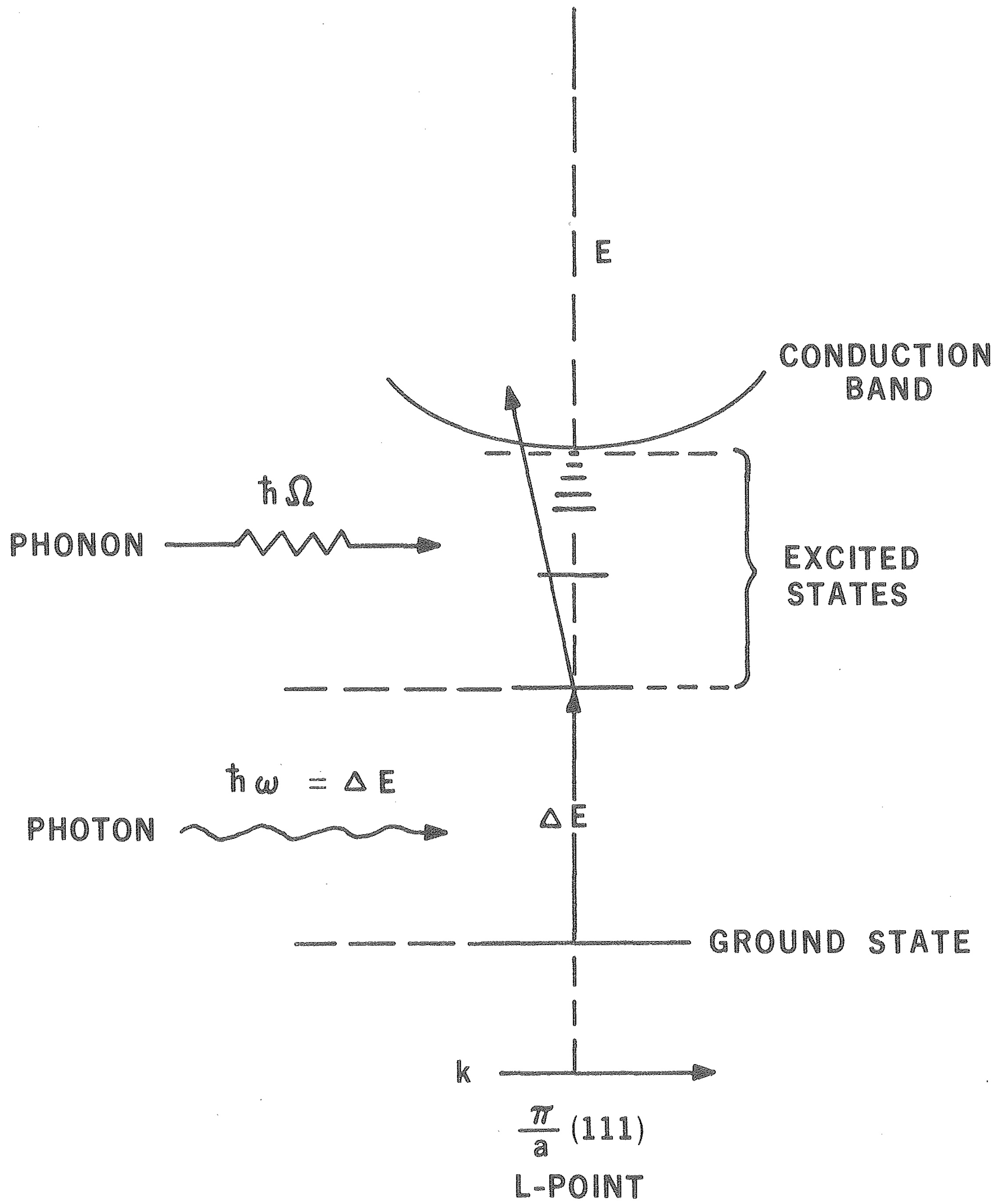

Figure 4.

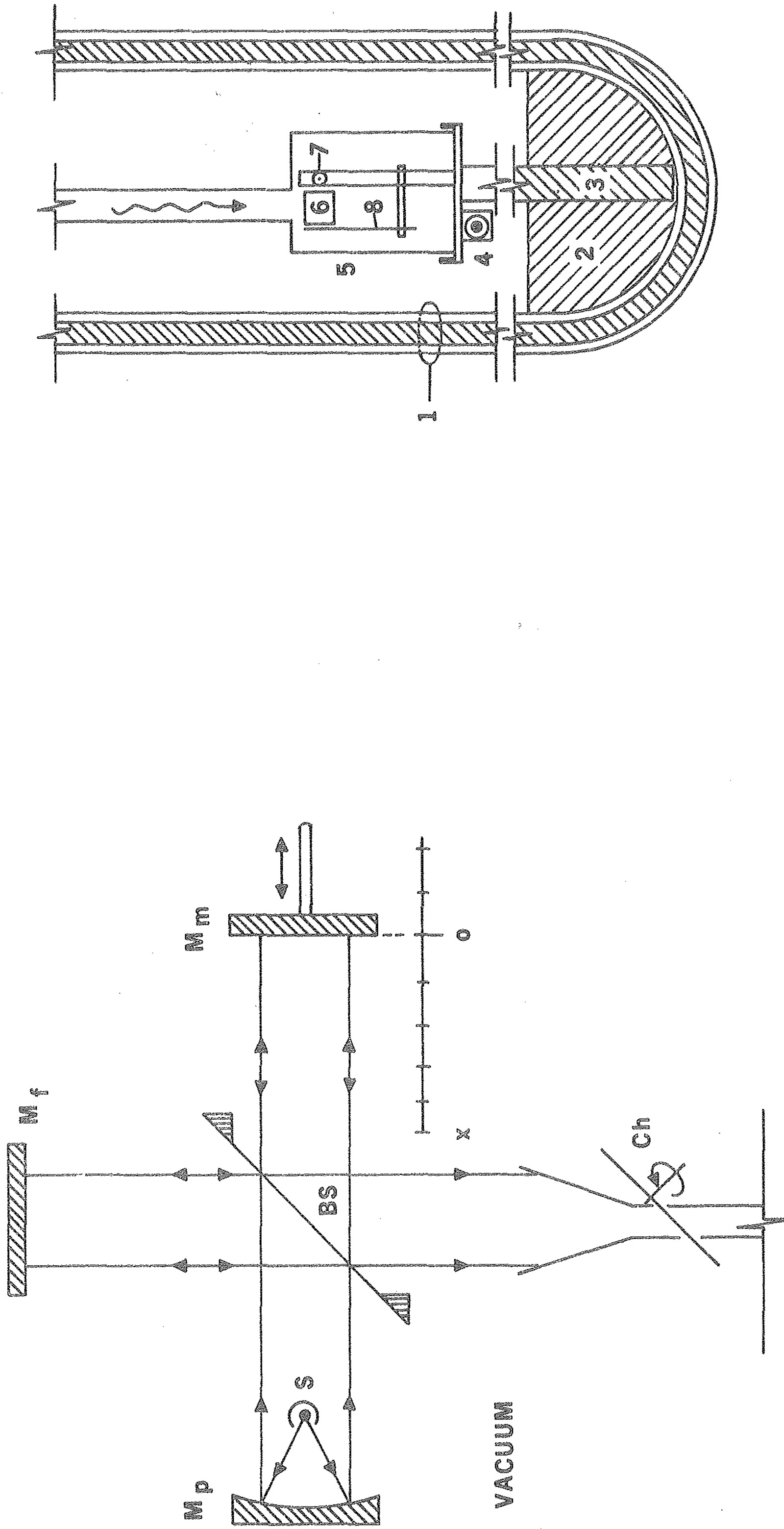

Figure 5.

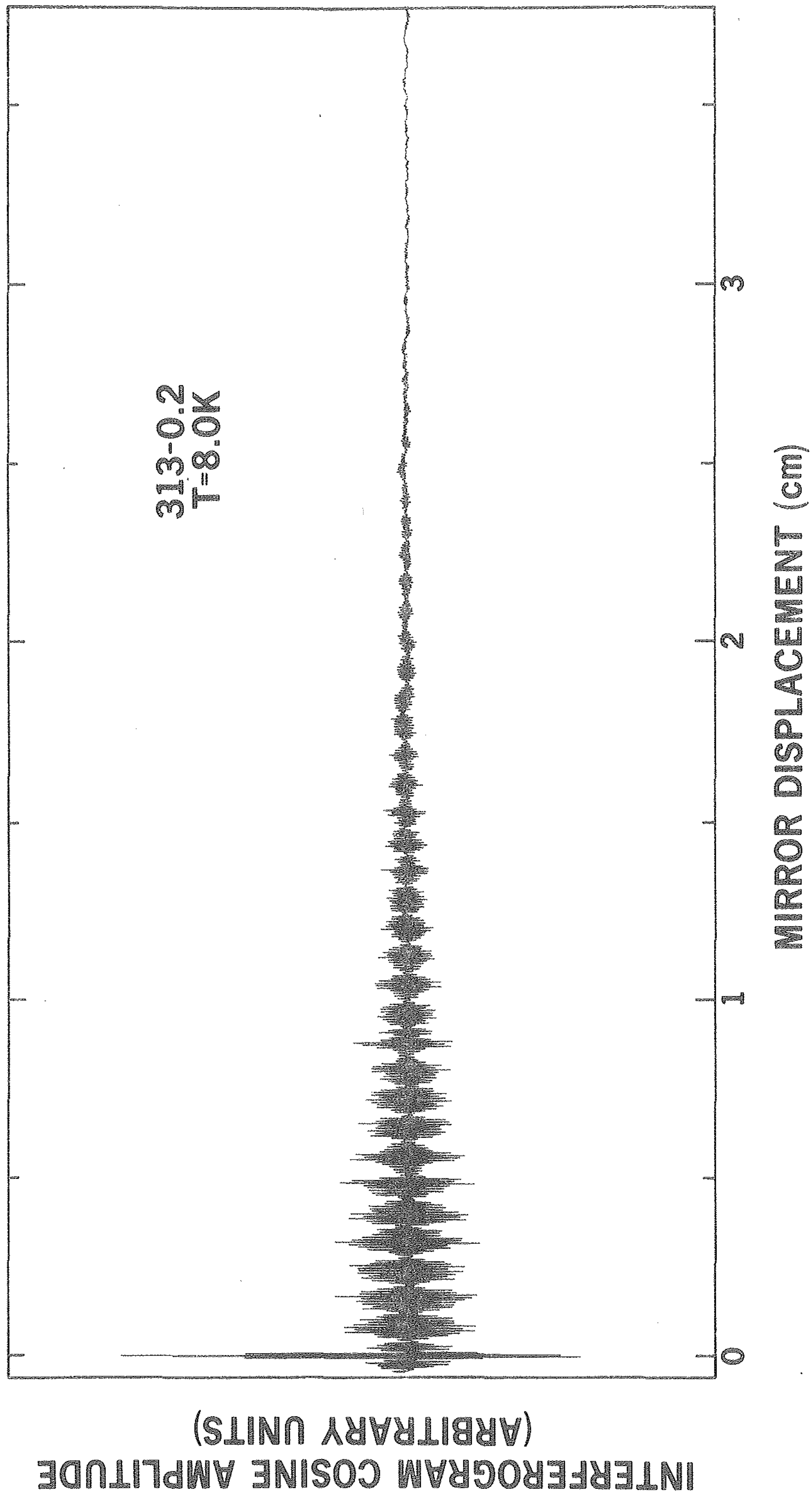

XBL 802-8048

Figure 6.

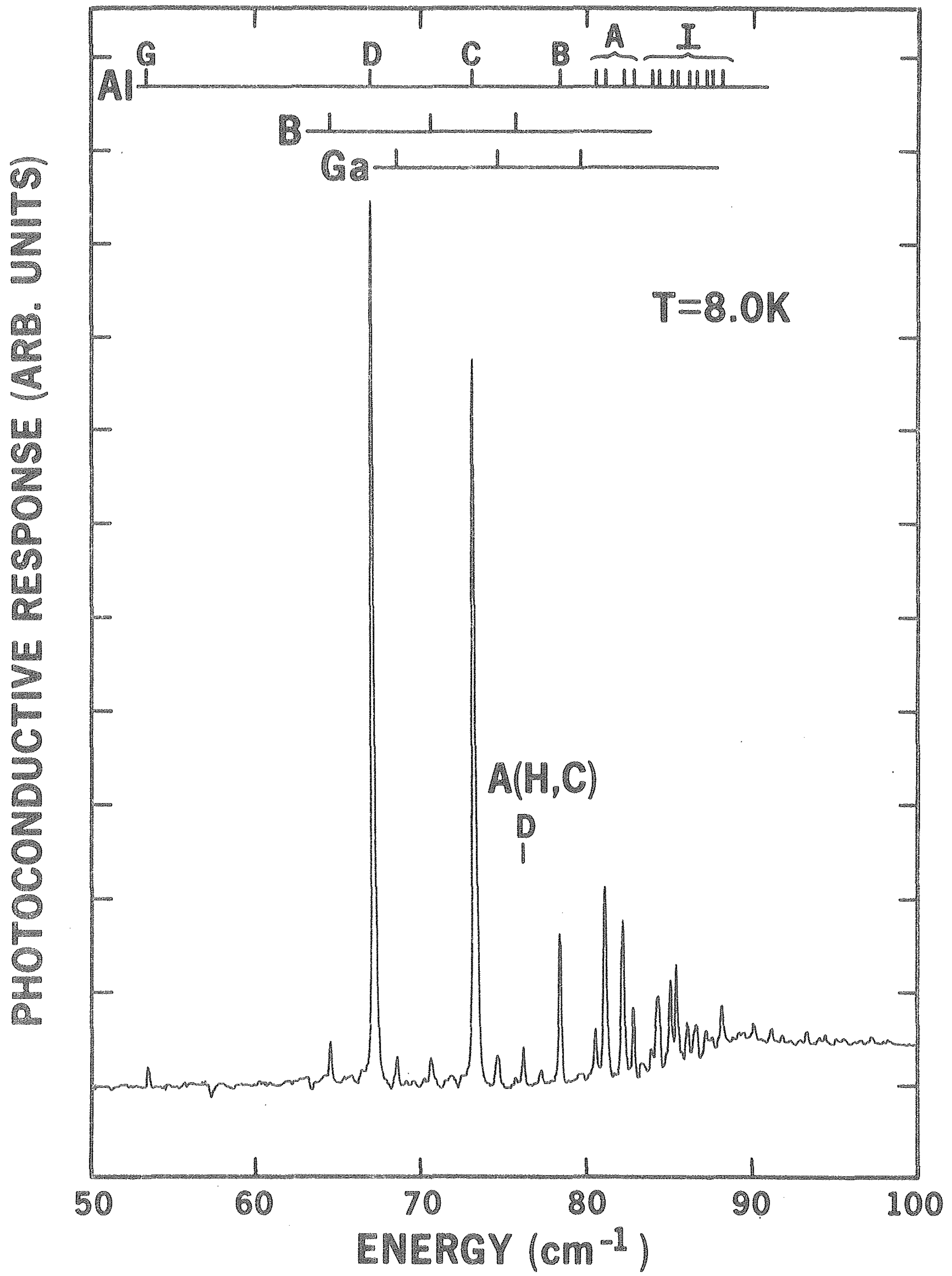

XBL 806-10176

Figure 7.

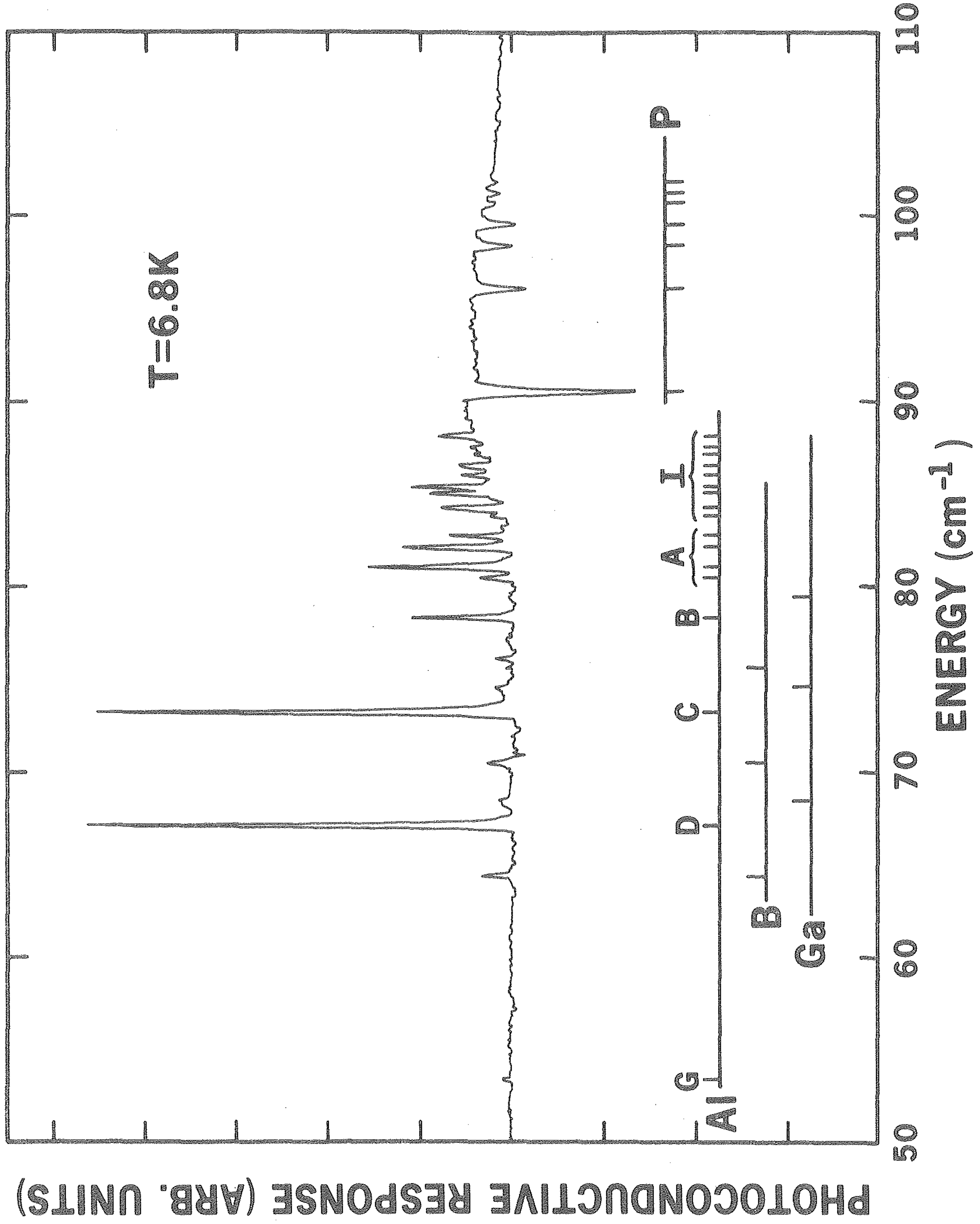

Figure 8.

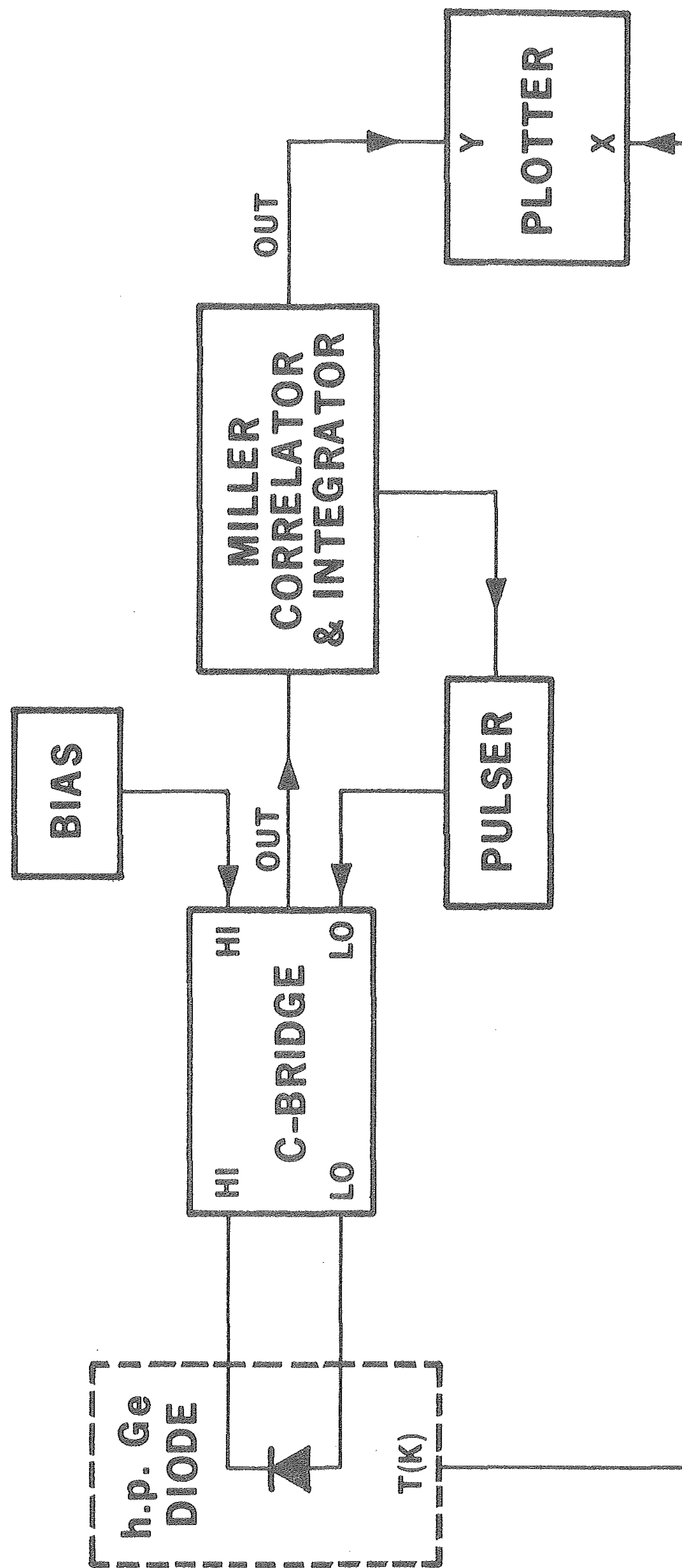

Figure 9.

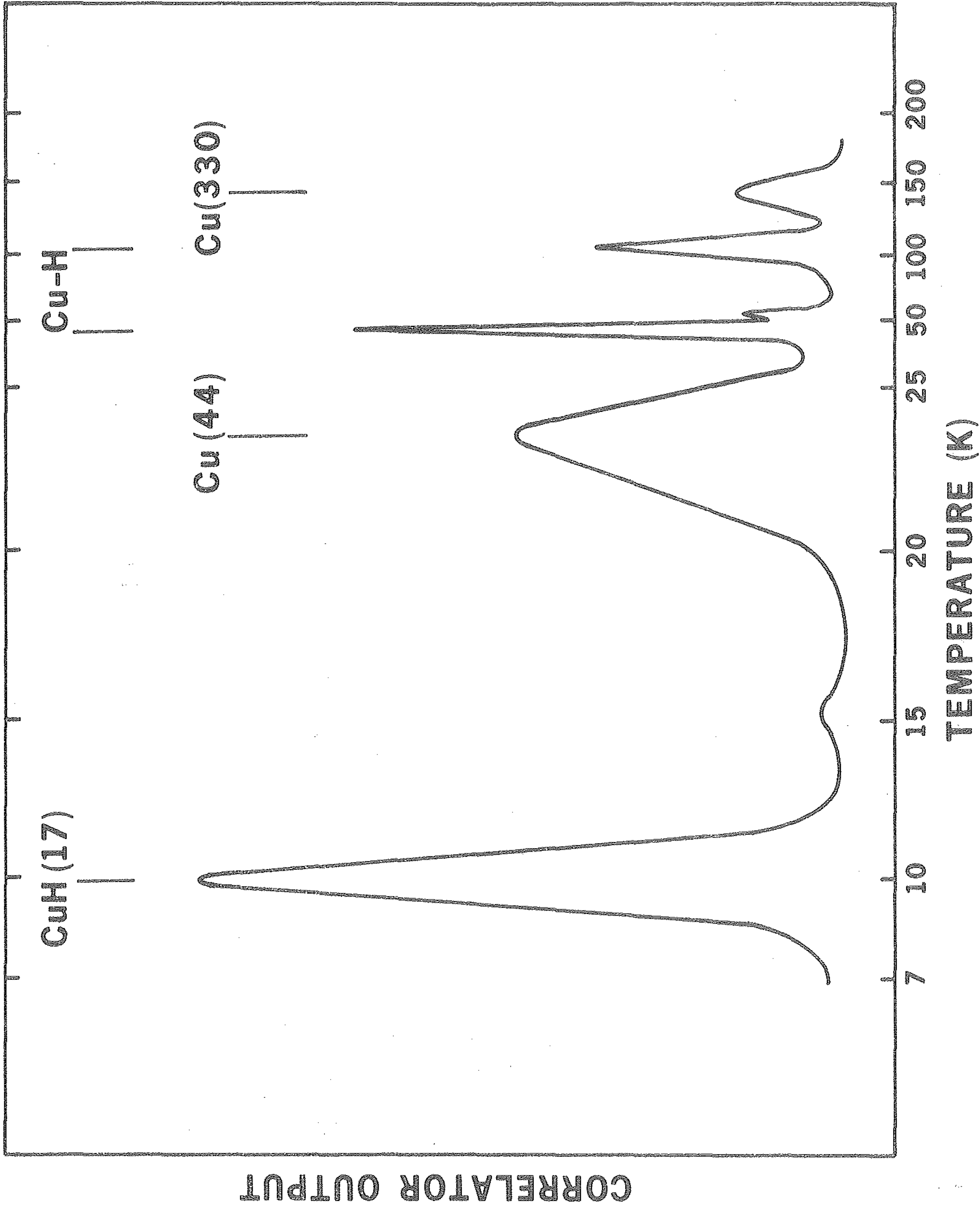

XBL 796-10138

Figure 10.

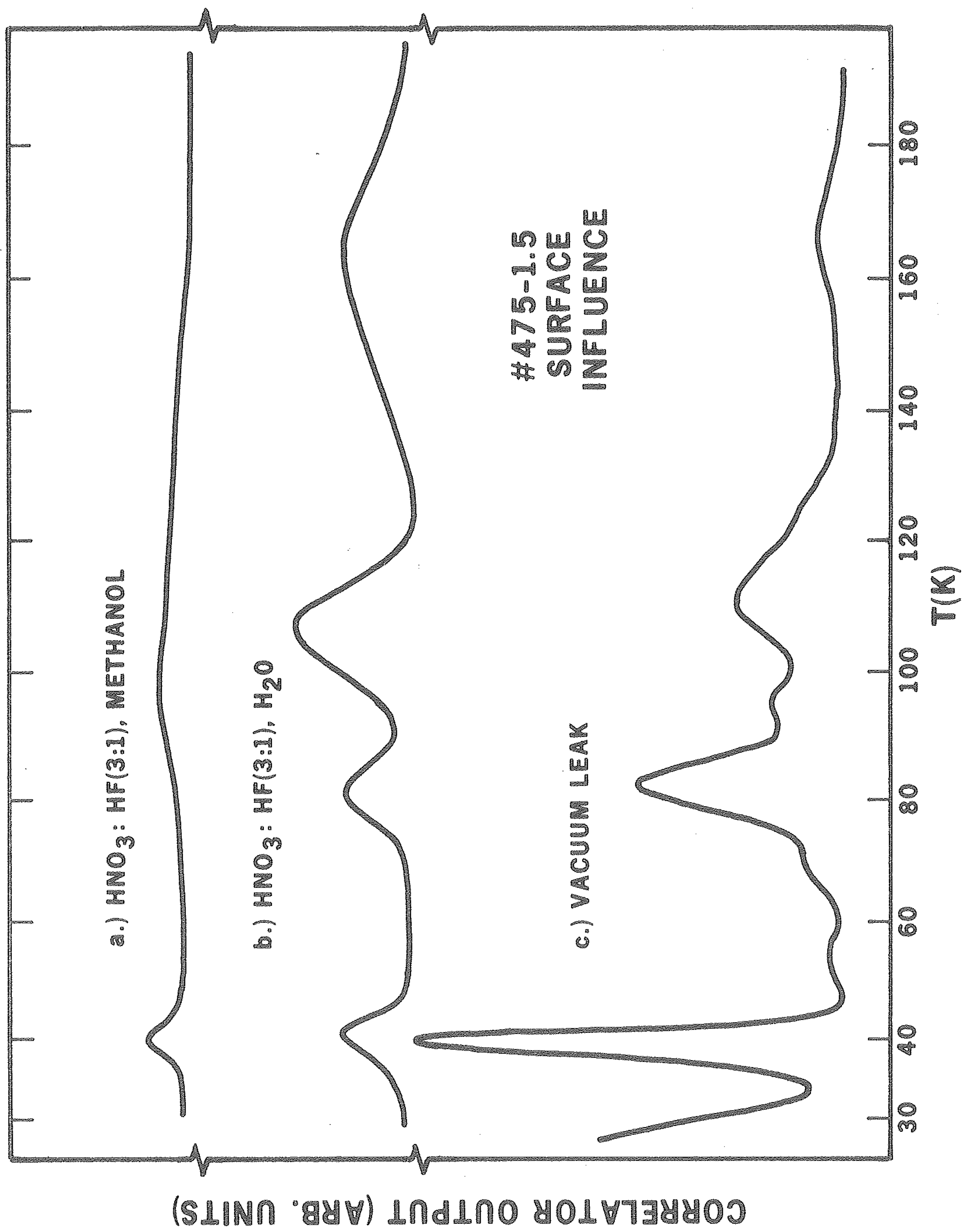

Figure 11.

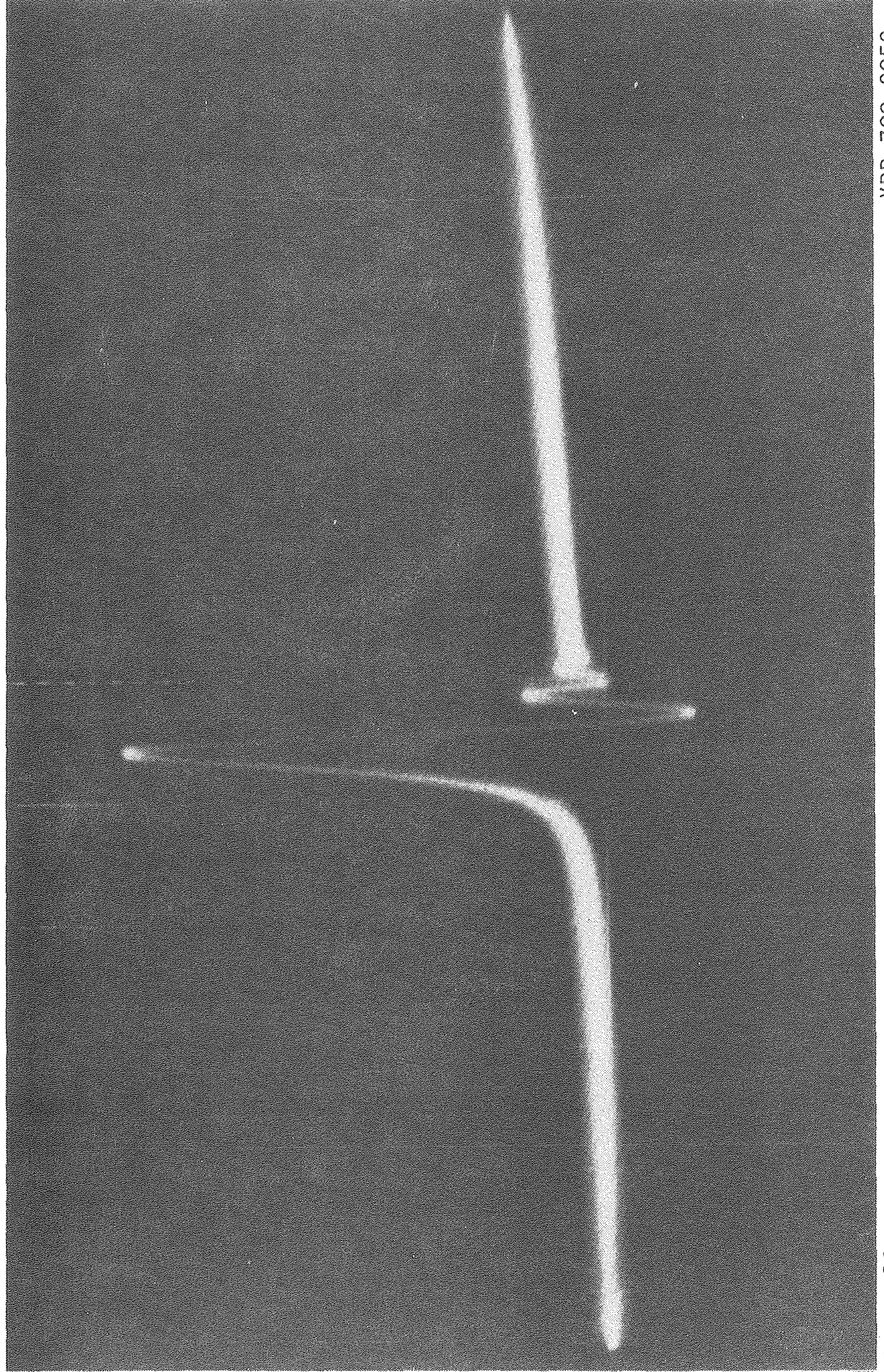

Figure 12

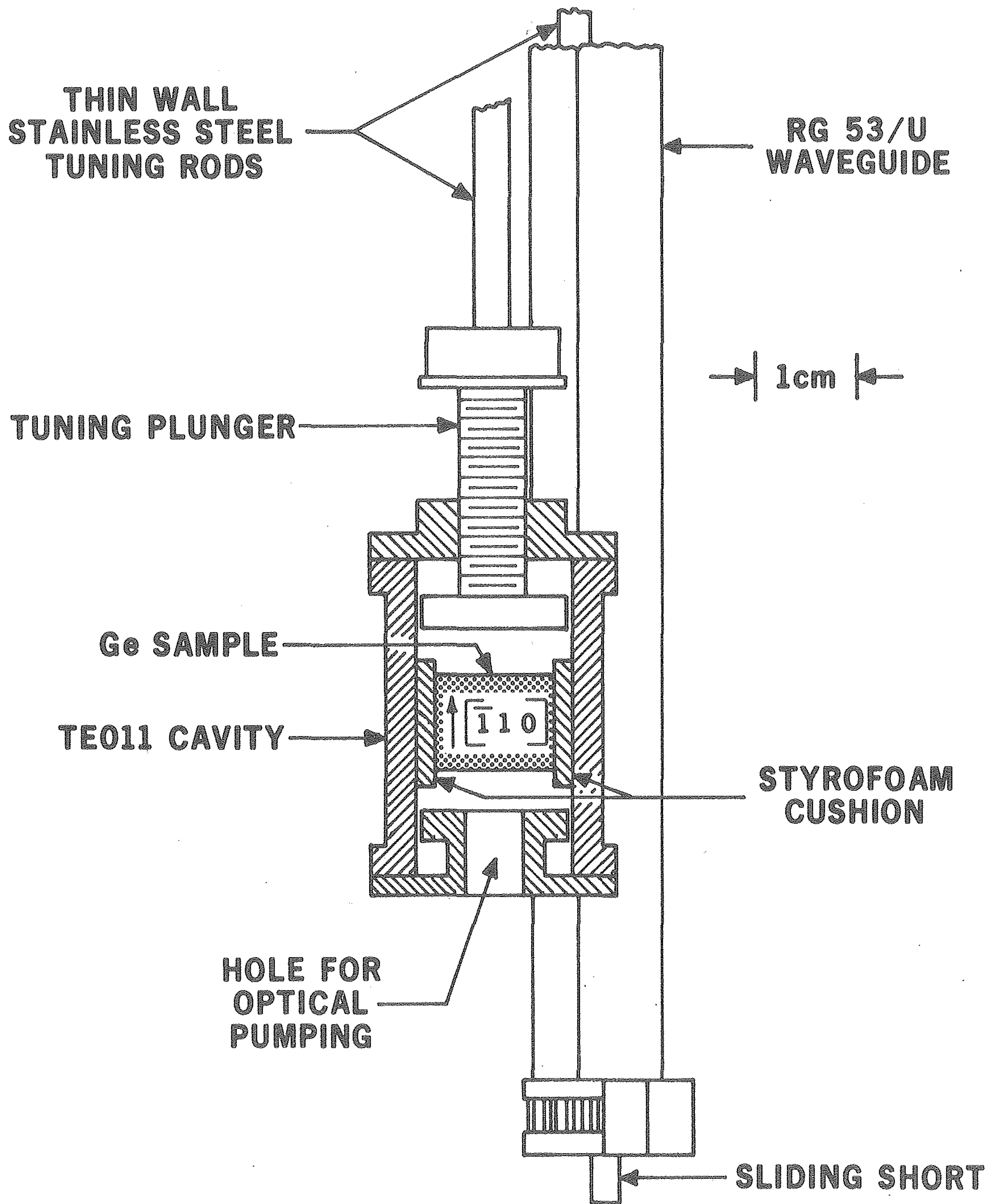

Figure 13.

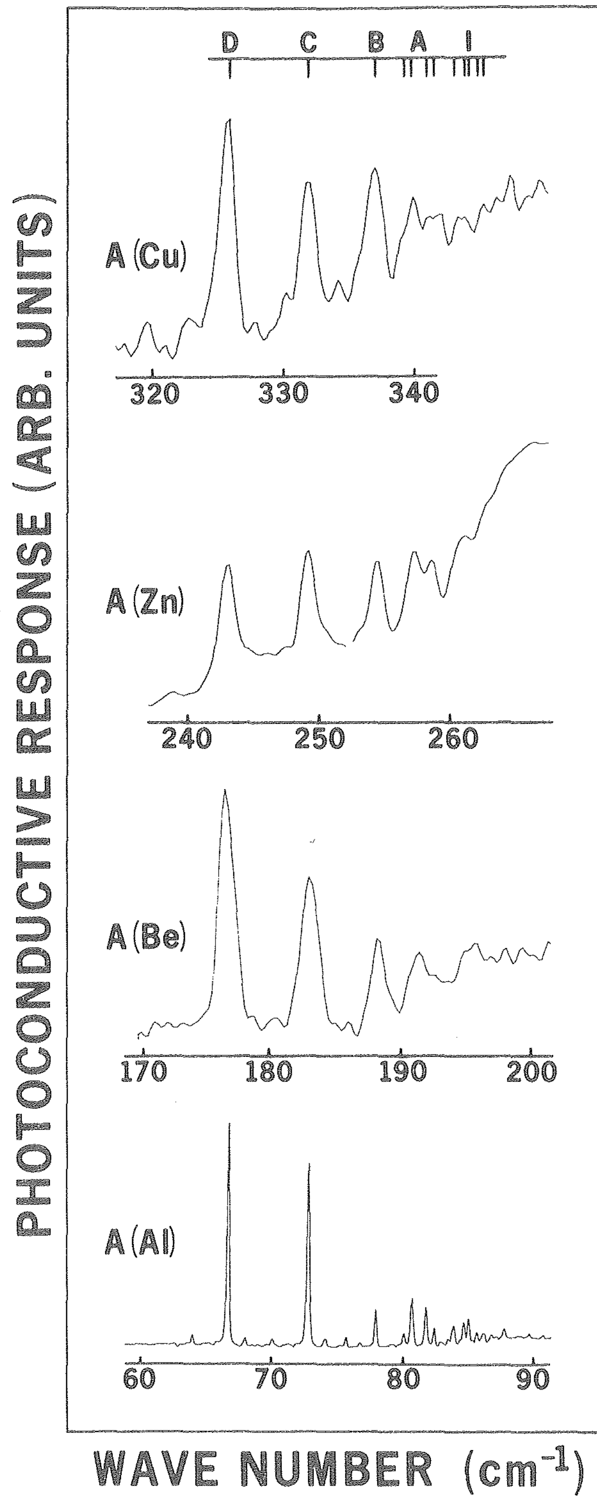

XBL 802-8202

Figure 14.

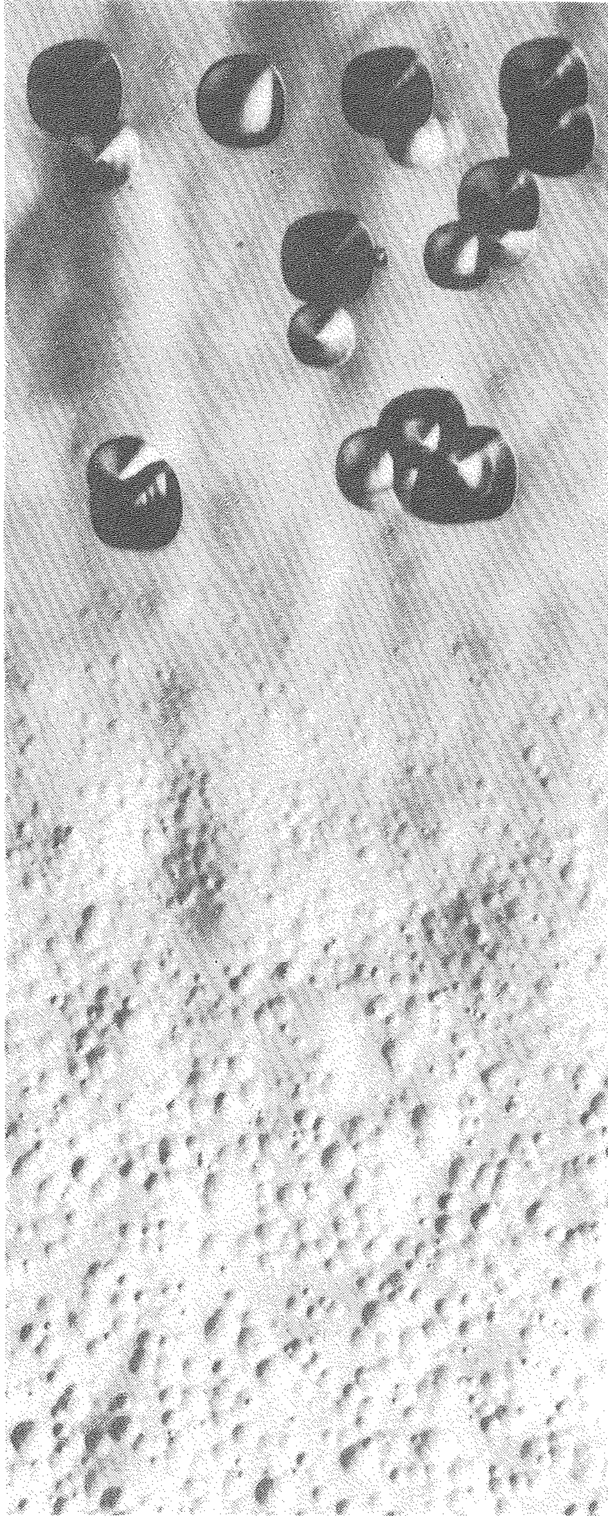

Figure 15

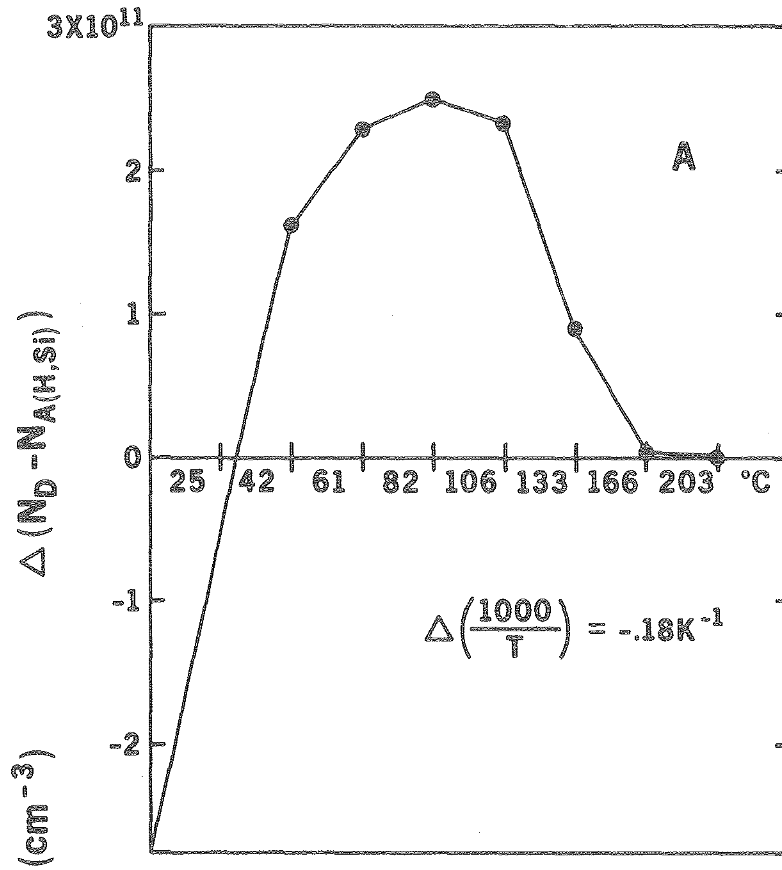

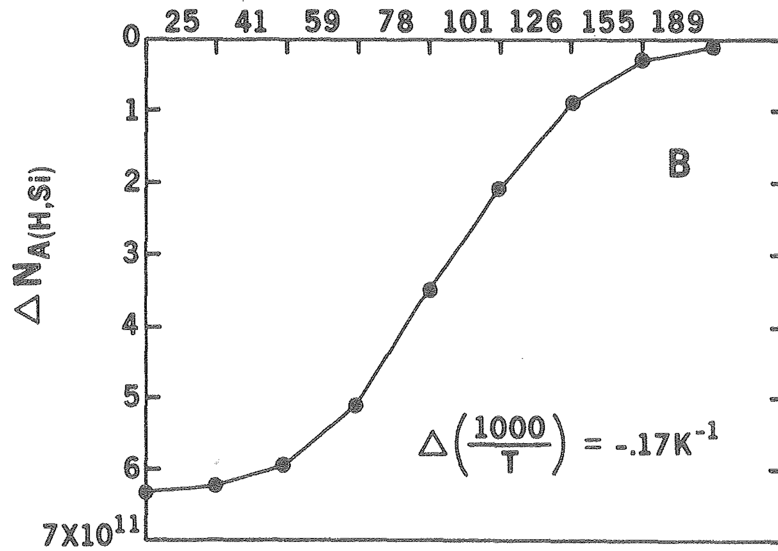

XBL 7911-12832

Figure 16.

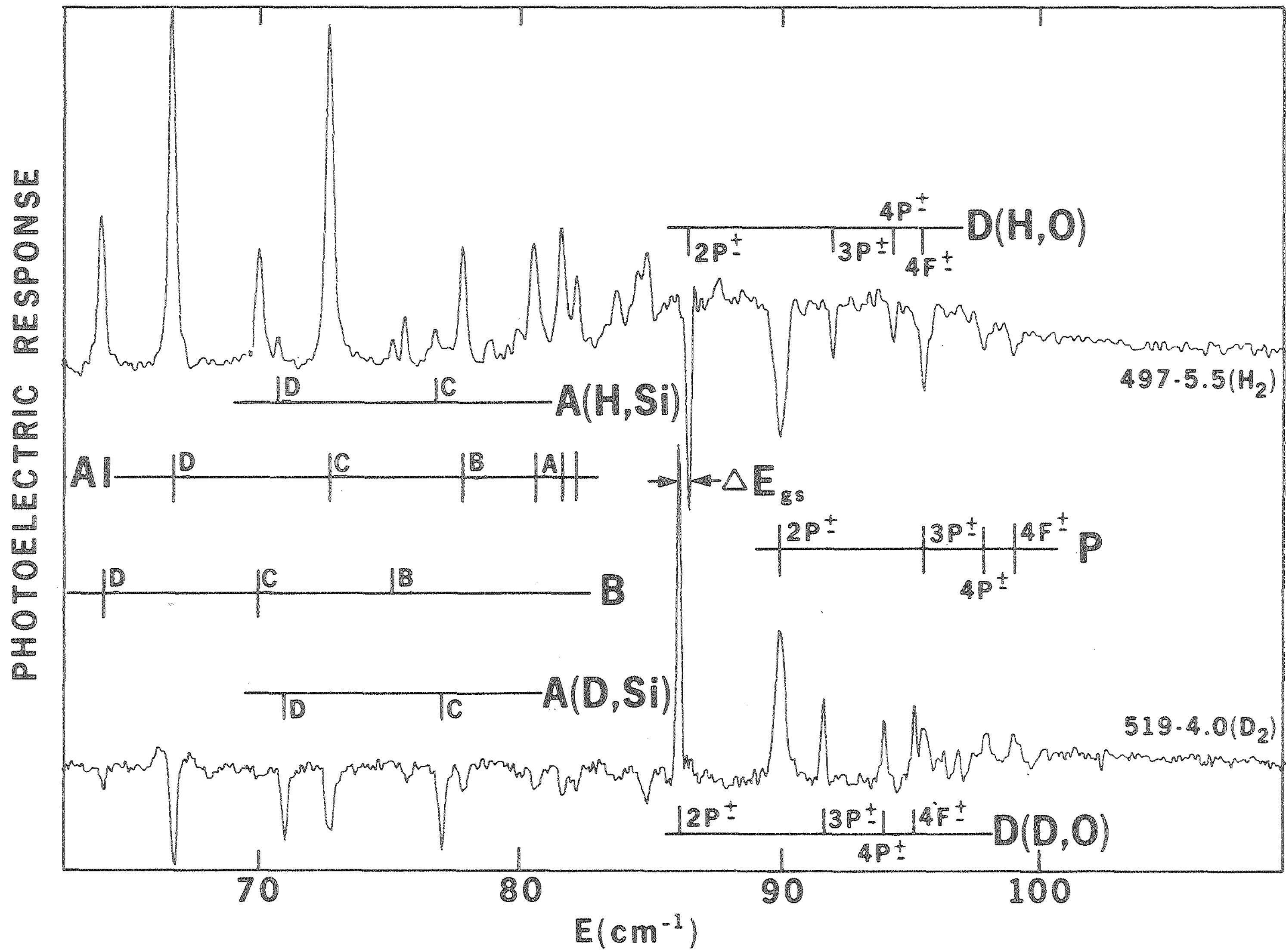

XBL 778 2792 A

Figure 17.

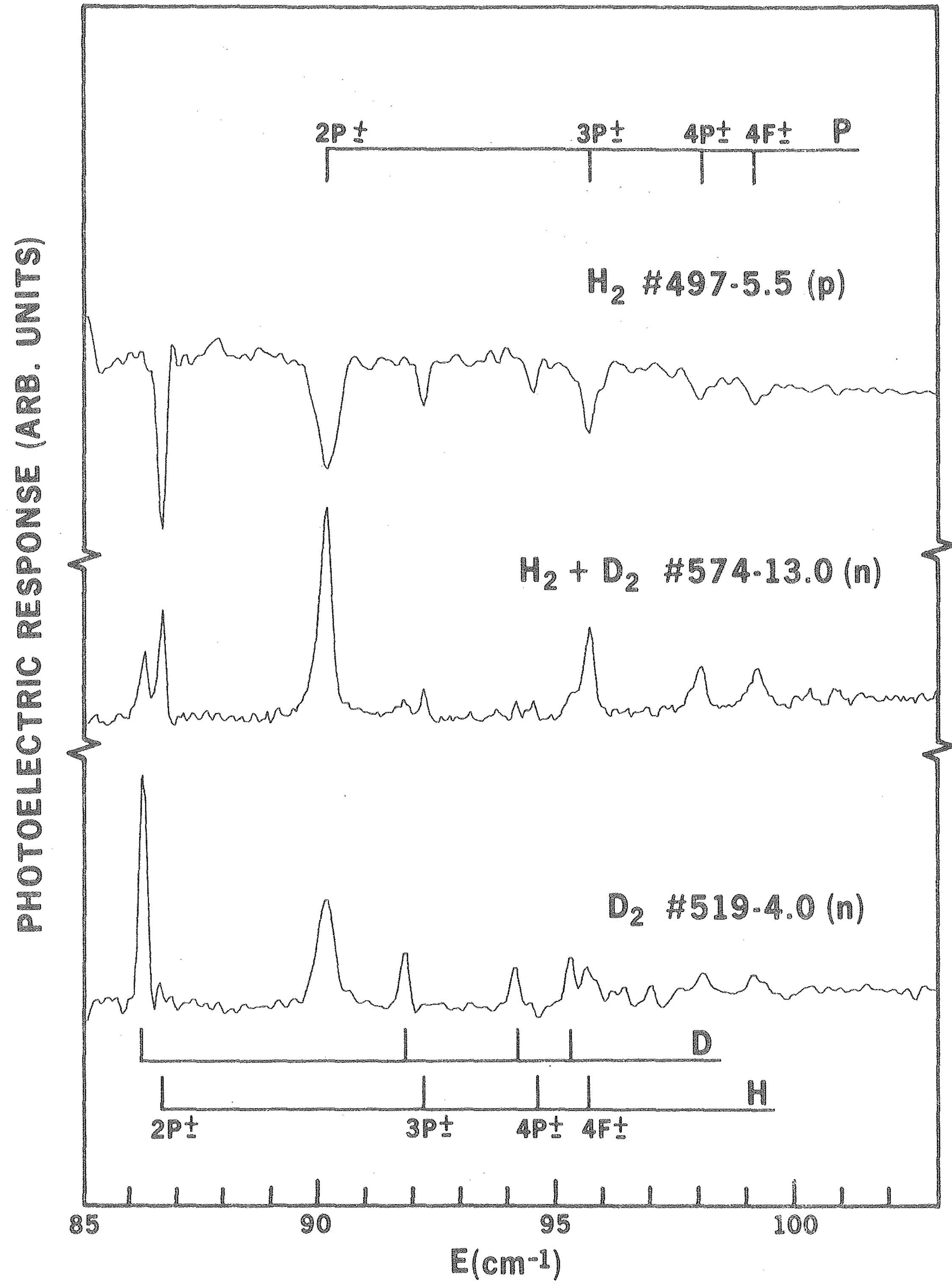

XBL 788-10100

Figure 18.

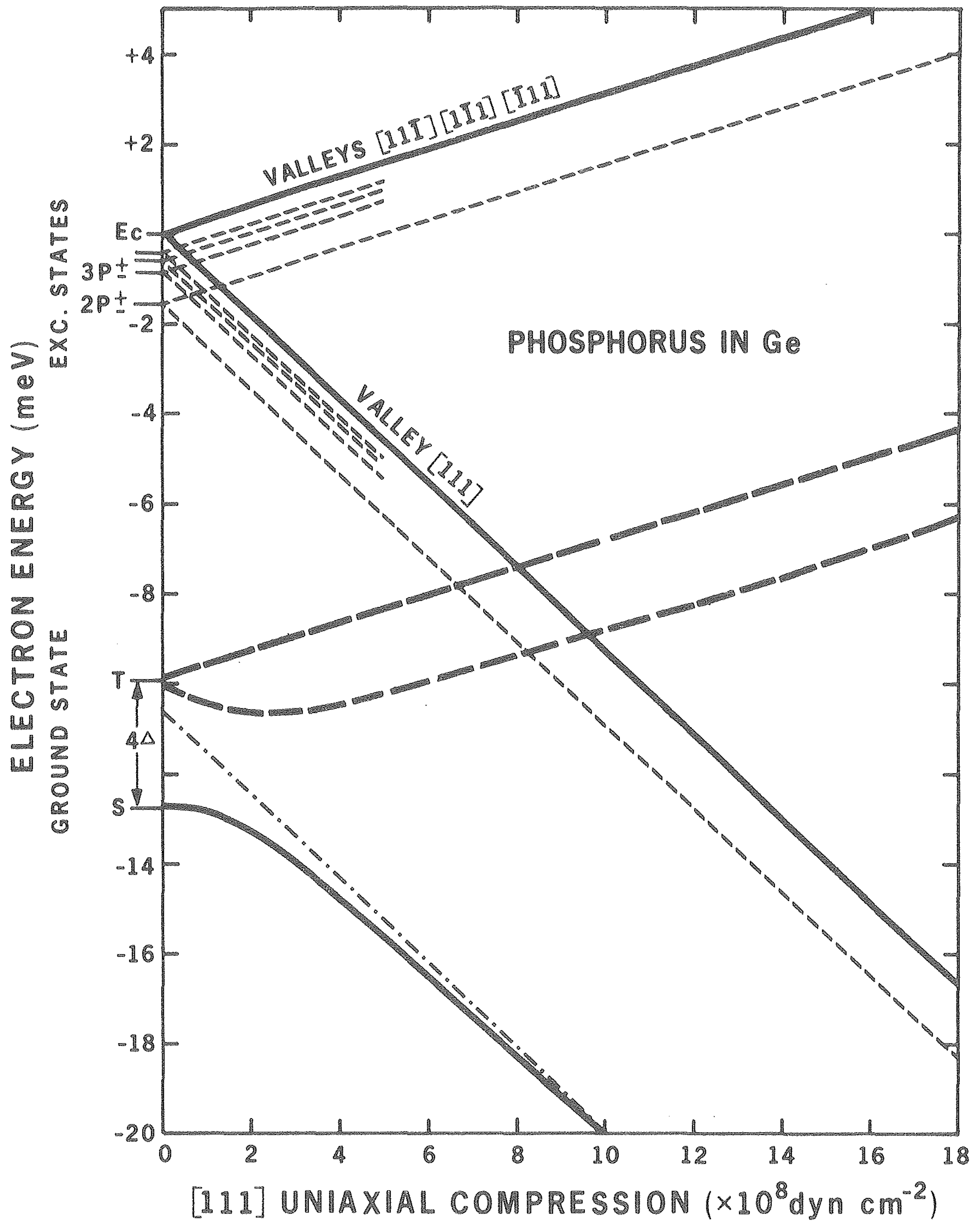

XBL 7710-10009

Figure 19.

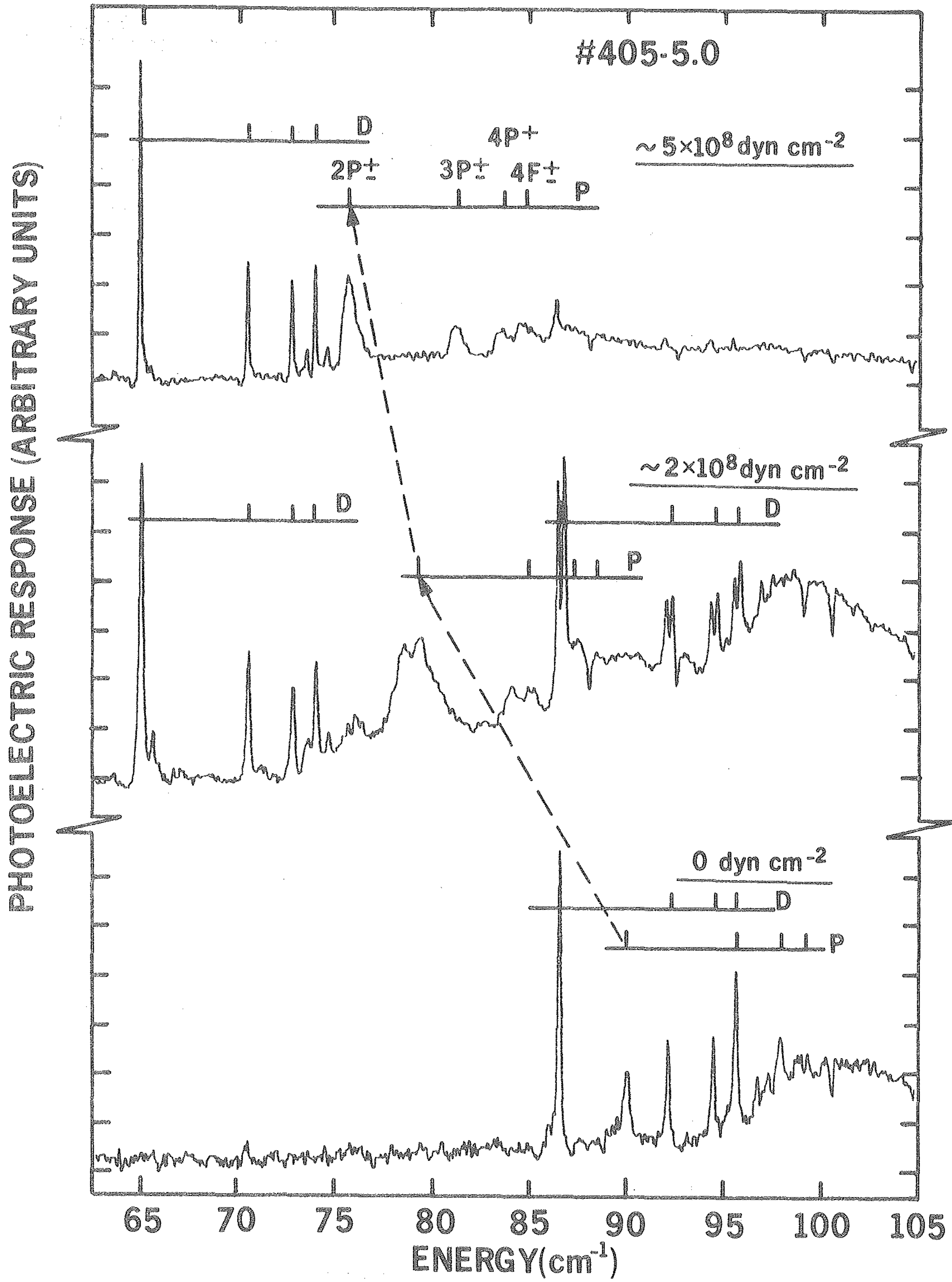

XBL 7710-6740 A

Figure 20.

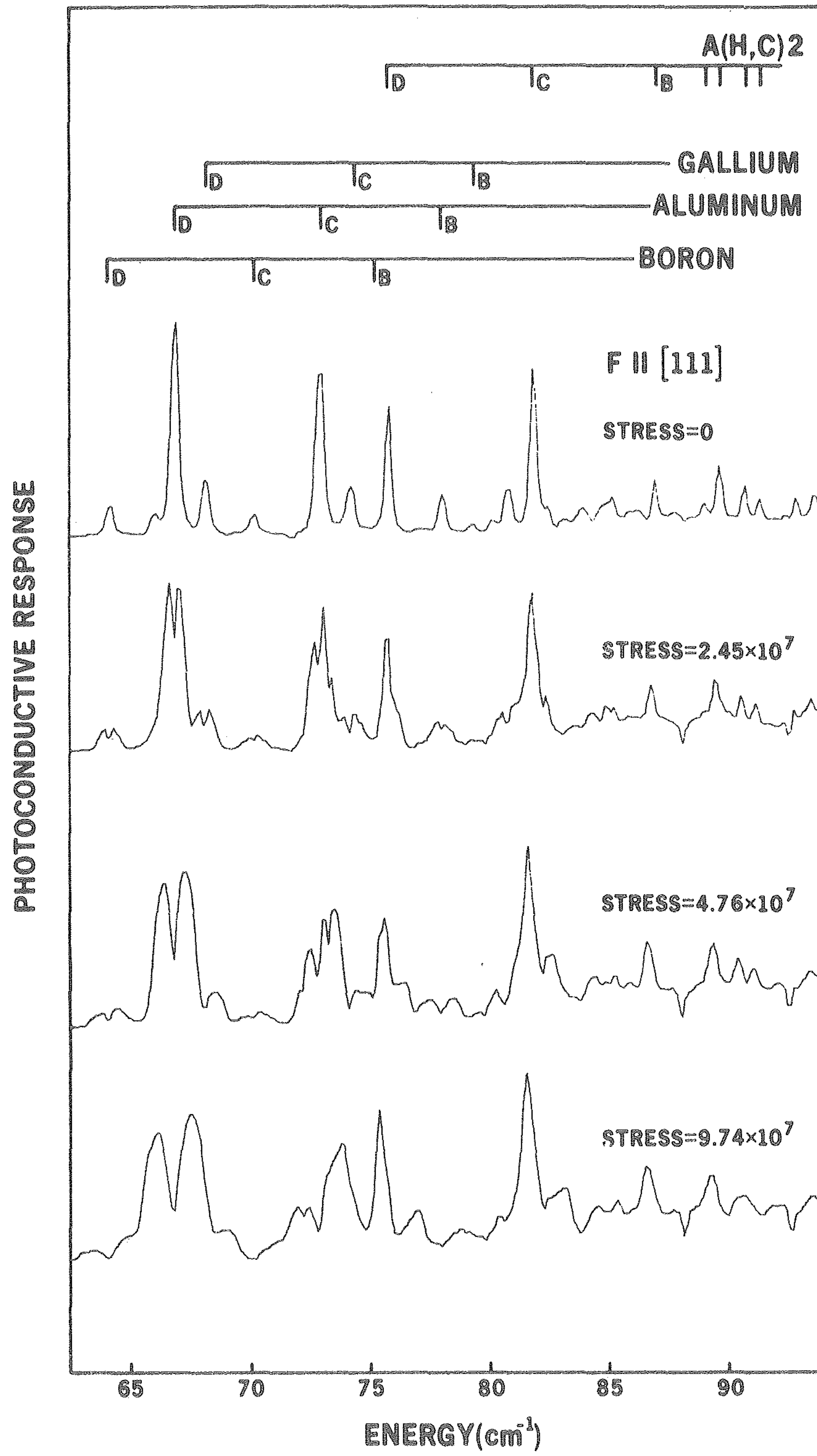

XBL 7911-12835

Figure 21.

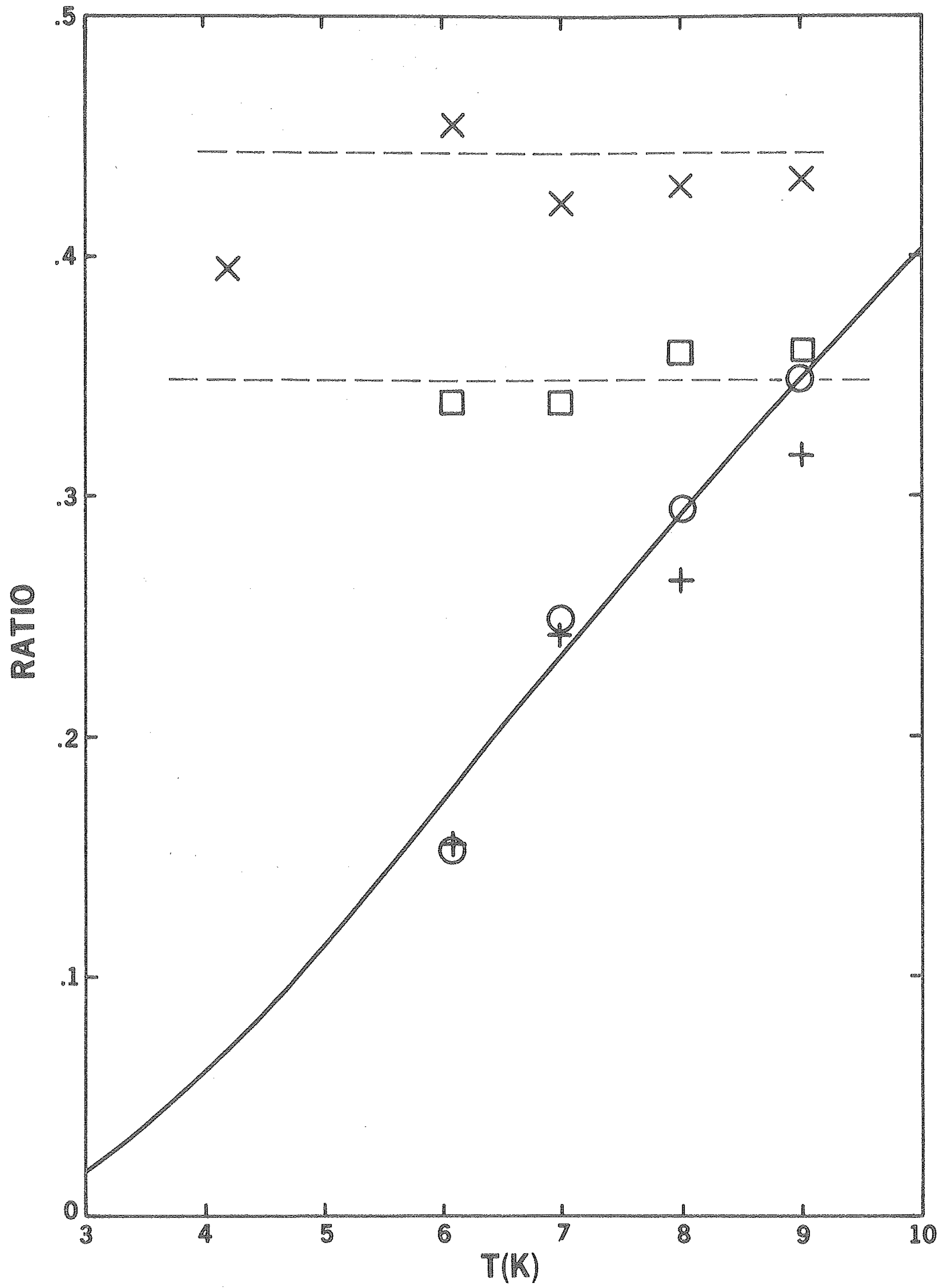

XBL 796-10139

Figure 22.

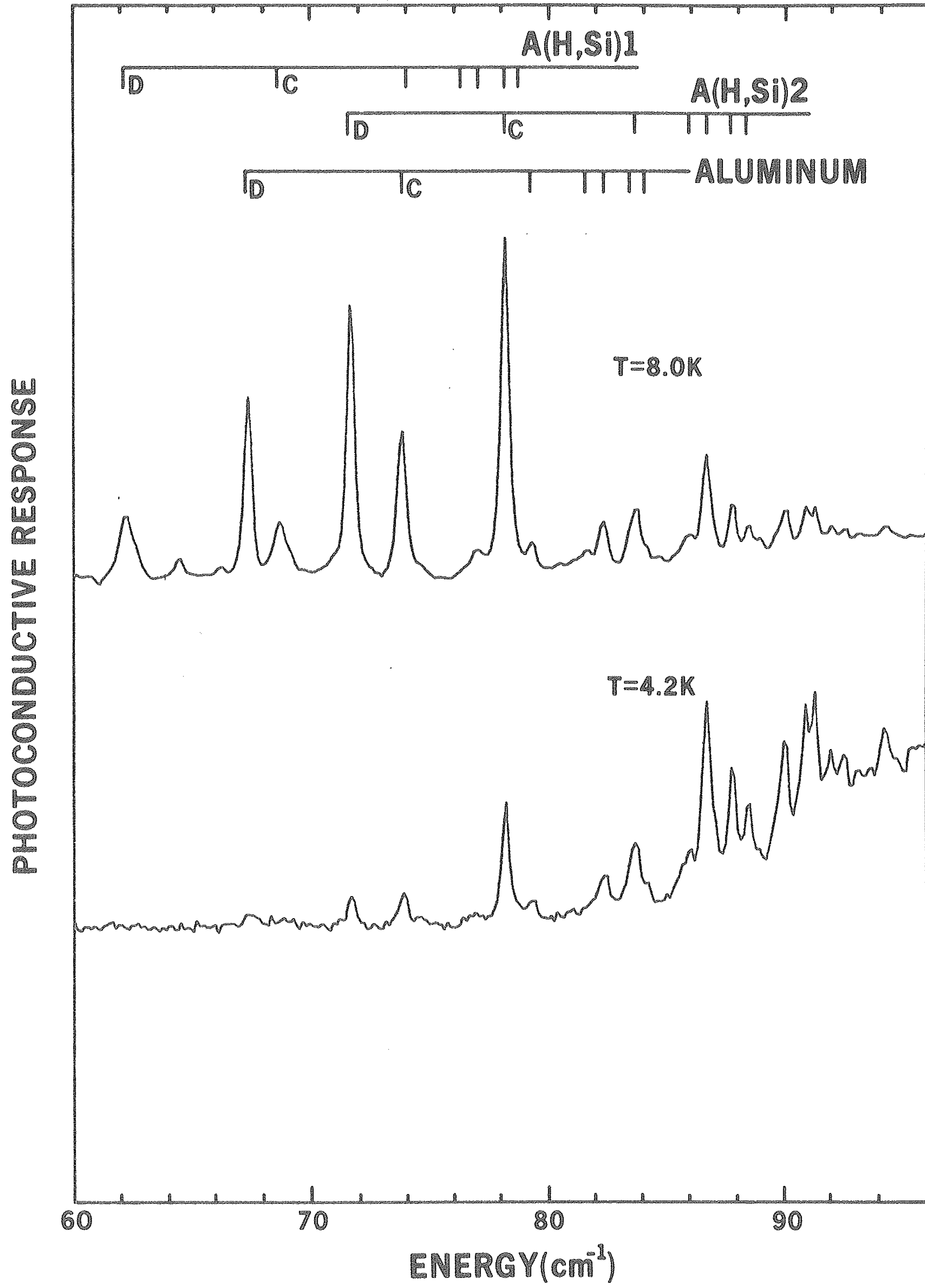

XBL 7911-12831

Figure 23.

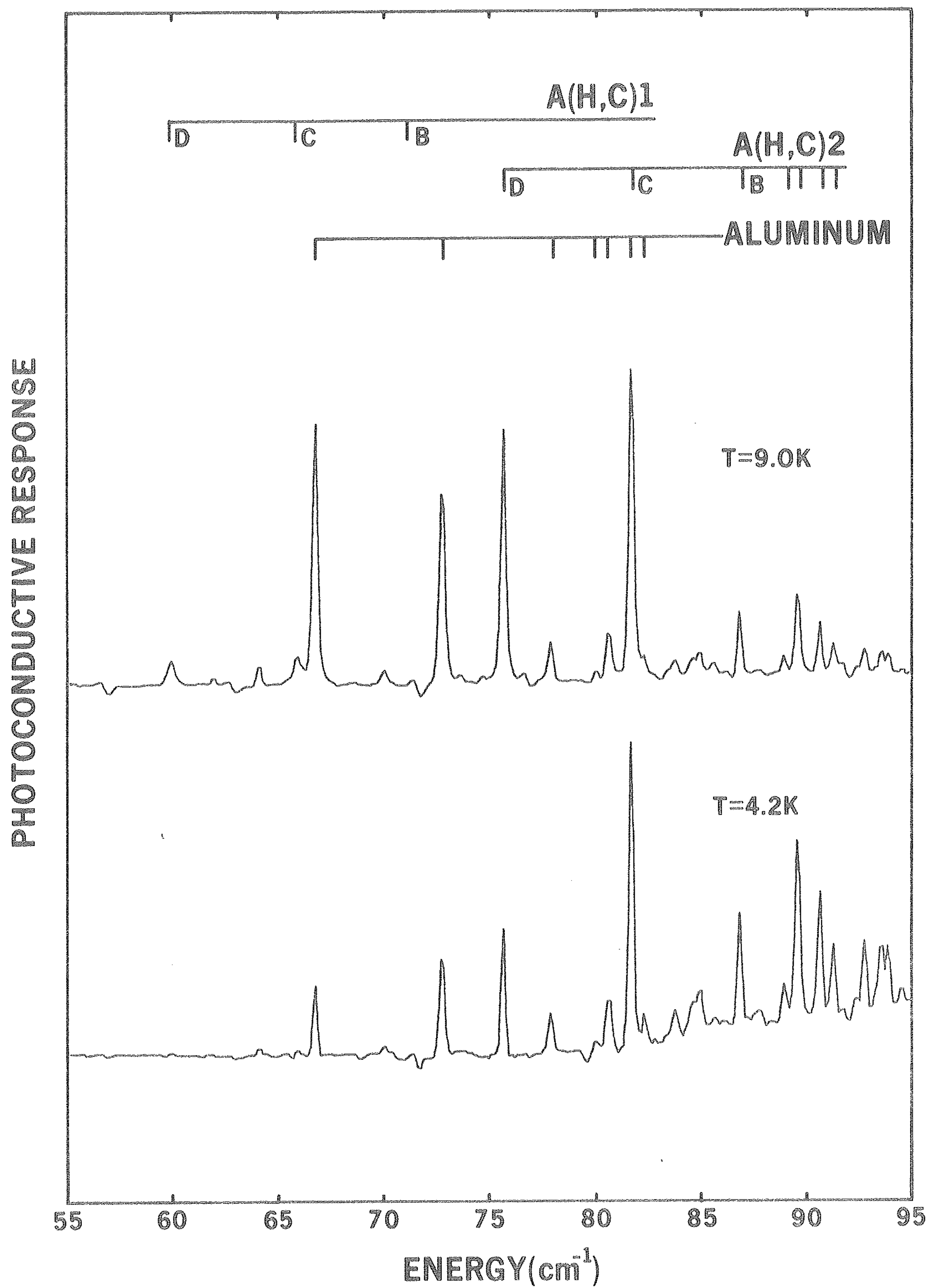

XBL 7911-12833

Figure 24.

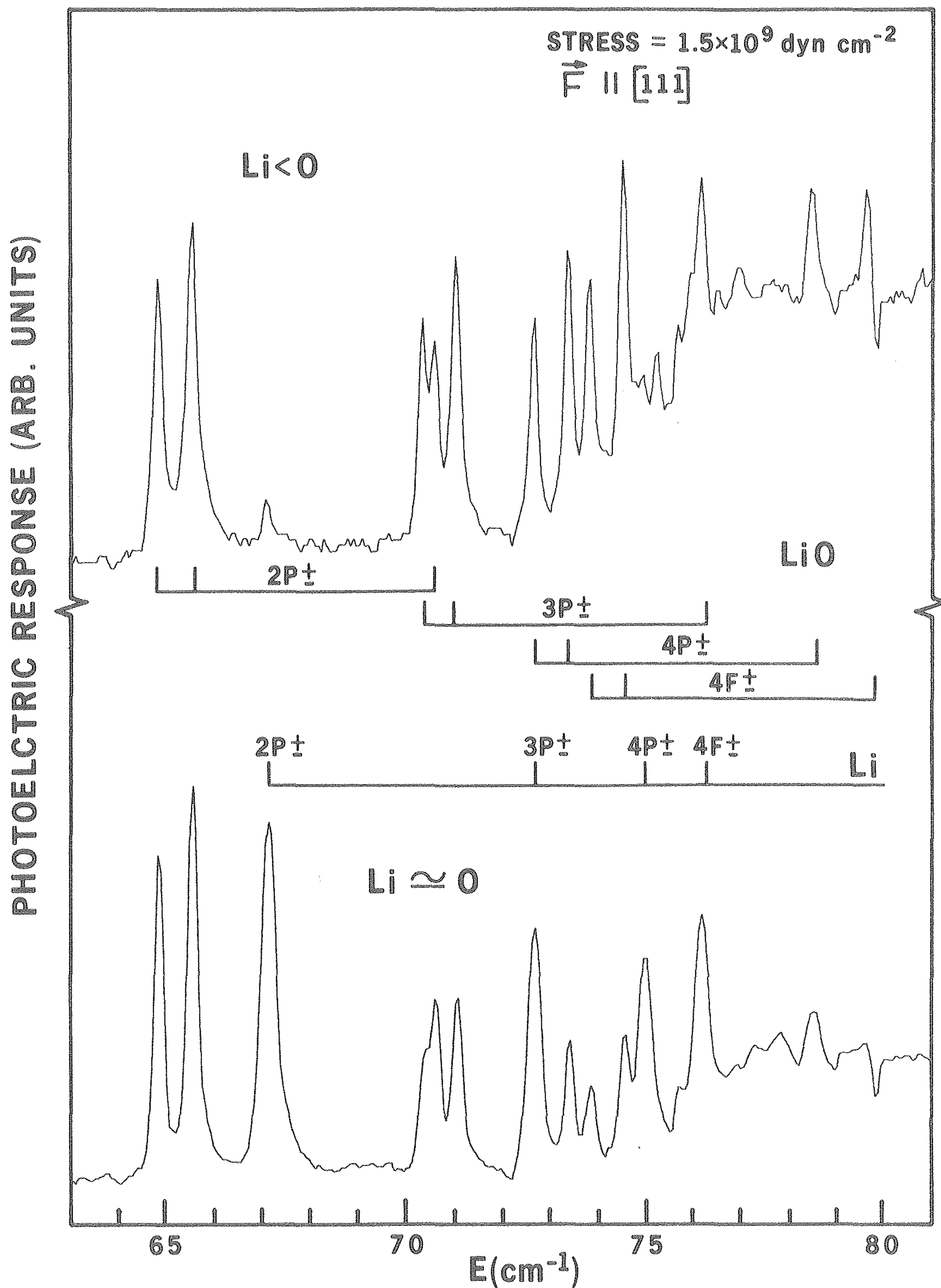

XBL 788-10103

Figure 25.

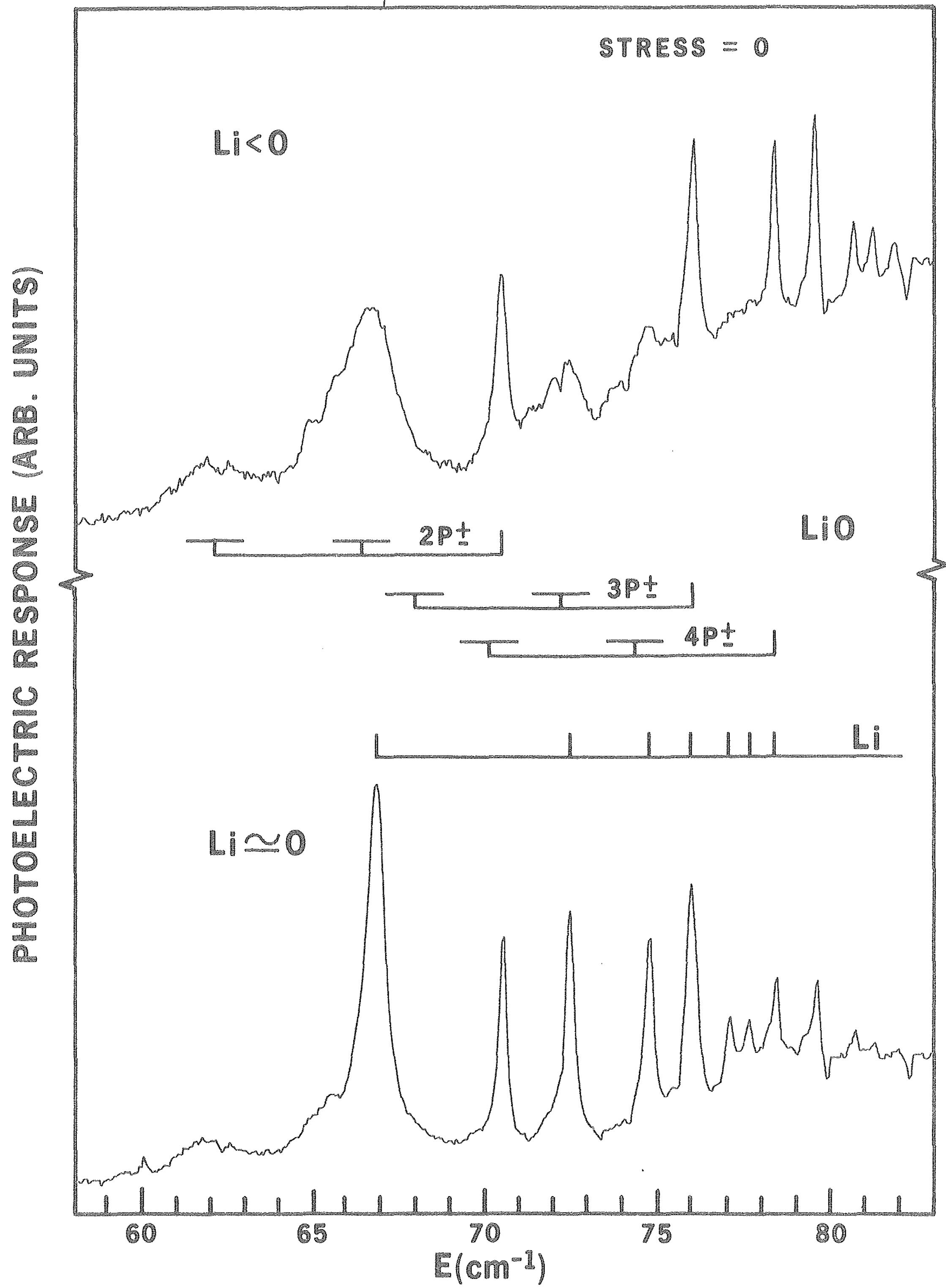

XBL 788-10102

Figure 26.

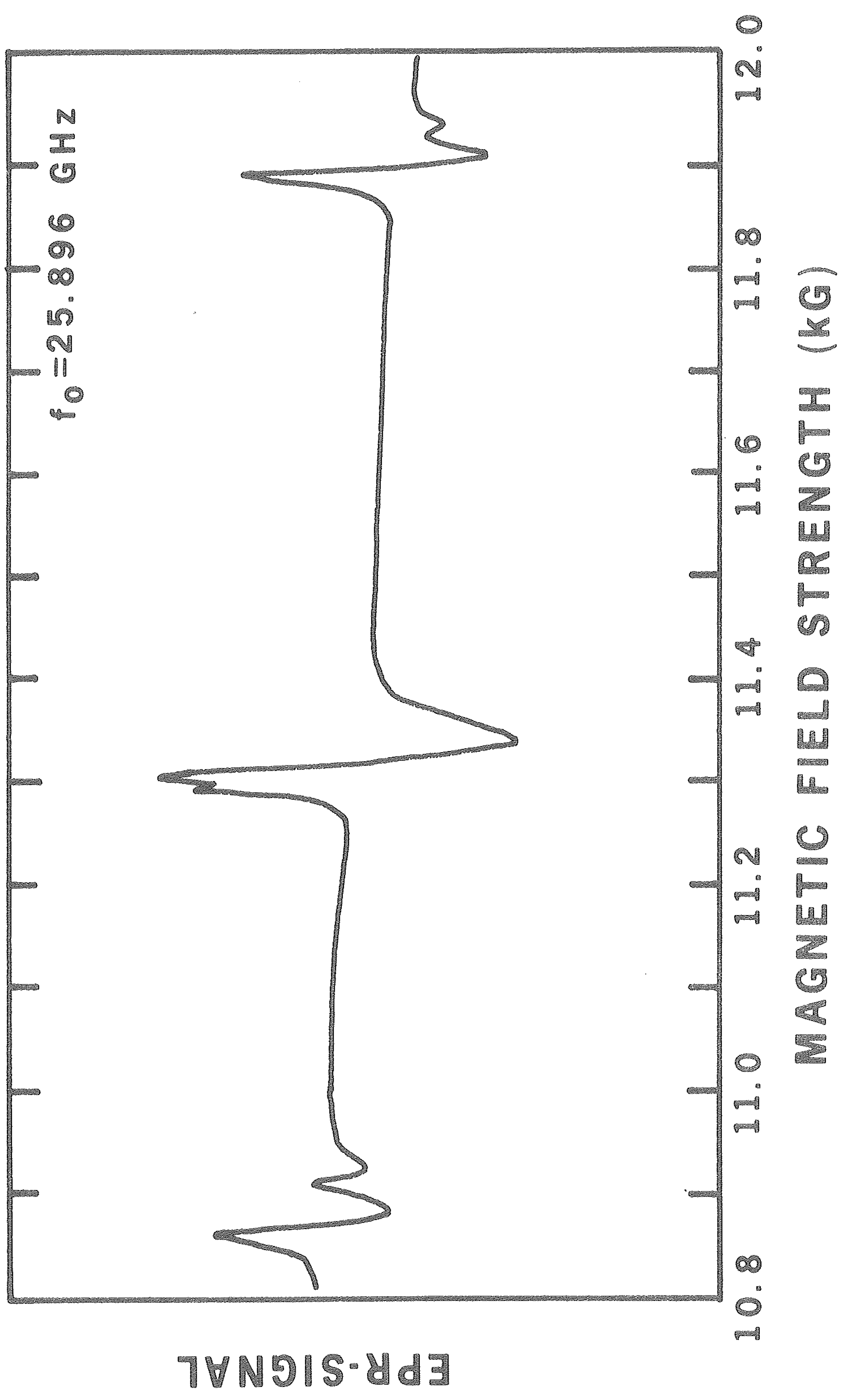

Figure 27.

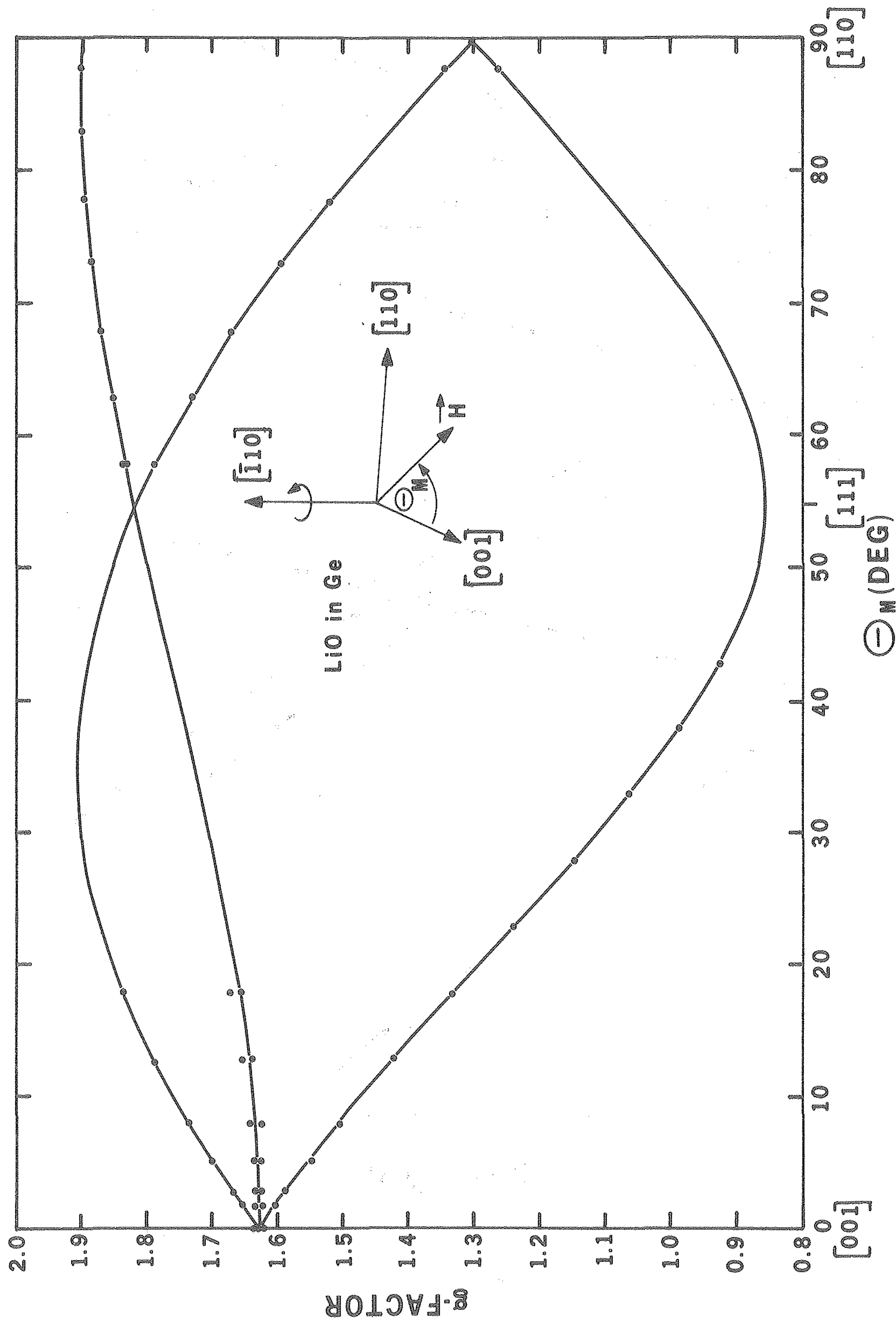

XBL 786-9185

Figure 28.

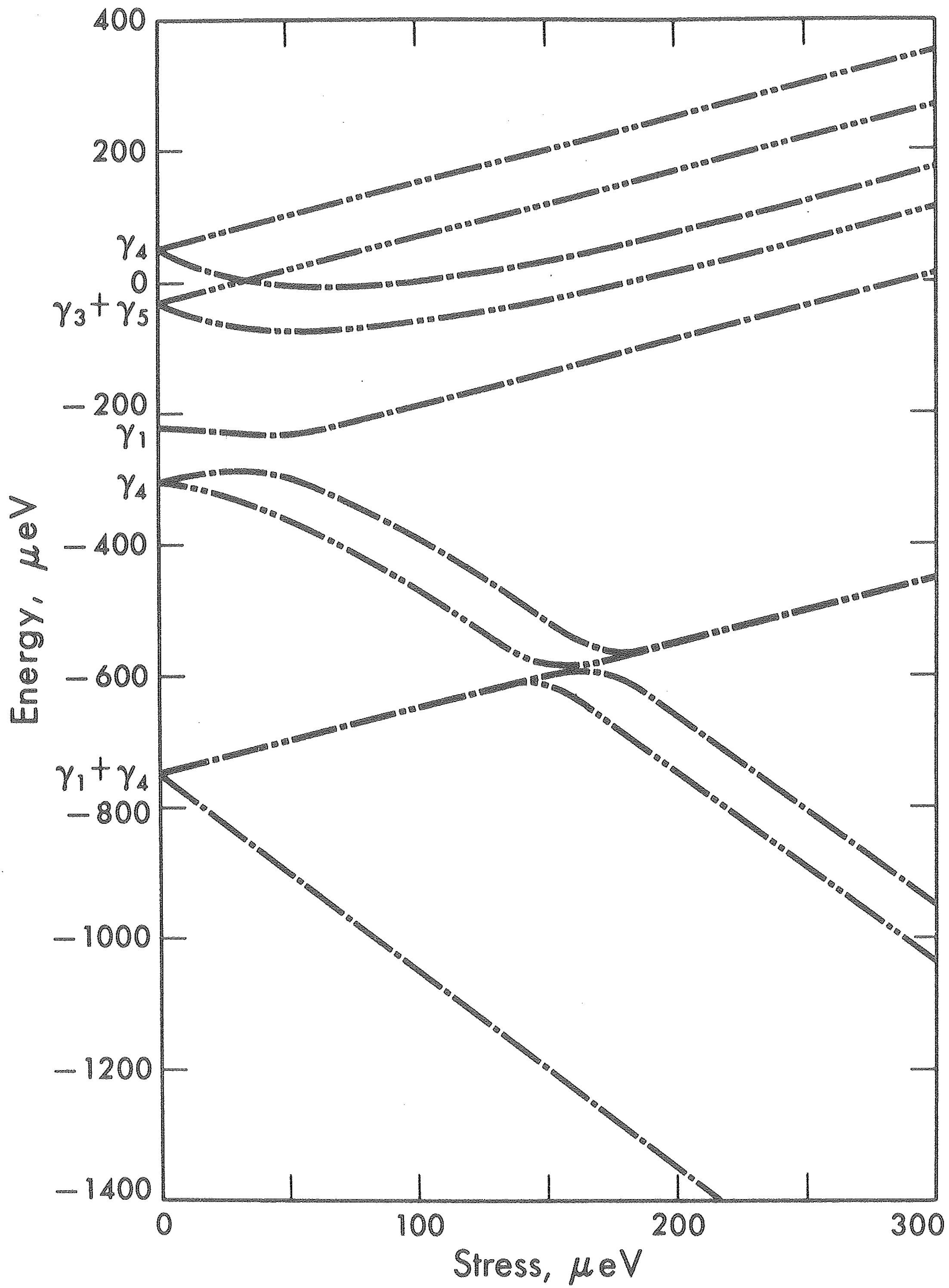

XBL 7810-11903

Figure 29.

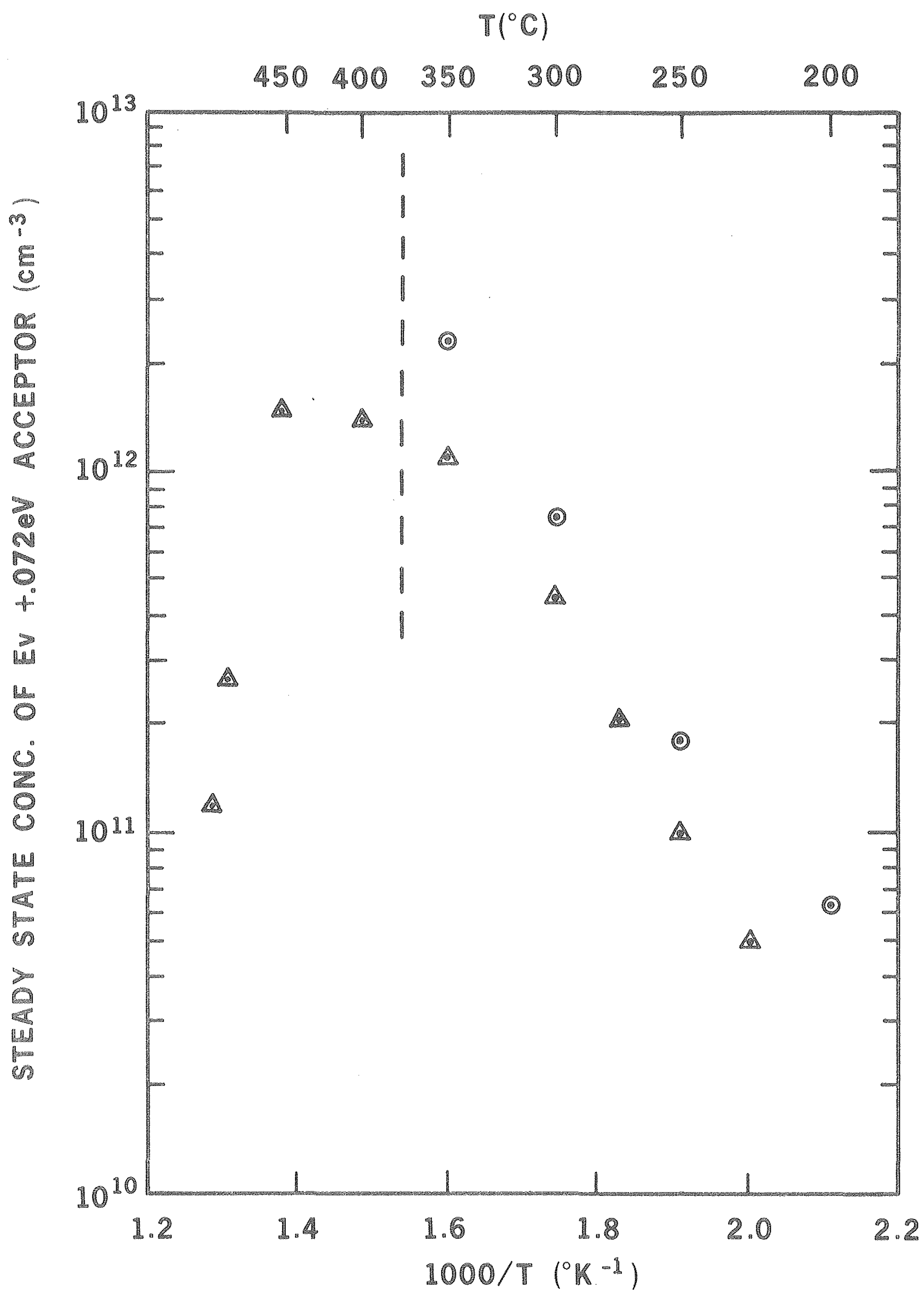

XBL 806-10438

Figure 30.

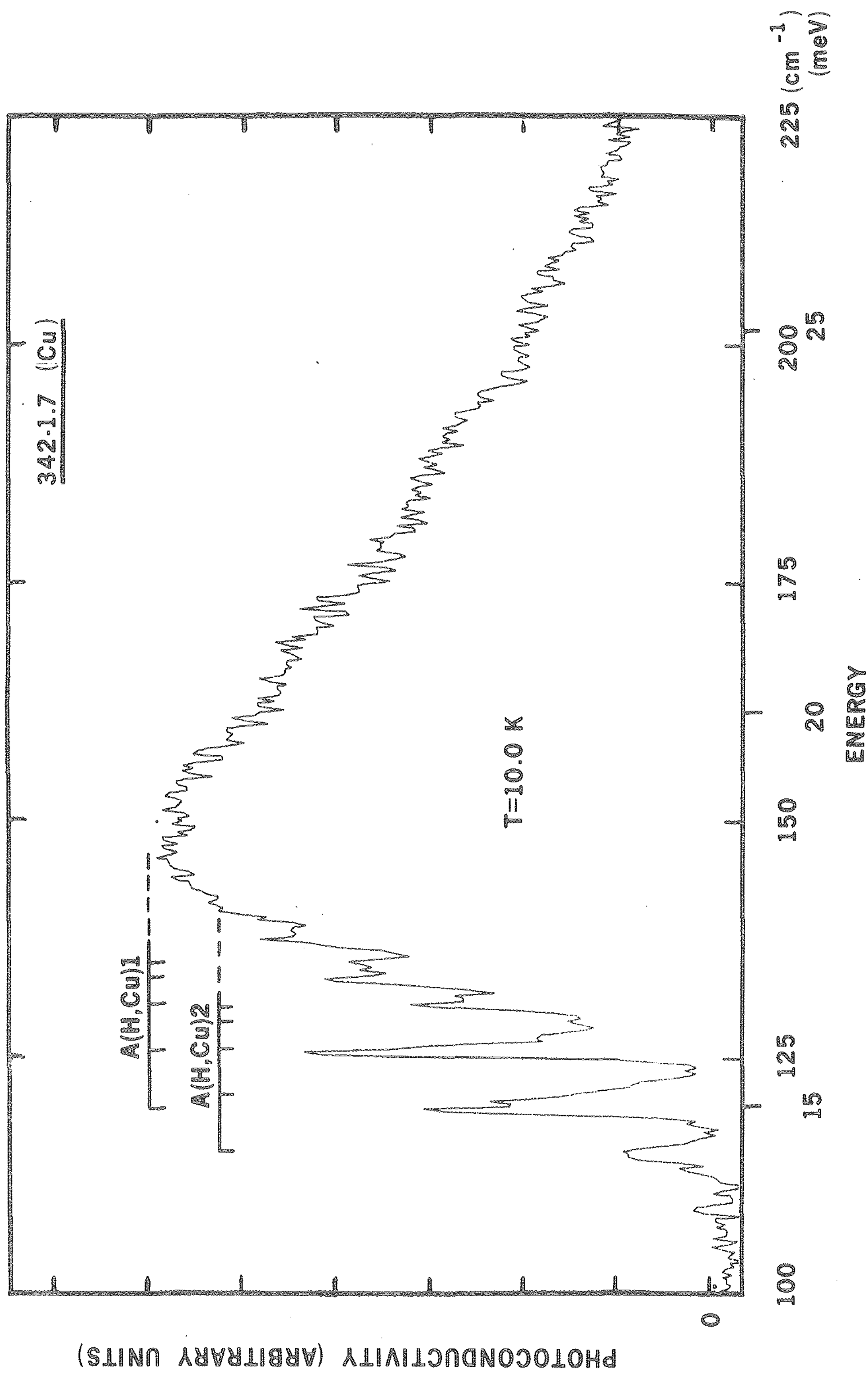

Figure 31.

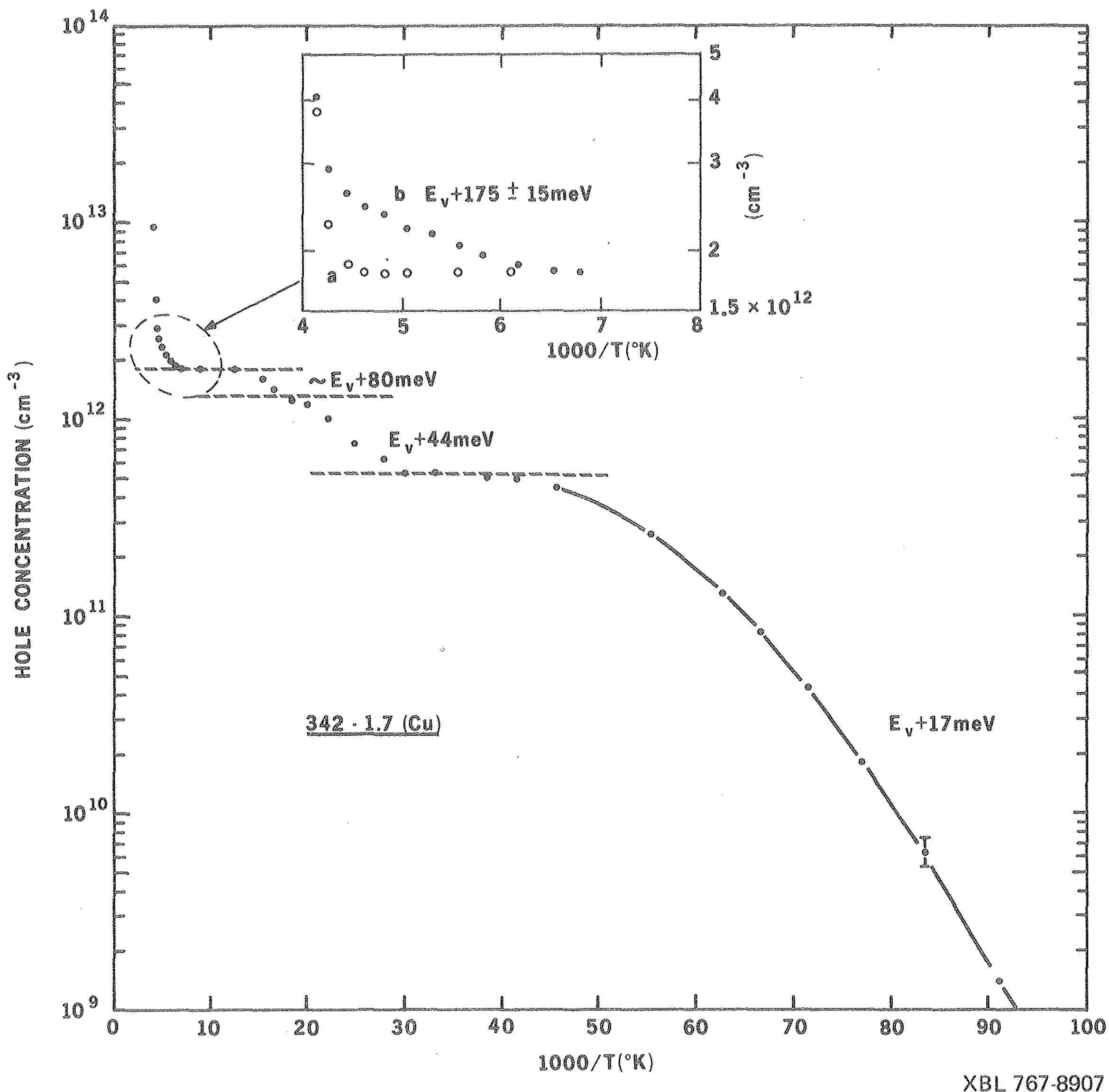

Figure 32.

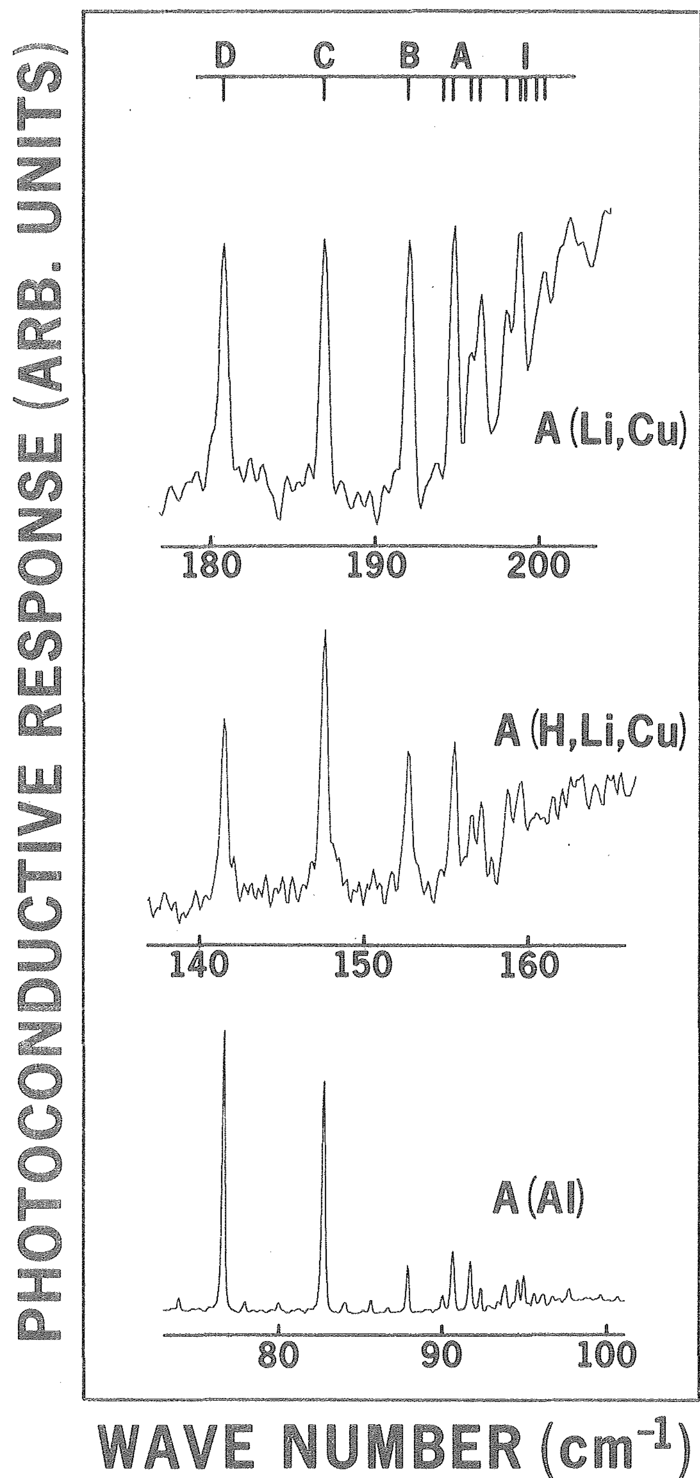

XBL 802-8203

Figure 33.

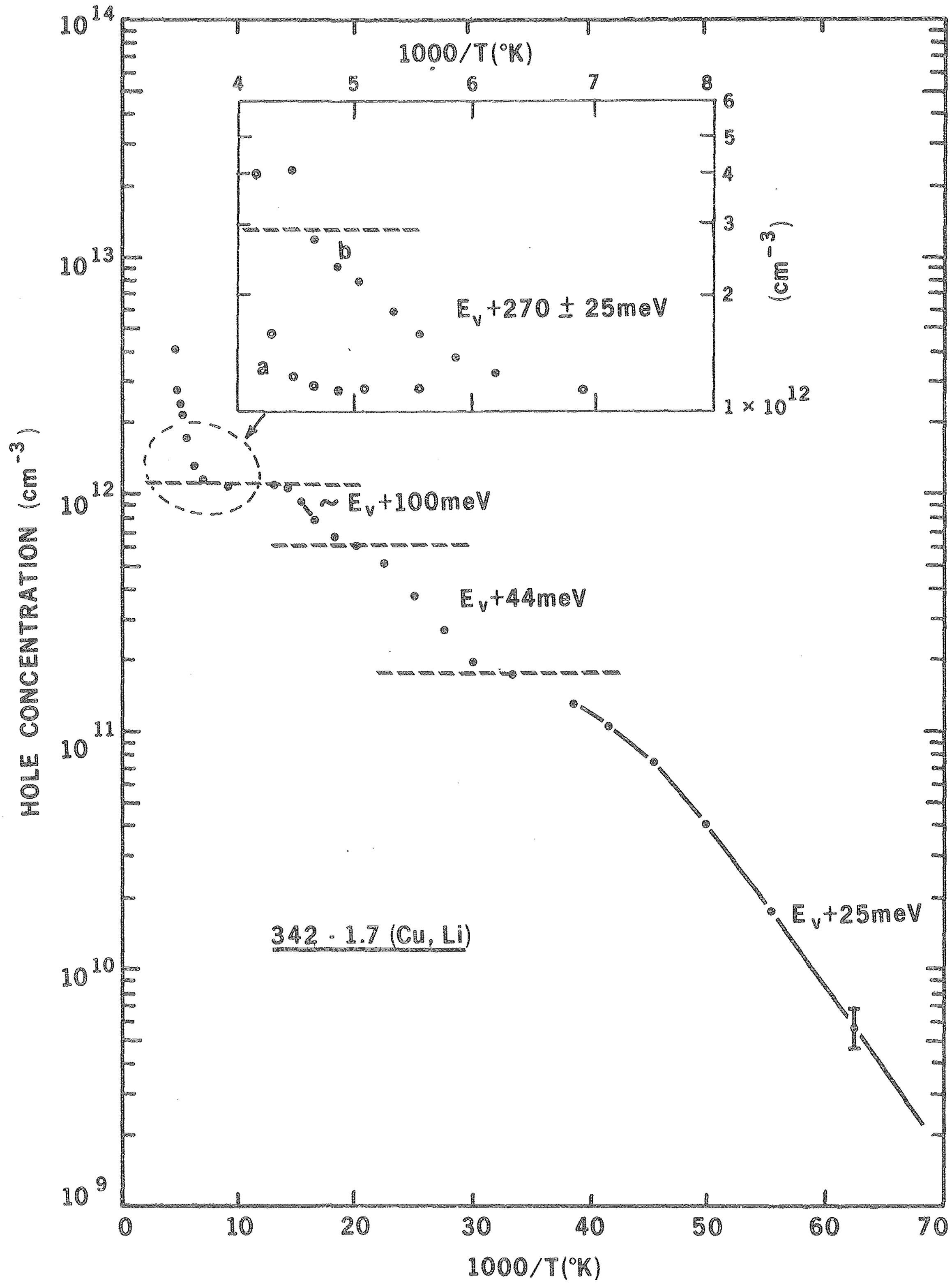

Figure 34.